Excess pore pressure generation due to pseudostatic tests in saturated sand

Marta Auleda Català

May 26, 2005

Abstract

Pile foundations are widely used, mainly to transmit structural load to an underlying stiffer soil or rock. This limit state load a certain pile can sustain without failure is known as *pile ultimate bearing capacity*. During design stage load-tests are performed in-situ on test piles to determine, among others, the value of the bearing capacity.

Commonly static tests are performed as they provide the most reliable data. Dynamic tests are much more cost-effective but have a series of shortcomings, mainly the fact that they introduce stress-waves on the pile and that require calibration with the static values. To overcome both nature-kind problems, a new type of test in-between the previous ones, i.e. the pseudostatic test, has been developed. It is still a dynamic test but the loading pulse lasts longer (70-150ms), 20 times the dynamic pulse, emphasizing the static component. Hence, it is both an economical and reliable option as requires no calibration with the static load-displacement curves. Therefore, it is interesting to get more insight on it.

Two main factors can influence the bearing capacity of a pile measured on the in-situ tests, namely, loading rate and excess pore pressures. In cases like The Netherlands, where end-bearing piles are driven into saturated sand, these two concepts may play an important role. A previous study had been carried out in dry sand and did not find a remarkable loading rate effect. However, for the case of saturated sand the soil response remains unknown. This research investigates the topic, the objective is to get more insight on the excess pore pressure generation and dissipation, evaluate the static-pseudostatic correlation and investigate the possibility of providing effective predictive tools.

The research has been structured in three parts. First a series of experimental scaled tests have been carried out for three loading rates: a CPT (20 mm/s), a static test (1 mm/s) and a pseudostatic test (up to 250 mm/s). The sample consisted in saturated sand that was prepared by means of a fluidizaton-vibration system. Standard sounding rots with a piezocone acted as the pile; five values were recorded: force on the pile head, shaft friction, tip resistance, displacement and acceleration.

Later on, the performed scaled tests have been modeled analytically and numerically. An analytical model based on the cone model of Wolf has been developed. Only the soil underneath the pile tip is considered and it is modeled as an elastoplastic material under static fully undrained loading followed by consolidation.

PLAXIS is the program used for the numerical model. The soil is represented by means of the Hardening Soil model and, although large deformations as the CPT are not allowed, the installation effects are accounted for. Static and low-frequency dynamic calculations have been performed, under fully drained and undrained loading conditions.

Finally conclusions can be drawn, if not form a quantitative point of view, from a qualitative one:

- There is a loading-rate effect on the generation of excess pore pressures, increasing loading velocities generate larger excess pore pressures, from an average of 0.003MPa for the static test to 0.03MPa for the pseudostatic one.

- Experimentally, though, the larger excess pore pressures do not affect values of tip and shaft resistance, thus, do not affect pile bearing capacity. Analytical and numerical models have been able to explain this fact by showing that the loading process is not fully undrained as first thought but partial drainage occurs instead.

- Static results and models fit appropriately the pseudostatic ones and vice versa, pointing towards the suitability of the use of pseudostatic tests even in saturated granular soils.

Evaluating the strong and weak points of the results and the robustness and limitations of the methodology used also some recommendations on further research have been proposed.

Acknowledgments

Contents

List of Figures

List of Tables

Chapter 1

Introduction

*'Scientific approaches to pile design have advanced enormously
in recent decades and yet, still, the most fundamental aspect of pile design
-that of estimating the axial capacity-
relies heavily upon empirical correlations'*
M.F.Randolph (2003)

Technology and development nowadays move at a vertiginous rate. High-raise buildings, bridges that communicate countries, increasing offshore construction, are just few examples that corroborate it. More and more there is an increasing necessity and use of deep piled foundations with higher capacity. Perhaps even more relevant, more and more there is an increasing necessity of evaluation and interpretation methods to optimize pile design, more cost-effective but equally reliable solutions are desired. This concept is the one moving this thesis.

Much of the design of pile foundations is still dominated by estimation of axial capacity. This research has been carried out aiming to be a little but hopefully useful contribution to the topic. Randolph [1] noted the existing dichotomy between (a) empirical correlations to quantitatively achieve a proper design and (b) the conceptual and analytical frameworks for estimating pile capacity. Ideally, any 'empirical' trend should be supported by 'science' in the form of models. Nevertheless, uncertainty and knowledge gaps appear in-between. This explains the scope of the current research: not only experimental testing has been performed, also, and more relevant for this concrete report, an attempt to develop a suitable analytical model has been made, as well as a numerical model. The purpose is to link all three approaches, to propose coherent and consistent conclusions and solutions from both technical and scientific point of view.

This report focuses on estimation of axial capacity for driven piles in saturated sand. More particularly, what attracts the interest is the methodology. The new pseudostatic test combine the reliability of the widespread static test with the efficiency of the dynamic one. It can be directly correlated to the static without need for calibration; however, it keeps the costs down, Bermingham (2004) compared the prices for US market: 100$/ton for the static test versus 10$/ton for the pseudostatic one.

However, it is still a dynamic test and this could be a source of complications. The main objective is to investigate the accuracy and applicability of this pseudostatic test in saturated sand. In this case, two factors may be critical: loading rate and generation of excess pore pressure. The first one was previously studied experimentally by Dijkstra (2004). Now the generation of excess pore pressures, how they can affect the effective stresses and the bearing capacity must be studied. A new series of tests equivalent to

those of Dijkstra but in saturated sand have been performed in cooperation with IHE-Unesco student E.Archeewa. Besides also the scientific insight has been questioned. An extensive literature study will present the potential and shortcomings of the available scientific models for the pseudostatic case. With the literature as background, an analytical model for the pseudostatic case will be developed. A numerical model by means of Finite Element Method with PLAXIS will also be presented. This two models will be compared with the experimental results. The intention is to merge 'science' and 'empirism'. *'...we must incorporate such science in our teaching and our practice, using empirical approaches to validate and calibrate them, but not replace, scientific theory.'M.F.Randolph (2003)*

1.1   Outline of the report

The report is structured in accordance with the research fields. After the introduction and the problem definition, the last somehow introductory chapter is chapter 3, which presents a detailed literature study.

Part 1 deals with the experimental testing. First, the test set-up and regime are described in chapter 4; the results are presented and evaluated in chapter 5.

Part 2 focuses in the analytical modeling. Based on the conclusions of the literature research, the developed model is presented in chapter 6 and the calculations can be found in chapter 7. Once more, the last chapter of the part, number 8, is reserved to the discussion of the results.

The last part is part 3 and concerns the numerical modeling with PLAXIS. A theoretical review of the Hardening Soil model as well as the reasons for its preference is the subject of chapter 9. Chapter 10 details the mode definition, input, geometry, calculations. Chapter 11 shows some significant results and these are contrasted with those of analytical modeling and experimental testing.

After part 3, chapter 12 consists in a wide perspective and general evaluation of the results of the full research (the three parts) as well as some proposals and recommendations for the applicability of the method and prospective research.
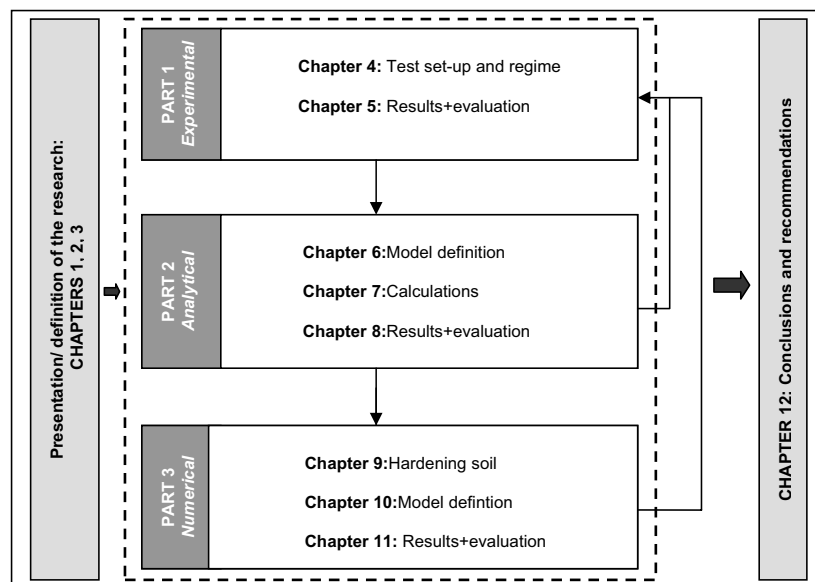
Figure 1.1: Reader's guide

Chapter 2

Problem analysis and objectives

To be able to carry a meaningful research and achieve consistent results or conclusions, a proper understanding of the issue and its related theoretical background is crucial. Dealing with a problem as an isolated question, without enough comprehension of its context, there is no way it can be properly solved. It is necessary not only to know which is the problem but also why this problem arises and which is its significance. This is the aim of this chapter. First, an extensive analysis of the problem is presented. Once this is understood, it is possible to define a coherent research program to get more insight, more answers, in the end, to resolve it. This structure is also detailed and justified in the following sections.

2.1 Problem analysis

In this section the tools for understanding and defining the problem are provided. First some related theoretical concepts related to the topic are explained [1], further on the problem itself can be stated and the reasons and significance of its solution. In following sections, objectives and limitations will be defined in order to get a clear idea of the boundaries, potential and shortcomings of the current research. With this frame in mind the next step will be to define the research to solve the problem hereby presented.

2.1.1 Introduction of the subject

Concepts on pile technology

A pile foundation is a relatively long and slender element that is pushed or driven into the soil or casted in-situ. They are mainly used to transmit the structural load to a firmer, less compressible soil or rock at greater depths. Other possible uses include:

- Sustain horizontal forces, like those from bridge abutments or retaining walls.

- Increase the stability of tall buildings

- Carry uplift forces

- Avoid scour damage

- Compact loose sands

---

[1]theoretical concepts extracted from Simons and Menzies [2] [3] books on foundation and piling engineering
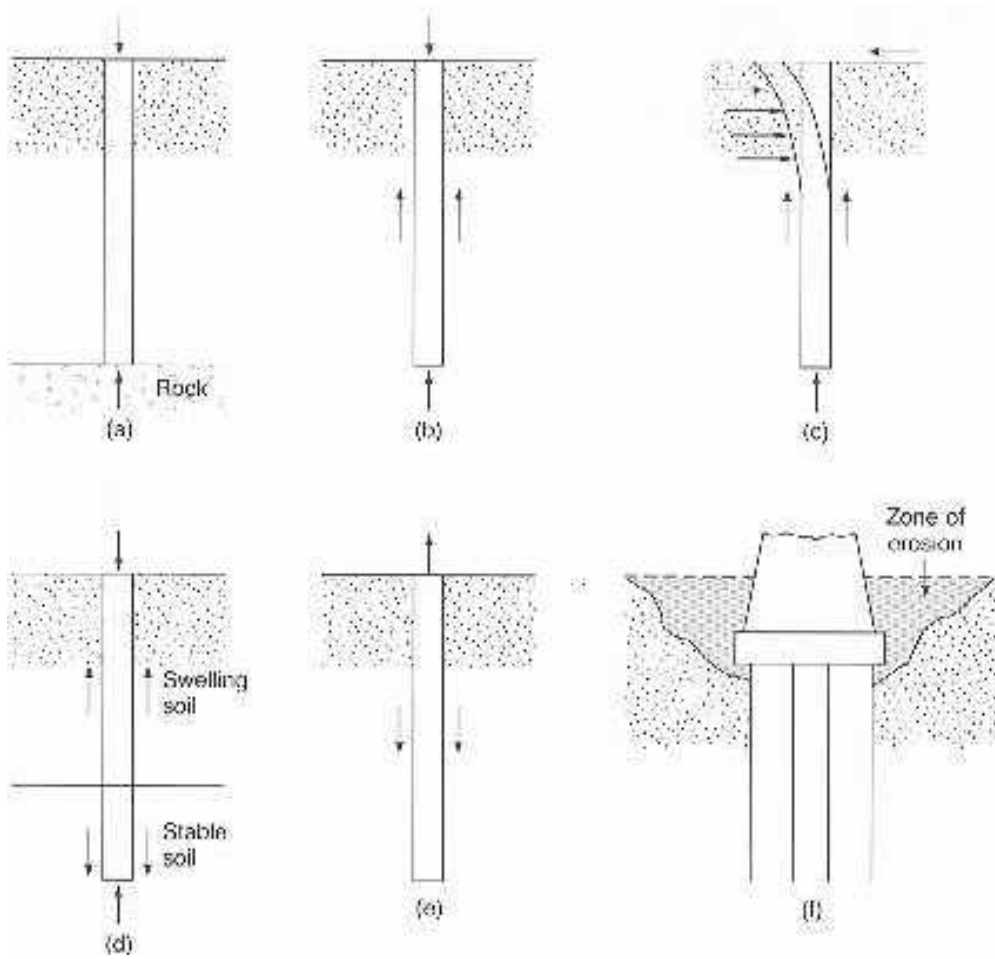
Figure 2.1: Pile uses

Piles can be classified according to the type of material they are made of, the mode of
load transfer, the method of installation or the degree of ground displacement during pile
installation. According to that we can find piles made of:

- Timber

- Concrete

- Steel

- Combinations of diverse materials

Piles transfer load to the soil in two ways, by lateral friction or directly to the soil below
the tip:

$$Q_{pile} = Q_{friction} + Q_{tip} \tag{2.1}$$

The relative proportions of load carried by side-resistance or end-resistance depends on the
shear strength and stiffness of the soil. It is interesting to note that the vertical movement
of the pile required to mobilize full end-resistance is much greater than that required to
mobilize full frictional resistance. Depending on the dominant mode, one can distinguish
between:

- **End-bearing piles**: they derive their resistance (from now on called capacity) mainly by axial transmission of the load to an underlying hard, impenetrable layer of soil or rock.

- **Friction piles**: if the pile cannot be driven to such a hard stratum, the load is then primarily borne by skin friction or adhesion between the lateral surface of the pile and the adjacent soil.

In function of the installation method, two more classes exist:

- **Bored pile**: Made from reinforced concrete cast in a pre-drilled hole in the ground.

- **Driven pile**: Made of steel, concrete or timber, they are hammered into the soil.

However, it is the last classification, according to the degree of ground displacement during installation, the most suitable one. Piles either fit in one of the three categories:

- Small displacement pile

- Large displacement pile

- No displacement pile

This research deals with *closed-end steel tubular displacement piles*. They are characterized by a high bending and buckling resistance, and have favorable energy absorbing characteristics for impact loading. They are not susceptible to damage caused by tensile stresses during driving and can withstand hard driving. All steel piles are driven ones. The study soil is *sand* and the pile will be axially loaded. Piles in granular soils mainly act as *end-bearing piles*.

Pile capacity and failure

The concept of *pile capacity*, as the ability of the pile to pursue its service, to meet the loading requirements, already been introduced. The pile capacity may be evaluated either considering the structural strength of the pile or the supporting strength of the soil, which is the perspective that interests the geotechnical engineer.

The *ultimate bearing capacity* is the limit state for which larger loads cause the pile to fail. For end-bearing piles it is directly linked, and may be identified, to the ultimate base capacity. The load causing ultimate failure of pile material or the load at which the bearing resistance of the soil is fully mobilized is known as *failure load*. But, from an engineering approach, failure may have occurred long before the ultimate load is reached, mainly with criteria related to serviceability state. There are different criteria depending on the different construction codes.

Load-settlement curve

The relationship pile vertical displacement versus applied axial load on top is a very useful tool. At early stages of the loading the settlement is very small and mostly due to elastic behavior. If the load were to be removed in such a point as A, the head of the pile would rebound almost to the original level. The largest portion of load is carried by side resistance on the upper part of the shaft. In a point as B exists some permanent settlement, indicating that plasticity has started to occur. Although still most load is laterally supported by friction, some of it is being carried at the pile tip. When point C is reached, settlement increases rapidly with little further load increase. The ultimate load has been reached and is mainly carried by end-bearing. The determination of this ultimate load on beforehand is then very important to the engineer.
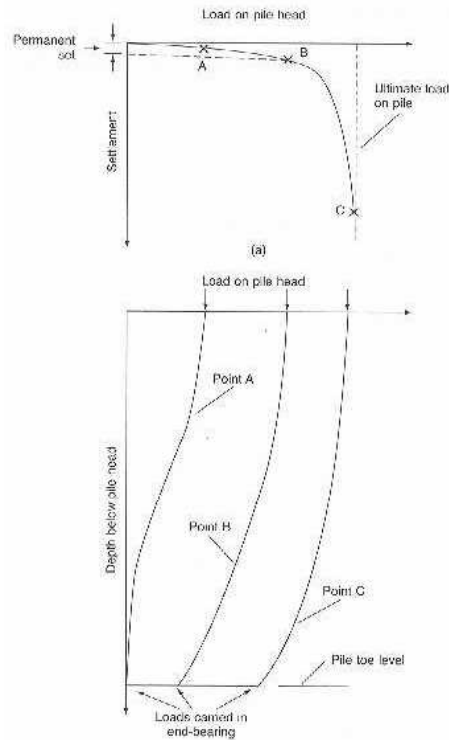
Figure 2.2: Effects of loading of a pile

Pile load tests

We have seen how important it is to know the capacity of a pile, even better, to know it's full load-displacement curve. Load tests are performed on-site on test-piles to determine these properties. Normally piles are initially designed according to analytical or experimental methods based on soil characteristics or estimated loads. During design stage pile load tests are performed to:

1. Determine settlement under working load

2. Determine ultimate bearing capacity

3. As a proof of acceptability.

Traditionally *static* load testing has been used as it provides reliable guaranty. However, its main shortcomings are:

- High costs

- Long time required

An alternative is provided by means of the *dynamic* test. Its main advantage versus the static one is that it doesn't require devices to obtain the reaction force because this is a result of a change of momentum, leading to less time required and minor costs. This reaction force can be assimilated to the ultimate pile bearing capacity, but it poses a major handicap: this measured pile capacity is a combination of both static and dynamic components, which implies that calibration with a static test is required. Besides, other remarkable disadvantages of the dynamic test are:
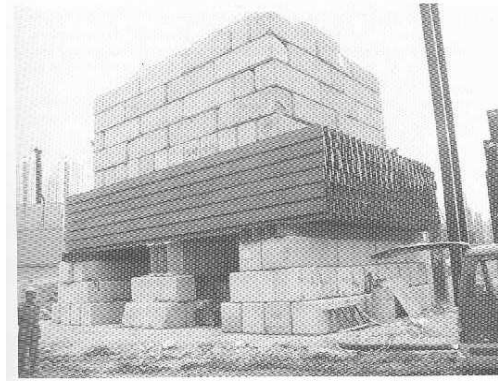
Figure 2.3: Kentledge reaction stack for static pile test

- Stress-wave phenomena introduces tension waves that can damage the pile

- Eccentric loading can introduce bending stresses, also risking to damage the pile

- The obtained results require cumbersome manipulation by means of signal-matching

- In some cases it may be difficult to mobilize the full capacity of the pile

To satisfy Industry's demand for cost-effective and accurate means of testing deep foundations, the **pseudostatic** test has been developed. Still considered a dynamic test, it combines high loads with low pile velocities and accelerations like in the static test, but with the quickness of the dynamic one. The required reaction mass is only 5-10 per cent of the one for static test and, apart from that, its long duration when compared to the dynamic test emphasizes the static component, allowing the operator to be able to establish in a straightforward manner the static load behavior without need for calibration. Hence, a test can be considered pseudostatic or quasistatic if the duration for which the load is above 50 per cent of the maximum load fulfills the condition:

$$t_{50} >> \frac{2l}{c} \tag{2.2}$$

where c is the wave celerity in the pile material. This relatively long duration keeps the pile always under compression, avoiding the possible development of tension stresses. Hence, it can be assumed that the pile reacts as a rigid body and, soil displacement and pile top displacement are equal. Moreover it guaranties the central location of the dropping mass, doesn't introduce eccentricity, it's fully axial loading.

2.1.2   Definition of the problem

The pseudostatic test combines the advantages of both static and dynamic tests, which turns it into a thrilling interesting new technology. It just has 'one', but determining, disadvantage: a lot of important questions about it have not been answered yet. TNO and Berminghammer developed the so-called *statnamic* device [4] and even proposed a simple model for it. Despite it, some question marks remain:

- **Loading rate effect**: increasing loading rates can alter the ultimate bearing capacity. This concept was investigated by Dijkstra [5], finding not remarkable influence of the loading rate in the pseudostatic test. More references to Dijkstra's work will be made along the report.

(a) Stanamic device   (b) Loading pulse
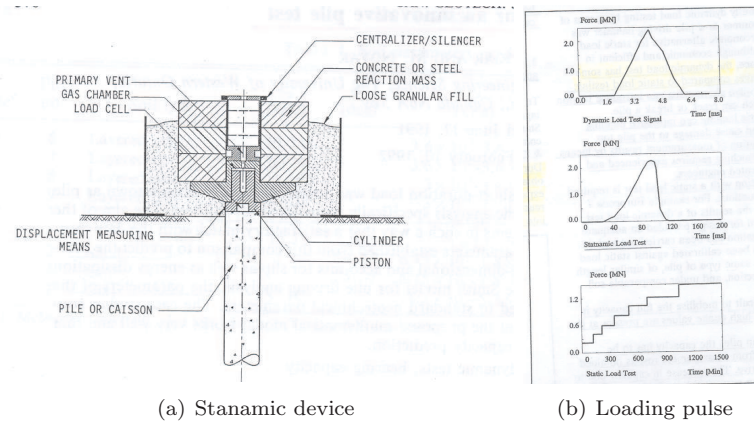
Figure 2.4: Statnamic testing

- **Excess pore pressures**: There is a research gap when considering saturated soils. Cohesive soils behave always undrained but for granular fine-grained soils like sand the effect of the rapid test in the water pressure is still unknown. Generally they are considered drained material but now, the larger loading rate can influence the soil behavior. As the excess pore pressures affect the effective stresses they may play a relevant role in the penetration resistance and thus the bearing capacity. Hence, is the pseudostatic method suitable to be used in saturated sands like the case of the Netherlands? Or may the test lead to erroneous results, compromising the design criteria of the foundation? Moreover, how reliable is the method when water is involved in the problem?

The second point is what defines the problem.

Problem definition: The applicability of the pseudostatic method in saturated sands is still unknown.To what extent due to higher loading rate excess pore pressures are generated and how they affect the bearing capacity needs further investigation.Correlation with the static values is necessary for the acceptance of the method.

2.2 Objectives

Once the problem is defined, obviously the objective shall be to solve it in the measure of this thesis scope.

Main objective: To extensively investigate, qualitative and quantitatively, how the generation of excess pore pressures due to pseudostatic testing in saturated sand affects the pile bearing capacity. It should result in a representative loading rate-excess pore pressure-bearing capacity relationship, with its correspondent load-settlement curves, that could be used to predict soil response under these conditions.

A series of secondary objectives may be defined:

1. Investigate relationship loading rate-excess pore pressure⇒Comparison among different loading rate tests in saturated sand

2. Investigate influence of pore pressures in bearing capacity⇒Comparison between saturated and dry conditions (Dijkstra [5] results)

	STATIC TEST	DYNAMIC TEST
Advantages	-Reliability of results	-Short time required -Low cost
Shortcomings	-Long time required -High costs	-Eccentric loading possible→Possible pile damage -Cumbersome result manipulation -Calibration with static required -Stree-wave phenomena→Tension waves -Difficult to mobilize full pile capacity

PSEUDOSTATIC *(still dynamic but emphasizes static component)*	
PSEUDOSTATIC vs STATIC	**PSEUDOSTATIC vs DYNAMIC**
Advantages -Short time required -Required reaction mass:5-10% of the static one -Lower costs	-Longer time (but quick enough)→Emphasizes static component -No stress-wave introduced→No tension waves (pile always under compression) -No need for calibration -Fully axial -Easy manipulation and model
Shortcoming	**PSEUDOSTATIC test still has to be better understood, especially in saturated granular soils there are 2 effects that need investigation:** 1. LOADING RATE→J.Dijkstra's thesis 2. EXCESS PORE PRESSURES→*Main purpose of this thesis*

Figure 2.5: Comparison among different load test methods

    3. Investigate the soil strength effect⇒Comparison among different soil densities

And, consequently:

- Propose correlation pseudostatic-static results

- Evaluate the suitability of importing pseudostatic testing into zones with fine-grained cohesionless saturated soils.

2.3   Scope of the research

It has been proposed as the main objective to carry on an exhaustive and coherent investigation about the topic in question. In this section how the objective will be met is explained. Therefore, the research can be said to embrace the following fields:
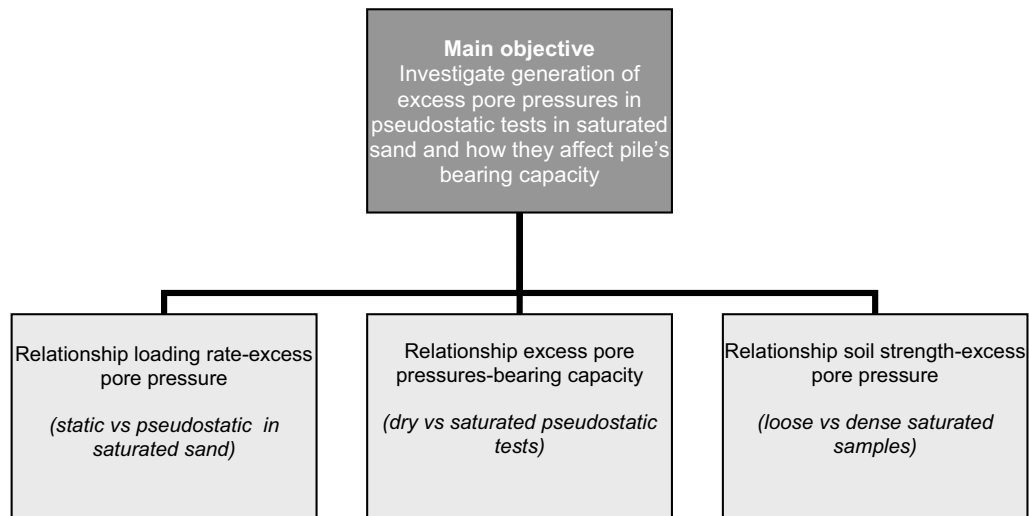
Figure 2.6: Objectives of the research

- **Experimental testing**: a series of tests have to be performed in the scale 1g condition model designed by Dijkstra [5]. The chosen test regime and series should meet the different requirements for a complete parametric study: different loading rates (static and pseudostatic), saturated sand, different densities. Analytical and numerical modeling results are to be calibrated with the experimental ones.

- **Analytical modeling**: There is no analytical model defined for such a problem. This approach passes by adapting the existent theories to the case and propose a good analytical fit.

- **Numerical modeling**: The experimental tests have to be modeled by FEM with the program PLAXIS. The numerical model should be defined to adjust the numerical results to the experimental ones.
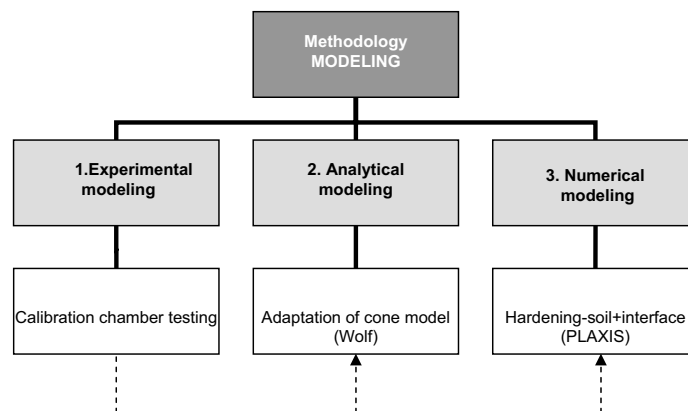
Figure 2.7: Scope of the research

Experimental results are going to be used to validate and calibrate the other models. So, implicitly, we are defining another objective:

- To evaluate the ability of the available analytical and numerical methods to model the problem and predict the soil response.

2.4   Limitations

The scope of the research needs to be properly delimited with restricted boundaries in order to make it feasible in the thesis context.

2.4.1   Experimental testing limitations

- **Pile**: Only one type of pile: 10 cm in diameter smooth steel pile

- **Soil condition**: Soil type is kept constant to fully saturated sand. The same sample in prepare again after each test, so we are always working with the same material. It is the same sand as used by Dijkstra [5] so the comparison is possible. The phreatic level is kept constant too. The only variable parameter is the vibration time (that controls the density), but its efficiency will be discussed. The soil conditions in the tank are not comprehensively known.

- **Amount of tests**: A statistical significant amount of tests should be carried out. The limitation of time need to be accounted for, though.

- **In-situ initial stresses**: They are not fully known or understood. Besides, the calibration chamber and the placement of the vibrators can affect them.

- **Loading system**: Only pressure forces, no tensional stresses.

2.4.2   Analytical modeling limitations

- **Model development**: The shortcoming of the literature presenting available analytical models that fit the case will be seen. Thus, a model will need to be developed, with all its limitations.

- **Applicability**: It is the experimental test that is modeled, thus not the real field case.

2.4.3   Numerical modeling limitations

- **Computer program**: PLAXIS will be used for the modeling. The standard available soil models are th only ones to be used. No user-defined model, which would better fit the case, are developed.

- **Applicability**: It is the experimental test that is modeled, thus not the real field case.

Chapter 3

Literature research

This chapter is meant to extend the understanding of the problem by presenting some theoretical background and important results of previous researches [1]. It begins with general considerations about the two key parameters governing the problem, the loading rate effects and the excess pore pressure effects. Afterwards literature conclusions related to experimental testing are available. It only focuses in the device itself (the calibration chamber) and excess pore pressure measurement. The reason for not developing so much this part is that the experimental set-up was designed by Dijkstra [5] in his MsC Thesis. Thus further information can be found in his report. Moreover, the tests were carried out in cooperation with E.Archeewa and the purpose of his thesis was precisely to evaluate in detail the experimental part. Also interesting reviews can be found in his report. Finally, there is a large review of the available analytical models. PLAXIS is the program to be used in the numerical model, so no literature research is explicitly required about finite element methods. In the corresponding chapter, the characteristics of the Hardening Soil model can be found, but it does not consist in literature research properly speaking.

3.1   General considerations

3.1.1   Loading-rate effects

The only scientists who have explicitly modeled pseudostatic testing were Middendorp, Bermighammer and Kuijper [4] and they developed the so-called Unloading Point Method (UPM).Without attempting to detail the method here, it is interesting to point out that in this method the rate effects are the part that should be subtracted to the measured statnamic load-displacement curve to obtain the static equivalent (if pore pressures could be neglected). It shows how remarkable the role of the loading rate can be.
Besides, damping is found to be significant in pseudostatic testing, it can be directly responsible for a pile capacity increase of up to a 30 per cent.

Other previous research stated that the bearing capacity of a pile (ultimate failure load) increases with increasing rate of loading. Al-Mhaidib [6] presented a relationship for sand as follows:

$$Q_u = C^*(LR)^n \tag{3.1}$$

where Q_u is the pile capacity corresponding to a loading rate LR, C is a constant and n is an exponent function of the sand density and the depth-to-diameter ratio. Especially

---

[1]The formulas and expressions are here shown as presented in the literature by their correspondent authors. The symbols have not been modified to homogenize them but, as further on the limitations of the available literature will be discussed and therefore an analytical model developed, it is not a problem as they are not used in the calculations in this thesis. The notations used in the model development are in the glossary

the sand density affects the relationship between loading rate and bearing capacity, when compared to the depth-to-diameter ratio, that has much slighter effects.

Another proposal to model the rate effect is the one of Briaud and Garland [7]:

$$\frac{Q_{DP}}{Q_{SP}} = \left(\frac{t_D}{t_S}\right)^n \tag{3.2}$$

where $Q_D P$ is the dynamic capacity, $Q_S P$ the static one, t_D and t_S are respectively the loading times for dynamic and static tests, and n is again an exponent function of the soil properties (0.01 for clean sand and 0.1 for soft, plastic clay).

Coyle and Gibson (1970) defined a power law:

$$R_t = R_s t(1 + J^* V^N) \tag{3.3}$$

where $R_s t$ is the static soil resistance, J^* is the rate-effect factor, V the penetration velocity and N an experimental exponent. El Naggar and Novak [8] choose $N = 0.5$ and $J^* = 0.1 - 0.15$ for sand, for the base of the pile only as they assume that the rate-effects are negligible for the pile shaft.

Also the local side friction increases with larger rates of penetration (Te Kamp [9]). This can be relevant as piles derive their strength largely from skin friction and only some 17 per cent is derived from end-bearing (Jones, Bermingham, Horvath [10]).

This is clear for cohesive soils, the dynamic-to-static ratio is directly proportional to the logarithm of the penetration velocity ratio; the proportionality constant was named 'soil viscosity coefficient' by Dayal and Allen [11] and it's inversely proportional to the soil strength. So on, we can affirm that the strength of clay increases significantly under dynamic loading, which could lead to overestimations of soil capacity. On the contrary, parallel research on granular soils showed that the effect of penetration velocity on cone and sleeve resistance is minimal, hence, dynamic effects are minimal for cohesionless soils. In dense sand there is almost no loading effect (Dayal and Allen [11], Eiksund and Nordal [12]). This means that, while pseudostatic may be too optimistic for clay, it should be suitable for sand (Brown [13]).

Related to the loading of the soil it must be noted that we are going to perform tests in the sequence: CPT-Static-Dynamic (Pseudostatic)-Static. This procedure, consisting in reloading cycles, can introduce some residual stresses that don't affect the load of the pile but do affect the initial slope of the load-settlement curve, that gets stiffer, and the load distribution of the pile (Briaud and Tucker [14]). Precisely, the aim of the second static test will be to evaluate these reloading effects and see whether they are significant or not.

The results of Dijkstra [5] are of special interest. He designed the test set-up to be used and performed the same series of tests but in dry sand. He found that a velocity increase from $1mm/s$ to $250mm/s$, the difference static-pseudostatic, did not imply any significance increase in bearing capacity, only 4% for the tip and 6% for the shaft resistance. Therefore, no loading rate effect on the pile capacity was found.

3.1.2 Excess pore pressure effects

During cone penetration or while driving a pile, the soil around the cone/pile is subjected to a combined compression and shear stress deformation and excess pore pressures are generated.

$$\bar{u} = \bar{u}_{oct} + \bar{u}_{shear} \tag{3.4}$$

Whether this excess pore pressures are detected by a piezometer on the shoulder of the cone will depend mainly on the permeability of the soil. Hence, Seed and Reese (1957) studied

the phenomena and showed that pressures created by pile driving are transfered into the soil largely as an increase in pore water pressure. When undrained soil is loaded, the main part of the hydrostatic stresses is carried by the water because water can be considered nearly incompressible, so small volumetric changes lead to large hydrostatic stresses. A sand can be expected to display a fully undrained behavior for permeability values lower than $10^{-7}m/s$. It is difficult to predict these pore pressures as they are function of the pile driving energy transfered into the soil, the type of pile, the local drainage conditions, the stress history and the soil type and density (Eigenbrod and Issigonis [15]).

Schmertmann (1974) pointed out that excess pore pressures affect the soil resistance values:

- Negative pore pressures$\Rightarrow$ increase on the effective stress$\Rightarrow$ larger shear strength$\Rightarrow$ larger resistance

- Positive pore pressures$\Rightarrow$ decrease on the effective stress$\Rightarrow$ smaller shear strength$\Rightarrow$ lower resistance

Influence of the density

The measured excess pore pressures will be positive or negative depending on the result of the combination of the two determining processes, namely, compression and shear deformation. Compression induced excess pore pressures are always positive, but shear-induces excess pore pressures can be either positive or negative. Volumetrical response to shear deformation is principally governed by soil density; density of the soil in relation to critical density can indicate whether the soil is contractant or not.

1 *Compression-induced excess pore pressures*: Always positive

2 *Shear-induced excess pore pressures*:

- Dense soil$\Rightarrow$ DILATANT BEHAVIOR: there is an increase of volume, and so the void ratio, giving negative values of the excess pore pressure.
- Loose soil$\Rightarrow$ CONTRACTING BEHAVIOR: there is a decrease in volume, and so the void ratio, giving positive values of the excess pore pressure.

So, in general, a penetration process in sand, that can often display a dilatant behavior, generates excess pore pressures as follows:

1 Soil is compressed by the cone$\Rightarrow$ Positive excess pore pressure generation in the displaced material

2 Soil around the shaft is subjected to local shear deformation$\Rightarrow$ Negative excess pore pressure until critical state is reached

However, it is also possible that in the case of the dynamic test, with rapid loading (high penetration rate), the shear stresses may be applied very quickly, not giving time for the volume to expand (Te Kamp [9]).This postulate reinforce the influence of loading rate into pore pressure generation.

Influence of the loading rate

However, there is another role factor in the generation of excess pore pressures, the loading rate. Thus, the two governing parameters on the generation of excess pore pressures in sand are:

1 Relative density

2 Loading rate

And these two factors are linked. Canou et al. especially constructed a minipiezocone of $1cm^2$ cross-section in a 180mm diameter triaxial cell at penetration rates between 0.1 and 100mm/s and found out that excess pore pressure in loose sand depends on relative density as well as on the penetration rate.
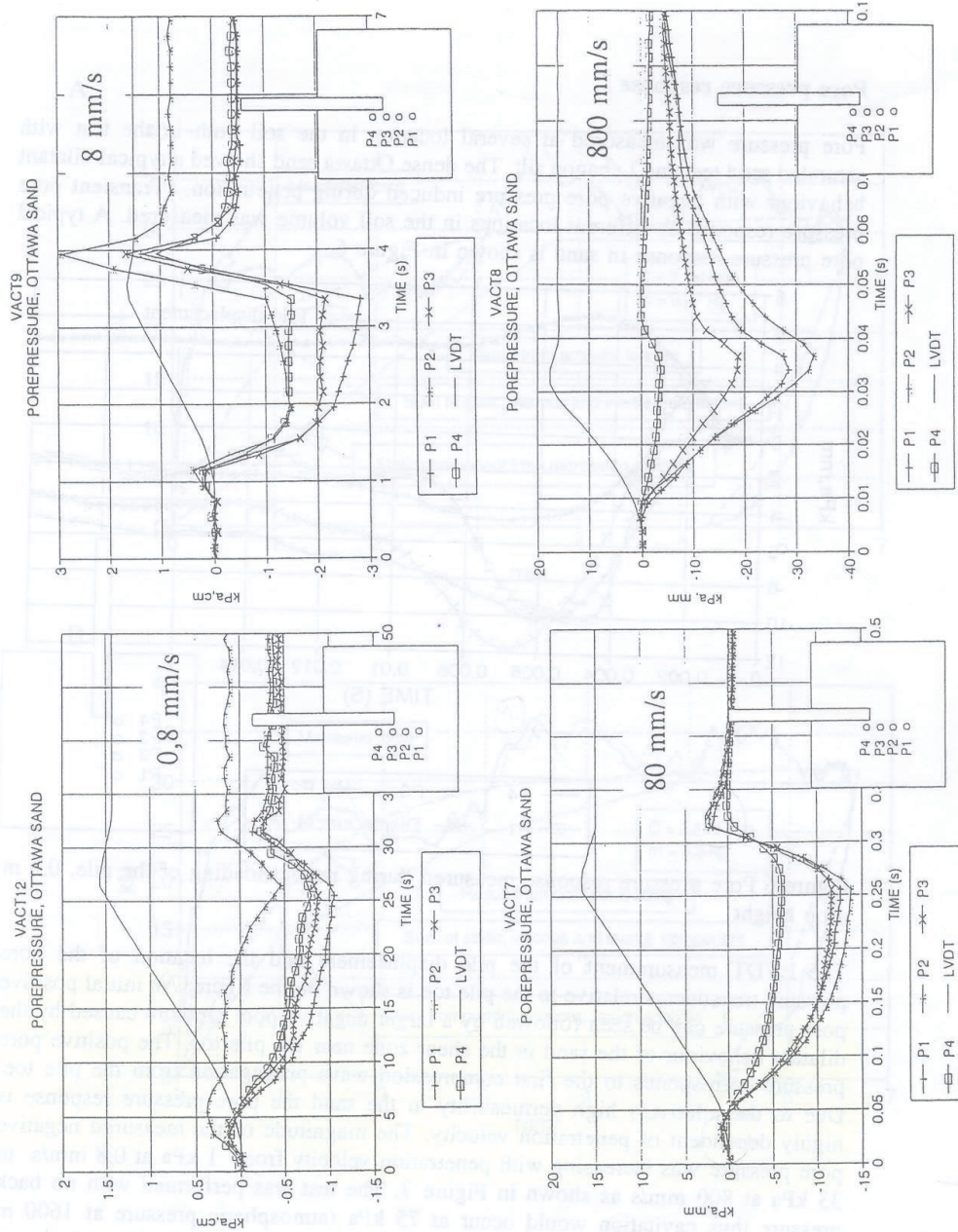
Figure 3.1: Pore pressure response in saturated sand for different penetration velocities

Firstly note that increasing penetration speeds (or loading rates) will shorten the dissipation time between the generation of the excess pore pressures and the observation by the piezometer, consequently, the possibility of observing the excess pore pressures in contrac-

tant soil before they dissipate will be larger.

Broere [16] performed high-speed CPT tests in the same calibration chamber at Geotechniek as this research. His results show that although larger excess pore pressure occur and are measured at higher than regular CPT penetration speed, there is no correlation with relative density other than that at higher densities greater negative excess pore pressures occur. Therefore, large negative excess pore pressures can indicate high relative density. On the contrary, large positive excess pore pressures do not provide any information about the sand density as positive excess pore pressures manifest themselves similarly for all density range.

3.2   Experimental testing

3.2.1   Calibration chamber testing

The tests will be performed in a **cylindrical calibration chamber**, filled with saturated sand. Holden (1977) studies these kind of tests and suggested 4 limiting conditions for calibration chambers:

1. σ_v ,σ_h constants

2. ϵ_v, ϵ_h constants

3. σ_v constant, $\epsilon_h = 0$

4. σ_h constant, $\epsilon_v = 0$

Parkin [17] noted that (1) and (3) are the most commonly applied.

It seems intuitive that a more densely packed sample (higher density) will suffer larger risk of boundary effects. The boundary effects from the chamber can be very significant, for these effects to be negligible the ratio chamber diameter-to-cone diameter needs to be in excess of about 35 for loose sands ($\rho_r \approx 30 percent$) and 60 for dense sands ($\rho_r \approx 90 percent$) (Wesley [18]). This is of special relevance as it has been demonstrated that the cone resistance in a sand of a given density depends primarily on the horizontal stress and the angle of friction, while it remains relatively unaffected by the vertical stress (Houlsby and Hitchman [19]); so the boundary effects could influence the horizontal stress. Linked to this is the concept that the friction ratio is closely related to the soil type (Begemann, 1965) and it's also very sensible to lateral stress and soil fabric (Huntsman, 1985, Houlsby et al. 1988).

Wesley [18] also found changes in the cone resistance with the chamber size. He argued that these may be due to changes in vertical stress arising from downward force exerted by the testing device while pushing the pile into the ground.

All authors seem to agree that the zone in which the soil will be affected by either the installation of the pile or the loading varies with soil density and pile installation method. Meyerhof (1959), Kishida (1963) and Robinski and Morrison (1964) report this area to be 3 to 8 pile diameters of extent. Logically, lateral deformations decrease with increasing distances from the pile. The largest area in extent affected will be found at a certain depth, in accordance with the radiation cone theory that postulates that the compressional wave generated by either installation or loading of the pile propagates vertically into a limited zone under the pile toe. Tests show that the measured cone angle is larger than the predicted one (Hölscher [20], [21], [22], [23]), thus, it should be possible and even expectable to exceed those 3 to 8 pile diameters mentioned above.

As to the influence of the depth, O'Neill (1991) proposed that the soil conditions at 5 diameters below the pile toe have little influence on the pile capacity.

3.2.2   Pore pressure measurement

There are, a grosso modo, two possibilities. Of course the best is to combine them. In first term the research is carried out only with a piezocone. If time available, the incorporation of transducers would be recommendable.

- **Piezocone**: the cone has an incorporated piezometer and measures pore pressures as it penetrates the soil. There are different positions of the porous element available, normally they are defined as follows:

    - *Position 1 (under the cone tip)*: records pore pressures generated by the compression of the soil by the cone,shear stress relative changes are small ($<$ 20%)(Baligh, 1986).
    - *Positions 2 and 3 (along the shaft)*: shear stresses become significant when related to the excess pore pressure generated, because the large normal compression stress acting on the tip undergoes stress relief in long the shaft.

  Thus, the stress regime directly behind the cone tip is more significantly affected by shear stresses than the area immediately located beneath the cone tip (Wroth, 1984, Campanella et al., 1986). The shear stresses only affect a limited thin annulus next to the body of the cone (1-10mm) but the normal stresses because of the compression is normally in the order of 10-20 diameters (or some 350-700 mm).

- **Transducers installed into the soil**: placing piezometers at different depths, relative to the cone penetration position, can provide useful information, especially to distinguish between compressive and shear deformation consequences.

Eiksund and Nordal [12] carried out a series of tests in Ottawa sand and they found the next tendency for pore pressure transducers installed in the soil beneath the pile toe: initial pore pressure that corresponds to the first compression wave form the pile toe followed by a larger negative pore pressure caused by the dilating behavior of sand. Once penetration stops the pile may rebound a little and some soil dilatation can be reversed, getting positive pore pressure response. Although we are also dealing with sand, and this results do much match with the sand dilatant character, it is important to reming that we are only measuring pore pressure at the cone (piezocone) and no transducers are installed in the soil, not allowing to follow the wave propagation so closely.

Broere [16] also investigated the different placements of piezometers into the soil for the case of loose sand. He embedded two high-precision piezometers in the sand bed at depths 20cm apart, p_1 being placed 1,2m below surface and p_2 1,40m. He compared it with the results obtained for the piezocone. The standard behavior of loose sand was: as the cone neared the deepest piezometer pore pressure started to rise slightly but for the nearest piezometer this behavior was interrupted by a sharp negative peak. Immediately afterwards, the pore pressure jumped again to positive values and once the cone had passed p_1 level, a time dependent pore pressure decay started until total pore pressure dissipation, 20s later. He attributed the original increase in pore pressure in part to the contraction of the sand as the cone displaced it and in part to the already existing pore water being displaced by the cone too. The sharp negative peak was attributed to the contractant behavior originated by the shear deformation that takes place once the cone has passed. Then sand should reach a critical state, no more deformation would take place, just consolidation process would start. He found less strong generation of positive pore pressures for
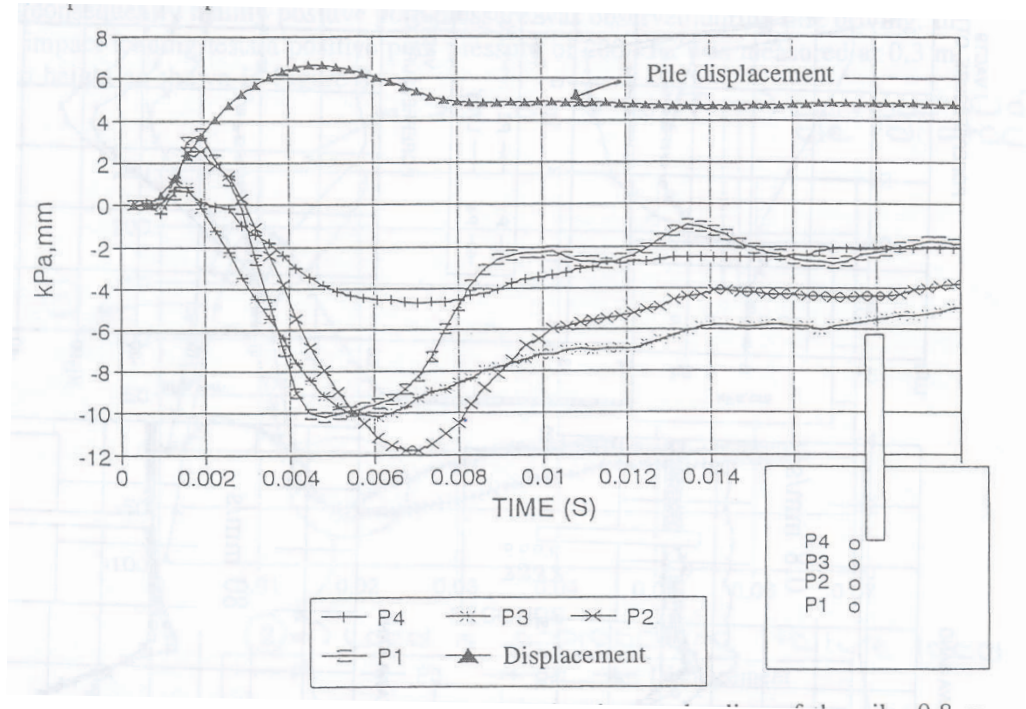
Figure 3.2: Pore pressure response at impact loading in dense Ottawa sand, 0.8m drop height

intermediate and high relative densities, only when $\rho_r = 80\%$ was considered the positive pore pressures were completely absent. He only observed a slow increase of pore pressure ver time until the hydrostatic value was reached again;, the sharp negative pressure peak was either not observed or less prominent than what happend in the case or loose specimens.

Comparison with piezocone results noted that although measurements made with piezometers in the sand bed are reliable, they do not correspond well with the measurements at cone shoulder of the piezocone and the extreme values did not clear up what relationship with density could be derived. Even though, from the piezometers results he concluded:

- Large negative shear-related pore pressures followed by positive ones indicate low density.

- Total absence of positive excess pore pressures indicates very high density.

- Absence of large pressure fluctuations indicates intermediate density.

3.3   Analytical modeling

3.3.1   Introduction

The behavior of saturated cohesionless soil under a dynamically (pseudostatic) loaded pile wants to be studied. To reflect all the components of this case, we first have to remark that any model, analytical or numerical, must take into account the 3 following parts:

- Modeling of the soil

- Modeling of the pile

- Modeling of the soil-pile interaction

Choosing an appropriate soil constitutive model is a key element for good understanding and insight into the topic. Hereby a review of some models is presented. A choice is taken and the reasons supporting it are presented.

Soil model

We are going to deal with saturated sand, hence, two phases a solid matrix that is a cohesionless frictional material and the fluid (water) filling the pores; this two phase approach must be reflected in the model to provide useful information on the effective stresses and pore water pressures, especially the knowledge about these last ones is one of the main purposes of the research due to the fact that during pseudostatic loading large excess pore pressures are generated and they can affect the pile bearing capacity. Discrete models cannot provide insight into the phenomena, then we elect the *continuum theory*, waves propagate through the continuum as in reality, and we can introduce the mass and stiffness of the soil.

Hence, to obtain information about the pore pressures a saturated porous model is required

Biot (1956) proposed the first two phase continuum model as in the form of a solid skeleton and a fluid. From the Biot-type models, Aubry and Modaressi [24] evaluated the $(u_s - u_{rf})$ model and the $(u_s - p)$ model. They recommended the first one for higher frequencies but noted that the second one, which neglects the relative acceleration of the fluid, posed a cost-effective and simple but equally valid option. No more insight is given here about these models as they do not account for pile-soil interaction.

Pile model

The steel pile is as an elastic single-phase material

The elastic parameters needed (Young modulus, E, and Poisson's ratio, ν) are the characteristic ones of this material.

Soil-pile interaction model

However, the interesting topic is the interaction of pile and soil, and this is the approach that interests us the most. Different types of models are available, they are explained and discussed in the next section.

3.3.2 Soil-pile interaction models

Statnamic model: Unloading Point Method (UPM)

This one presented here is the only model that explicitly takes into consideration the pseudostatic character of the pile tests. The other models presented below are models for *dynamic* pile behavior or pile behavior in general.

Middendorp, Bermingham and Kuiper [4] performed series of tests with the so-called *statnamic* testing device, developed by TNO and Berminghammer. They corroborated that all pile parts move in the same direction with almost the same velocity, permitting to model the pile as a rigid body with simple forces acting on it:

- Statnamic load

- Inertia forces

- Soil resistance

The displacement dependent forces represent the static soil resistance and pore pressure resistance, the velocity dependent forces account for the soil damping and the acceleration dependent ones for the inertia. In fact, we have seen that it should be possible to model the pile and the soil that surrounds it as a single mass. We get more insight and understanding on the rough model presented above by proposing also a mode that physically reflects the forces (inertia and soil resistance) acting on the pile-soil mass M. This mass is then supported by a spring (stiffness, K) and a dashpot (damping coefficient, c) in parallel. The spring represents the force-displacement behavior under static loading (F_u) and the dashpot represents the velocity dependent viscous soil resistance (F_v).

This method, supported on the assumption of rigid pile behavior, and the consequent model have proved to be accurate and effective in approaching the static load-settlement curve. It works by determining a constant damping coefficient hat when multiplied by the velocity gives the viscous soil resistance that may be subtracted from the pseudostatic load to give the static one. The magnitude of this damping coefficient is obtained by first determining the static soil resistance at the unloading point. In this point, the peculiarity is that, although the pile's inertia is not zero (there is a displacement going on), the velocity and the damping are zero. Then, this static soil resistance together with the inertia is subtracted from the maximum measured pseudostatic load to determine the viscous component of the resistance. So we can summarize that the following assumptions are made:

- The pile is a rigid body

- The damping model is linear (c=constant)

- The soil is perfectly elastoplastic

- Inertia effects are only restricted to the pile

- Pore pressure effects are not considered
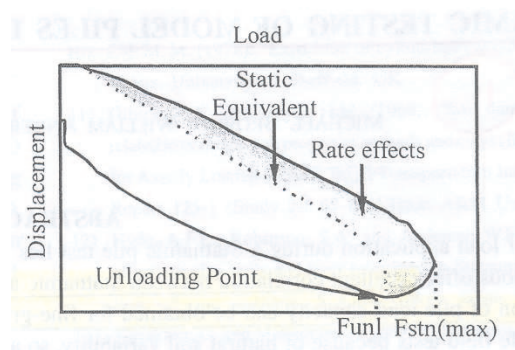
Figure 3.3: Statnamic results interpretation

Stress-wave theory

Pseudostatic is still a dynamic test, hence, stress-wave theory is applicable to its analysis. Stress-wave theory consists on the estimation of the pile static bearing capacity by the

stress-wave matching technique using a wave equation model.This has been proved to give reliable estimates of the pile static bearing capacity in a rapid and economical manner. The principle is as follows: either the force- or velocity-time trace at the pile head is used as a boundary condition, replacing the driving system, in a wave-equation analysis The soil resistance along the pile shaft and at the pile toe, together with the soil parameters used in the wave-equation model are adjusted with consideration for the mechanics of the stress-wave theory until another computer trace agrees closely with the measured one or no further improving can be made. When a reasonable match is achieved, the associated soil parameters are assumed to be the best fit the operator could obtain, close enough to the actual values, and then the mobilized soil static resistance is considered as the pile bearing capacity. Fellenius(1988) pointed out that the total static resistance computed will show little variation among different operators, but the distribution of this capacity between the shaft and the base may vary. In the case that some static data is available, Bruno and Randolph [25] recommend using it as initial input, then we will only need to perform some minor adjustments.

In this approach, the soil continuum is replaced by series of 'load-transfer' models distributed down the length of the pile and at the pile base (Randolph, Deeks [26]). The soil is split in layers and each layer is assumed to act independently from the neighboring ones. Some models available are presented below.

Smith-model

Smith (1960) presented a solution for the calculation of dynamic pile behavior. It is a 1D wave-equation model. His rheological model represents the total soil resistance to pile motion by a series of springs and dashpots whose constants are empirically determined from the back analysis of pile driving records an pile load tests. The total resistance comprises two components, a static component and a dynamic component. In his model he defined the soil quake as the maximum soil elastic deformation corresponding to the maximum soil strength and the *soil damping* as the effect related to the dynamic soil response. In particular, he considered linear viscous damping, with a damping constant proportional to the static portion of the soil resistance. The dashpot response is then:

$$R_t = R_s \left(1 + J_v\right) \tag{3.5}$$

where R_s is the static resistance (from the spring and the slider), v the velocity and J the damping coefficient.
Further on, Coyle and Gibson (1970) discussed that the increase in resistance with velocity may not be a linear relationship and presented a power-law relationship instead, but it ignored the effect of the acceleration.
However, Eiksund and Nordal [12] performed some dynamic pile testing and found that the resistance is almost independent of the velocity in the case of sand, so there should be no need for any viscous component in its modeling. This insinuates the little dynamical effect we may find in sand. For the static part they prefer a more curved relationship than the simple bilinear elastoplastic relation as it gives too low initial stiffness that must be then compensated by increasing the value of the damping constant.
Ealy and Justasson [27] performed some static and statnamic tests of a pile group in sand and concluded that possibly a strain-dependent model would fit better the reality, they observed that the damping constant dropped as the velocity or settlement increased.

Modified Smith model (Nguyen et al., 1988)

This model differs from the Smith one by the position of the plastic slider (see figure) and uses Lysmer spring and dashpot constants, found for a spring in parallel with a linear dashpot, which simulates the response of an elastic semi-infinite half space to an oscillating

circular rigid footing (Lysmer, Richart, 1966).

Nevertheless, different authors noted that Smith models are essentially empirical and the parameters proposed lack physical significance. This makes the interpretation procedure much cumbersome.
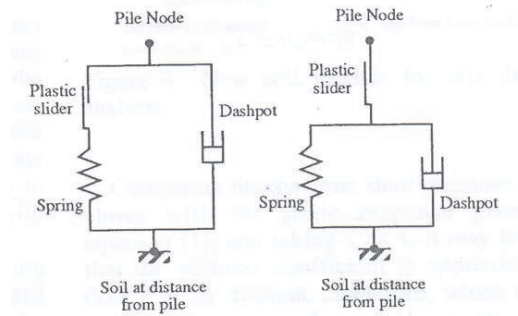
Figure 3.4: Smith model and modified Smiht model

Base model

Deeks (1992) proposed a model based on that of Wolf (1988) for the vibration of a circular rigid footing on the surface of a half-space. Wolf's model, however, was only valid for small dimensionless frequencies (Randolph, Deeks [26]). The author also showed that the model might be extended to inelastic behavior by incorporating the plastic slide in series with the spring and the dashpot.

Eventhough the improvement, it is still too rough to model accurately our problem and does not propose any solution for the pore pressure effects.

Shaft model

The energy delivered by the pile driving will mainly generate shear wave in the soil, leading to vertical accelerations, velocities and displacements into the soil.At some stage the pile will slip relative to the adjacent soil, leading to very high shear strain rates in a narrow slip zone close to the shaft, The above mentioned Smith models are unable to capture inertial damping due to outward energy propagation. This can be solved by including lumped masses and dashpots (Likins et al. [28]).

In contrapostition to the *statnamic* model by Middendorp et al. [4], the shaft model does not assume the pile to behave rigidly, on the contrary, it can be modeled as a flexible body. In this dynamic point of view, a one-dimensional model discretizes the pile and soil into elements (layers). In each layer, the soil is subdivided into a linear outer region and a non-linear inner region. The model allows to divide the soil into different layers along the shaft. Novak et al. (1978) considered the elastodynamic response of each soil layer and modeled it by a spring and a dashpot in parallel. By separating this elastodynamic response of the far-field soil from the slip zone close to the pile they introduced a degree of freedom. The motion of the soil adjacent to the pile shaft is traced independently from that of the pile to permit slippage at the soil-pile interface to take place. Outside the slippage zone, soil nonlinearity is accounted for by means of a reduction in the soil shear modulus of the inner region (also called weakened zone) and an increase in material damping.

El Naggar and Novak [8] adjusted the spring stiffness that represented the weakened zone
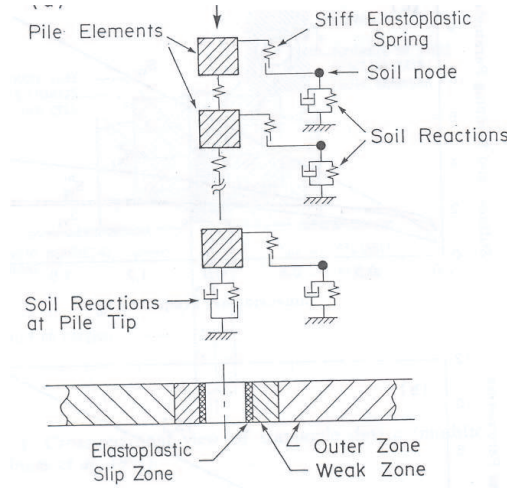
Figure 3.5: Shaft model

according to the stress level, following an hyperbolic stress-strain relationship (Kondner, 1963).

Rheology

- *Outer soil region*: The stiffness of the outer soil region is modeled using plane strain solution for an infinitely long mass cylinder that vibrates in an homogeneous half-space (Novak et al. 1978). A spring and a dashpot with frequency independent constants are used:

$$k_s = 2.75G \tag{3.6}$$

$$c_s = 2\pi r_0 \sqrt{G\rho_s} \tag{3.7}$$

where k_s is the spring stiffness, c_s the damping constant, r_0 the pile radius and ρ_s the mass density of the soil (El Naggar and Novak, 1994)

- *Inner soil region (weakened zone)*: The nonlinear behavior is confined into a region that extends from the outer pile surface (with r_0) to a certain fixed radius r_1. Stress-strain relationships can be used to model the soil nonlinearity, for instance as proposed by Kondner (1963):

$$\frac{\gamma}{\gamma_r} = \frac{\eta}{1 - \eta} \tag{3.8}$$

where $\eta = \tau/\tau_f$ with τ being the shear stress and τ_f the ultimate shear strength; γ is the shear deformation and $\gamma_r = \tau_f/G_s$ is the reference shear strain, with G_s being the maximum soil shear modulus.
We can therefore express the stiffness of the inner region:

$$K_{n1} = \frac{2\pi G_s}{\ln\left(\frac{r_1/r_0 - \eta_0}{1 - \eta_0}\right)} \tag{3.9}$$

where $\eta_0 = \tau_0/\tau_f$ in which $\tau_0 = \tau$ at $r = r_0$. This relationship shows that the stiffness decreases as the shear stress increases. When the shear stress reaches the ultimate soil strength, the soil behaves purely plastic and the stiffness disappears, leading the soil to constant resistance to pile movement. To consider the rate effects as well, the ultimate soil resistance should be expressed:

$$\tau_d = \tau_s \left[1 + \alpha \left(v_r/v_0\right)^\beta\right] \tag{3.10}$$

where τ_d is the dynamic shear strength of the soil, τ_s is the static one, v_r is the relative velocity pile-soil, $v_0 = 1m/s$ is the reference velocity, $\beta = 0.2$ and α ranges from 0 in the case of dry sand to 1 for clay.

There is a rigid plastic slider that connects the pile node and the inner field element. When the force in this slider exceeds the ultimate dynamic soil resistance, the slider disconnects and slippage occurs. During slippage soil resistance is not constant due to rate effects.

Stiffness in the unloading phase is supposed to be completely elastic ($\eta_0 = 0$). Another assumption is that the damping in this region is small, although it could be taken into account by means of adding a dashpot in parallel.

Hence, we may conclude:

  – Slip and plastic deformations are confined to the soil-pile interface, the spring and the dashpot representing the outer zone are always elastic.

  – Soil nonlinearity, associated with large displacements outside the slippage zone, is accounted for by the reduction of the soil shear modulus in this weakened zone and an increase in material damping.

- *Soil resistance at pile toe*: The soil before plastic yield is modeled by the reaction of an elstic half-space to a rigid massless circular disk undergoing harmonical vibration. Disk stiffness is assumed static, whereas the damping:

$$K_t = \frac{4Gr_0}{1 - \nu_s} \tag{3.11}$$

$$C_t = \frac{3.4r_0^2(G\rho_s)^{1/2}}{1 - \nu_s} \tag{3.12}$$

where K_t is the pile base stiffness, C_t is the pile damping coefficient and ν_s is the soil Poisson's ratio and ρ_s its density (for closed-end piles as it is our case).

- *Loading rate effects*: loading rate effects follow the Coyle and Gibson (1970) power law:

$$R_t = R_{st}(1 + J^*V^N) \tag{3.13}$$

where R_{st} is the static soil resistance, J^* is the rate-effect factor, V the penetration velocity and N an experimental exponent. El Naggar and Novak [8] elect $N = 0.5$ and $J^* = 0.1 - 0.15$ for sand, for the base of the pile only, as they assume that the rate-effects are negligible for the pile shaft. This expression can be rewritten as the limiting soil resistance, with V_r instead of V, representing the relative velocity pile-adjacent soil. Before this limiting value of resistance is reached, the soil and the pile have the same motion, this is ensured by linking the pile to the adjacent soil by a rate-dependent elastoplastic spring with elevated stiffness K_1. The force in this link is:

$$F_1 = K_1W_r(1 + J^*V_r^N) \tag{3.14}$$

where W_r is the real displacement pile-adjacent soil. K_1 should be high enough to guaranty that the pile-soil connection behaves as a rigid when $F_1 < R_t$.

- *Strain hardening and softening*: Once applying a shear stress into a sand we can reach and even excess its shear strength, leading to plastic behavior and unrecoverable deformations; reorganization of the granular package due to shearing may lead to strain hardening or softening, depending on the original density of the affected

material.This model introduces the post-peak factor to represent this soil stiffness variation during the unloading phase:

$$K_{nl} = \left[\frac{2\pi G_s}{\ln(r_1/r_0)} \right] R_p \tag{3.15}$$

  – Loose sand$\Rightarrow$ Hardening$\Rightarrow R_p = 1 - 2$
  – Dense sand$\Rightarrow$ Softening$\Rightarrow R_p = 0 - 1$

Calculations

- *Energy balance*:It consists in, analytically, perform an energy balance between input energy from the dynamic source and work done by the pile movement.

- *CASE method*: The motion of a stress-wave through an elastic rod in axial direction leads to an expression for the static capacity that introduces a Case damping coefficient and pile impedances (Rausche et al.,1985)

  These two calculation processes are cumbersome and usually require calibrations with static tests;they do not suit our requirements.

- *Signal-matching technique*: A numerical calculation seems the most feasible and trustful procedure, the main drawback is the fact that iteration is a time-consuming process.

Cavity expansion theory

This theory is a good tool to give us more insight into what happens as the pile penetrates the soil. There are four fundamental equations in cavity expansion (Collins, Yu [29]):

1. Conservation of mass

2. Quasistatic equilibrium

3. Yield condition

4. Elastoplastic flow rule

In undrained cavity expansion, like it is our case of interest, (1) is automatically satisfied since the total volume of soil element remains constant. Then (2) serves only to determine excess pore pressure distribution at the end of the calculation, after the effective stress distribution has been found integrating (3) and (4).

Cylindrical cavity expansion

The pile and the piezocone can be modeled as a cylinder that makes the soil surrounding it to open radially around it. While the pile is assumed to be linear elastic, the soil at its vicinity has been shown to behave largely inelastically. Mabsout, Sadek and Smayra [?] used it to model numerically the radial static displacement of the soil below the pile, to provide an opening equivalent to its penetration.

Spherical cavity expansion

Ladanyi(1961) suggested that the deformation bulb beneath the pile resembled a spherical cavity expanded in an infinite medium. Vesic(1973) developed the theory that made it

suitable for the prediction of end-bearing capacities of piles in sand, taking into account the compressibility and the failure envelope curvature the slope of the Mohr-Coulomb envelope in sands normally displays a curved shape (Yasufuku, Hyde [30])).

The pressure exerted at the boundary of the bulb of soil immediately beneath the pile tip is equal to the limit pressure required to expand a spherical cavity. Baligh (1976) and Bolton (1986) proposed different expressions for the shear of the soil, in function of the tangent of the secant, to be able to reproduce the curved shape of the envelope.
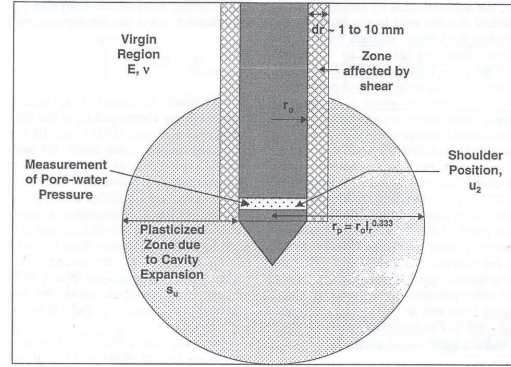
Figure 3.6: Spherical cavity expansion

Cone model and simple physical models

This models rely also on the stress-wave theory. However, they are interesting enough as to deserve an apart evaluation.[2]

Wolf presented the use of *simple physical models* to represent the soil under dynamic conditions. They may lead to some loss of precision, when compared to *rigorous models* but they have other advantages, for instance, lower budget, lower computational costs and less time required. This kind of models are a major step towards developing a *strength-of-materials approach to foundation dynamics*.The physical models proposed are:

1. CONES: Translational and rotational trucanted semi-infinite single and double cones to represent soil half- and full-space are based on rod (bar) theory, plane deformations remain plane, with 1-D displacements.

2. LUMPED-PARAMETER MODELS: Consists in representing the soil with a series of springs, dashpots and masses with frequency-independent coefficients. These models can be conceptually constructed from cones by assembling their exact discrete-element models in parallel and by calibrating with rigorous solutions.

3. PRESCRIBED WAVE PATTERNS IN HORIZONTAL PLANE: One-dimensional body and surface waves on the free surface and cylindrical waves.

In general, they fulfill the next requirements:

- Conceptual clarity and physical insight

- Simple physical description

- Sufficient scope of application

---

[2]Theory of cone model extracted from Wolf [31], [32], [33], [34] and Meek and Wolf's [35], [36], [37], [38] works.

- Sufficient accuracy

- Appropriate to explain the physical phenomena

- Direct use in engineering practice

- Possibility to generalize the concepts, directly linking them to the more rigorous solutions

The cone model for translational motion was postulated half a century ago by Ehlers and Meek and Veletsos extended the idea to the cone for rotational motion some 20 years ago. As introduced before, it is important to know that cones are dynamically equivalent to an interconnection of a small number of masses, springs and dashpots with frequency-independent coefficients.However, researchers have had reservations against the cone models for mainly three reasons:

1. They are based on strength-of-materials and not on the rigorous theory of the elastic half-space

2. The portion of the half-space outside the cone is neglected

3. They cannot represent the influence of Rayleigh waves.

Meek and Wolf [36] proved those prejudices to be unfounded. They verified the correctness of some aspects of the cones by means of the rigorous Boussinesq results for the half-space:

1. For low-frequency motion the equivalent vertical damping is finite, but the equivalent rocking starts from zero.

2. The apex of the cone is located above the surface of the soil.

3. The radius of the cone increases linearly with depth.

4. The assumption that plane sections remain plane is approximately valid.

5. The cones are doubly asymptotic solutions, correct for very high and very low frequencies too.

The authors also proved that it is physically correct to assume that the region of the soil half-space outside the cone is essentially inactive and can be neglected. They also found that the proportions of the cones are compatible with the proper wave-propagation velocities in the horizontal direction.

Finally, they demonstrated that no Rayleigh waves exist in the portion of the half-space occupied by the cones in the case of low-frequency excitation and that, for high-frequency excitation, the energy transmitted by the Rayleigh waves is negligible.

It has been enumerated why cone models can represent the soil half-space. No more detail is given in this report about these demonstrations, the reader is referred to the literature.

Disk on the surface of a half-space

The simplest case is that of a disk resting on the surface of a homogeneous soil half-space. As first approximation, the soil is idealized to be a semi-infinite elastic cone with apex height z_0. Depending on the nature of the deformation, there are two types of cones available:

1. TRANSLATIONAL CONE for vertical and horizontal motion

2. ROTATIONAL CONE for rocking and torsional motion
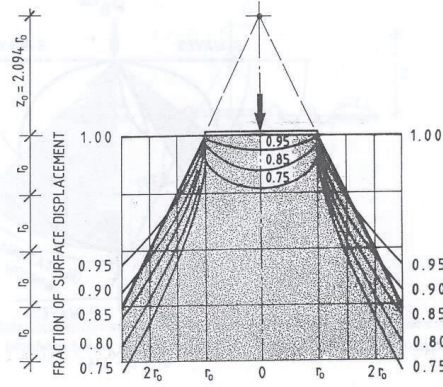
Figure 3.7: Ratio of underground vertical displacements to surface vertical displacements for statically loaded rigid disk on half-space with $\nu = 0.3$
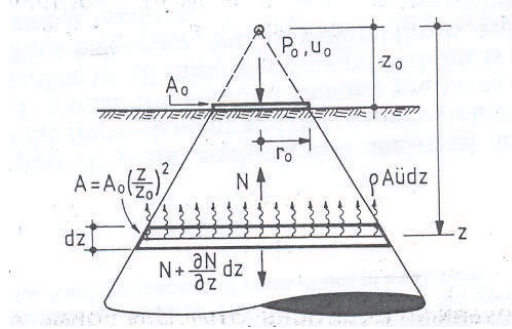
Figure 3.8: Translational cone

In the first approach the soil is considered to be an unlayered linearly elastic semi-infinite medium and no material damping is considered in the beginning. In cone theory, the two defining properties needed for this soil are the propagation velocities of shear waves c_s and of dilatational waves c_p. In our case of cone in vertical motion, axial deformation, the wave velocity to use is c_p. This feature makes the vertical cones to be slender ($z_o/r_0 > 1$) whereas horizontal cones, with predominance of shear waves are squatty ($z_o/r_0 < 1$). When working with a compressional cone, the dilatational velocity c_p should never be taken greater than $2,264c_s$, otherwise the radiation damping would be overestimated. Some authors prefer using in this case the Lysmer apparent velocity:

$$c_{La} = \frac{3.4c_s}{\pi(1-\nu)} \tag{3.16}$$

In the case of saturated sand, it is almost incompressible ($\nu = 0.5$) due to the hight incompressibility of the water filling the pores. Then $c_{La} = 2.165c_s$. Wolf also proposed to use $2c_s$ instead of c_p. Another consideration for nearly incompressible soil to take into account is that a trapped mass ΔM is assigned to the basemat (and thus, we should also add it to the governing equations, hereby presented without including it).
The aspect ratio determining the opening angle follows from equating the static-stiffness coefficient of the cone to that of the disk on a half-space. For a translational cone:

$$K = \rho c^2 A_0 / z_0 \tag{3.17}$$

and for the disk:

$$K_v = \frac{4Gr_0}{1 - \nu} \tag{3.18}$$

This results, for vertical motion cone, in:

$$\frac{z_0}{r_0} = \frac{\pi}{4}(1 - \nu)(\frac{c}{c_s})^2 \tag{3.19}$$

The dynamic equilibrium of the translational cone:

$$\frac{\partial N}{\partial z} = \rho A \ddot{u} \tag{3.20}$$

Substituting the relationships: $A = A_0(z/z_0)^2$ where A_0 is the area of the disk and $N = \rho c^2 A \partial u / \partial z$ we get the governing differential equation of motion:

$$\frac{\partial^2 u}{\partial z^2} + \frac{2}{z}\frac{\partial u}{\partial z} = \frac{\ddot{u}}{c^2} \tag{3.21}$$

z is the depth below the apex and u the displacement. There are two possible ways to solve the equation of motion:

- *Stiffness formulation*: displacements are regarded as an input and the corresponding force is the output.The result has the shape of:

$$P_0 = Ku_0 + C\dot{u}_0 \tag{3.22}$$

  in which $K = \rho c^2 A_0 / z_0$ and $C = \rho c A_0$ may be interpreted as an ordinary spring and an ordinary dashpot. The values of the constants are dependent on the apex height (i.e. cone geometry), making the static stiffness of the cone equal to that of the half-space.

- *Flexibility formulation*: the roles of input and output are reversed: forces are regarded as the input and displacements are the output. The fundamental solution for this case is the displacement due to a Delta-dirac impulse (normalized force P_0/K). Noting $h(t)$ this Delta-dirac response, it turns out to be a simple exponential function:

$$h_1(t) = \begin{cases} \frac{c}{z_0}e^{-ct/z_0} & \text{for } t \geq 0 \\ 0 & \text{for } t < 0 \end{cases}$$

Formally, the flexibility formulation expresses the resulting displacement as convolutions (Duhamel's integrals) of force with an impulse h_1:

$$u_0(t) = h_1 * \frac{P_0}{K} = \int_0^t h_1(t - \tau)\frac{P_0(\tau)}{K}d\tau \tag{3.23}$$

It is computationally inefficient to perform convolution directly by the numerical quadrature of Duhamel's integral. A more desirable method is the use of recursion formulas, but it falls beyond the scope of this thesis.

If we would like to consider material damping too, this should be introduced in the frequency domain based on the correspondence principle applied to the elastic solution.

Disk on surface of soil layer on rigid rock

A step further on the complexity of the cone model and towards a more precise representation of the experimental test-set up: the disk is not resting on the surface of a half-space anymore but instead it lays on the free surface of a soil layer with a rigid rock in its bottom. In this case, the *layered cone* needs to be introduced. In addition to the decay

in amplitudes as the wave propagates, the layered cone includes reflections at rock inter-
face and on the free surface, the so-called *echo constants*. The original dilatational wave
propagating downwards form the disk is named *incident wave* and it propagates along the
same cone as in the half-space.

No more detail on this case is provided as in our tests we can neglect this bottom rigid
boundary because the ratio pile diameter-to-depth excess the required margin to avoid
boundary effects.

Embedded disk

Wolf demonstrated that it is not possible to extend the concept of a single truncated
semi-infinite cone to an embedded foundation, it gives poor results. When the disk is not
resting on the surface but embedded, it shall be represented by a *double-cone model* within
the elastic fullspace. The aspect ratio z_0/r_0 which determines the opening angle also results
from equating the static-stiffness coefficient to that of the disk on a half-space. The only
difference is that now the static-stiffness coefficient K is doubled; thus, by symmetry the
applied load is resisted half in tension (upper cone) and half in compression (lower cone).
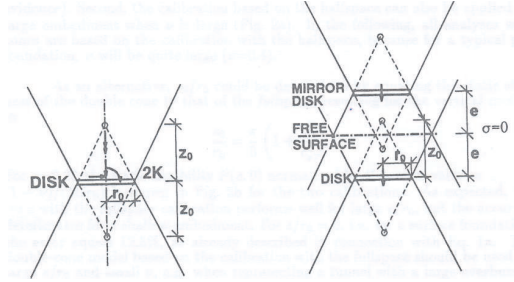
Figure 3.9: Double cone:(a)Disk embedded in fullspace, (b)Disk embedded in halfspace
with antisymmetry

The displacement field defines approximate Green's functions for use in a matrix formu-
lation of structural mechanics. The Green function applies in time domain, hence, giving
the displacement at a receiver point located at a distance a from the source disk, which is
excited at $t = 0$ by a unit-impulse force.

$$g(a, t - \frac{a}{c}) = \frac{1}{2K} \frac{1}{1 + \frac{a}{z_0}} h_1(t - \frac{a}{c}) \tag{3.24}$$

with the unit-impulse response function:

$$h_1(t) = \begin{cases} \frac{c}{z_0} e^{-ct/z_0} & \text{for } t \geq 0 \\ 0 & \text{for } t < 0 \end{cases}$$

For the case of large embedment depth, some times larger than the disk radius, the double-
cone model for the vertical degree of freedom seems to be too flexible at large distances
from the loaded disk. In this case, the Green's function needs to be modified and be equal
to the weightened Green's function of the double cone and that of the fullspace for a point
load:

$$g(a, \omega) = w(a)g_{cone}(a, \omega) + (1 - w(a))g_{fullspace}(a, \omega) \tag{3.25}$$

The frequency-domain expressions can be found in the literature. It is convenient to ana-
lyze the embedded foundations in frequency-domain.

Pile foundation

Its dynamic analysis is analogous to that of the embedded foundation. We consider an embedded disk of the same radius as the pile, with its correspondent double-cone model. The same Green's functions in time domain apply for this case. The soil region within the pile is modeled as a sandwich of m disks which will later be analytically excavated and replaced by pile material, where m must be chosen large enough that the slice thickness $\Delta e = e/(m-1)$ does not exceed about one sixth of the shortest wavelength of the vertically propagating waves. Standard matrix methods of structural analysis can then be used to develop the stiffness- and flexibility-formulations in time and frequency domain.

Conclusion

Although several of the most relevant models for pile analysis have been reviewed *none* of them accounts *explicitly* for excess pore pressure generation and effects.

3.3.3   Pore pressure and consolidation models

As said previously, there is a gap in the literature when searching for pile models that include excess pore pressure generation and the consolidation in sands. Hereby, some works on clay will be introduced.

Excess pore pressure generation

There are two approaches widely used in the literature for predicting excess pore pressures when a pile is driven in clay, namely (a) the strain-path method (Baligh, 1985, 1986), and (b) the analogy of cavity expansion, which Gibson and Anderson extrapolated to excess pore pressure generation in 1961. Both methods quantify stress changes due to pile installation and these stress changes can be related to water pressures. Although Randolph [1] concluded that Baligh's strain path method provided more realistic and detailed predictions for the immediate vicinity of the pile, if the few diameters close to the pile tip are ignored, comparison of the two approaches shows that radial displacement fields are extremely similar. In fact, in the literature mostly cavity expansion is used.

Gibson and Anderson (1961) applied simple cavity expansion to an elastic, perfectly plastic soil with shear modulus G and undrained shear strength s_u and obtained the following excess pore pressure distribution:

$$\frac{\bar{u}}{s_u} = \ln(\frac{\rho G}{s_u}) - 2\ln(\frac{r}{r_{pile}}) \tag{3.26}$$

This expression, though, does no account for changes in mean effective stress as the soil is sheared and remoulded, which may be a significant factor together with increases in mean total stress due to 'outward' expansion of the soil to accommodate the pile.

Burns and Mayne [39] controlled and calculated analytically the monotonic and dilatory pore-pressure decay during piezocone tests in clay. First they needed to calculate the excess pore pressures generated. They developed a model based on the premise that the excess pore pressures which generate during penetration are due to changes in both normal and shear stresses. They used cavity expansion to represent the octahedral normal component of the excess pore pressure in combination with Modified Cam-Clay to quantify the shear-induced component. The equations where those derived by Torstensson [40] for the case of cone penetration testing:

$$\bar{u} = \frac{4}{3}s_u \ln(\frac{G}{s_u}) \tag{3.27}$$

for the case of a spherical cavity. And,

$$\bar{u} = s_u \ln(\frac{G}{s_u}) \tag{3.28}$$

for a cylindrical one. The initial magnitude of induced excess pore pressures was calculated using spherical cavity expansion, despite noting that the zone around a shoulder position filter in a piezocone is neither fully spherical nor fully cylindrical, but instead represents a transition between those two.

Randolph and Wroth [41] derived an analytical solution for the consolidation around a driven pile in clay. Once more, the first step was to derive the initial excess pore pressure distribution. They the expansion of a cylindrical cavity from zero radius to that of the pile to model the installation. Considering an elastic perfectly plastic material, they calculated the stress changes and the extent of the plastic zone. Assuming that, in undrained conditions the mean effective stress remains constant, the excess pore pressures were equal to the change in total mean stress:

$$\bar{u} = \frac{1}{3}(\delta\sigma_r + \delta\sigma_\theta + \delta\sigma_z) = \frac{1}{2}(\delta\sigma_r + \delta\sigma_\theta) = s_u[\ln(G/s_u) - 2\ln(r/r_0)] \tag{3.29}$$

Outside the plastic zone the excess pore pressures in the model were zero.

Also Rocha Filho [42] derived a similar expression by means of spherical cavity expansion combined with Skempton (1954) theory:

$$\frac{\bar{u}}{s_u} = \frac{4}{3}[\ln(\frac{E}{3s_u}) + 1] + 2A - 0,7 \tag{3.30}$$

where A is the pore water pressure defined by Skempton.

Consolidation

The same studies that computed the generation of excess pore pressures continued evaluating the dissipation of those, thus, the consolidation. As pore pressures dissipate, soil increases strength and there will be a increase in pile capacity, hence, it is a key concept to evaluate. Axisymmetric consolidation is a classical boundary problem in Geotechnics. Under some circumstances an analysis in which the changes in pore pressure, effective stress and displacement can be uncoupled from each other is sufficient, leading to a Terzaghi formulation of the axisymmetric consolidation equation in terms of pore pressure. The representation of the Mandel-Cryer effect -that is, sudden increase in pore pressure just after the start of the consolidation, followed by the usual dissipation- usually requires more complex, coupled, Biot formulations (J.D. McKinley [43]).

Mostly researchers have used the Terzaghi-type of formulation. Burns and Mayne [39] include in their report about pore pressure decay during piezocone tests in clay an interesting table about the historical development of piezocone dissipation modeling, modified after Lunne (1997) and Jamiolkowski (1995). They noted that because the volume affected by the mormal stress is much larger than the one affected by the shear stress, the dissipation of shear-induced pressures will occur more rapidly than that of the normal-induced pore pressures. Their model relied on an analytical solution to the radial consolidation equation. Evidence suggests that radial drainage most strongly governs consolidation in pile driving (Bjerrum and Johanessen, 1961, Koizumi and Ito, 1967, Randolph and Wroth, 1979).

$$\frac{\partial u}{\partial t} = c_h \frac{\partial^2 u}{\partial r^2} + \frac{c_h}{r} \frac{\partial u}{\partial r} \tag{3.31}$$

where c_h is the horizontal coefficient of consolidation, u is the pore pressure, r is the radius, and t is the time. This equation must best be solved by numerical methods. The initial distribution of excess pore pressures within the plastic zone was used as the initial condition to solve the one-dimensional, uncoupled partial differential equation for radial drainage. While they had used spherical cavity expansion for the generation of the initial excess pore pressures, the cylindrical one was chosen for the dissipation. The boundary conditions assumed that there was no increase in excess pore pressure outside the plastic zone ($\Delta u = 0$) and that the cone body was an impermeable boundary. With this the problem was defined and they run the numerical program iteratively for values of c_h until a good fit with experimental results was attained.

Of special interest is the work of Randolph and Wroth [41] on the consolidation around a driven pile. Again they noted that the major pore pressure gradients are radial. They derived the following equation:

$$\frac{\partial u}{\partial t} = c[\frac{1}{r}\frac{\partial}{\partial r}(r\frac{\partial u}{\partial r})] + g(t) = c\nabla^2 u + g(t) \tag{3.32}$$

where:

$$c = \frac{k}{\gamma_w}\frac{2G(1-\nu)}{(1-2\nu)} \tag{3.33}$$

Apart from the integration constant $g(t)$, which depends on the boundary conditions, the equation is identical to Terzaghi's. The same boundary conditions of no excess pore pressure at the limit plastic-elastic and impermeability of the pile ($\partial u/\partial r = 0$ at $r = r_0$) were used. The initial excess pore pressures distribution was the input initial condition. The equation was solved by means of separation of variables and Bessel functions, achieving:

$$u = \sum_{n=1}^{\infty} B_n \exp^{-\alpha_n^2 t} C_0(\lambda_n r) \tag{3.34}$$

where the coefficients B_n depend on the initial condition and may be obtained integrating:

$$\int_{r_{pile}}^{r_{plastic}} u_0 r C_0(\lambda_n r) dr = \frac{B_n}{2}[r^{plastic2}C_1^2(\lambda_n r^{pile}) - r_{pile}^2 C_0^2(\lambda_n r_{pile})] \tag{3.35}$$

where $C_i(\lambda r)$ are cylinder functions of ith order, linear combination of: $J_i(\lambda r) + \mu Y_i(\lambda r)$, being J_i Bessel functions of first kind and Y_i Bessel functions of second kind. Once more, the solution was evaluated by means of numerical algorithms.

Imre, Rosza [44] modelled the consolidation around a pile tip. Their problem was, though, more complicated as entailed bidimensional consolidation:

$$-c\frac{\partial}{\partial r}\frac{1}{r}\frac{\partial}{\partial r}(r\frac{\partial u}{\partial r}) + \frac{\partial^2 u}{\partial t \partial y} = 0 \tag{3.36}$$

where c is the consolidation coefficient. Once more with the same boundary conditions of no pore pressure at the plastic limit and zero flux at the pile (impermeability), they added an extra one because of the higher degree of the equation, no flux at the plastic limit. The solution obtained, which is not detailed here, consisted of a linear combination of sine and cosine functions whose amplitude decayed with some negative power of r.

Conclusion

The most extended approach to the problem of generation and dissipation of excess pore pressures is that of cavity expansion in spite of strain path, which gives better results but is cumbersome. For clay, fully undrained loading is assumed and then the mean

total stress change is related to the excess pore pressures. Authors coincide in localizing the generation of water pressures in the plastified zone. The consolidation problem is of crucial importance and mainly solved uncoupled for the radial case, for experimentally the gradients are more important in the radial direction. Although 2-D would be more suitable, this is very complicated to calculate and certainly requires of numerical methods. Even the radial equation need of computer programs and Bessel functions to be calculated, thus it is not trivial. The boundary conditions of impermeability at the pile and zero pressure at the plastic limit are the most extended.

3.3.4 Conclusion

Shortcoming of the available literature and related studies

Problem: There is a gap in the literature when it comes to analytical modeling of pseudostatic tests in saturated sand, thus, accounting for the generation and dissipation of excess pore pressures.

Most models either assume penetration in sand is fully drained or, when considering undrained behavior, it always relates to clay. No modeling of undrained sand response has been carried out yet, therefore, no insight into the response of saturated sand under fast (pseudostatic or dynamic) penetration has been acquainted for. The only model explicitly pseudostatic, the UPM method, does not consider the presence of water. One of the main objectives of this research is then to choose and adapt one of the available models to the case.

Evaluation and proposal

There are static and dynamic models available. Dynamic theories have been developed for elasticity. Excess pore pressure generation is, however, related to volumetric strain and plastic deformation. This means that the soil must certainly be modeled as an elastoplastic material. Combining plasticity with dynamics is far more complicated than this thesis allows for. Consequently, the analytical model will be under static loading. This hypothesis should not be so incorrect as the thesis involves pseudostatic tests; precisely, the direct correlation with static results is the most powerful feature of this kind of tests, thus, stress-wave theory should be possibly neglected. Still, it could be possible to intrinsically introduce some somehow 'dynamic' portion. For instance, the cone geometry of Wolf [31], [32], [33], [34], which was defined due to the wave propagation patterns, can be used as input model geometry, while keeping the calculations static. If the results of the static model were not satisfactory, indicating that dynamic calculations are necessary, the analytical model could be easier modified to account for that.

Cavity expansion is the most extended model for pile penetration and supposes elastoplasticity but it's fully static. Although Verruijt [45] developed a dynamic solution for cavity expansion, once more the solution is only elastic. Also static cavity expansion could be an option for a first contact. Nevertheless, Wolf's cone would account for some dynamic behavior, even if it were only in its definition, thus it seems an interesting choice. Cavity expansion has been used for estimating pore pressures, but only in clay. No parallel formulas are yet available for sand, so the ones of clay could be extrapolated or looking back at the theory of cavity expansion for granular materials, the stress variations could be deduced and related to excess pore pressures. Anyway, the power of cavity expansion, that was its widespread application, is weakened if one needs to modify and extrapolate the previous related studies.

> **Proposal**:Not being able to find a fully satisfying solution, the analytical model will be derived from an adaptation for the Wolf theory.

Besides, as the objectives point towards the pore pressures and these will mainly be generated from compression at the pile tip, focusing in this area only seems appropriate. The excess pore pressures will be calculated following the premises of Randolph and Wroth [41], using the same concepts: for undrained case, excess pore pressures are only generate in the plastic zone and are due to mean total stress changes. Also for the consolidation, similar boundary conditions will be applied and the generated pore pressure distributions will be used as initial condition too (see chapter 9).

The coming chapters will describe and calculated this model, a static and elastoplastic adaptation of Wolf [31], [32], [33], [34] cone model with generation and dissipation of excess pore pressures based on Randolph and Wroth [41] model.

MODEL		Reasons for its possible suitability	Reasons for its refusal	CHOICE
1.Statnamic model (UPM)		-It was especifically conceived to model pseudostatic tests	-Explicitly neglects excess pore pressure generation	-NOT appropriate
2. Stress wave theory	2.1.Smith	-Pseudostatic test is still a dynamic one→stress-wave theory is applicable	-Parameters lack physical significance -Doesn't include excess pore pressures	-NOT appropriate
	2.2.Nguyen		-Parameters lack physical significance -Doesn't include excess pore pressures	-NOT appropriate
	2.3.Base		-Doesn't include excess pore pressures, difficult to include	-NOT appropriate
	2.4.Shaft		-Doesn't include excess pore pressures, maybe could be included, but the calculation would be too complicated	-NOT appropriate
3. Cavity expansion	3.1. Cylindrical	-It is a very good model, widely used in literature, to represent pile penetration -Has been used to evaluate excess pore pressures in clay	-Represents pile shaft, not suitable for zone beneath the tip -Difficult application dynamics	-NOT appropriate
	3.2. Spherical		-Difficult application dynamics	-Could be a good option but:previously only used in clay→extrapolate to sand? -NOT preferred
4. Cone model (Wolf)		-Can be assimilated to a simple rheological model→Physical significance -Simple and accurate -Flexible, offers the possibility to manipulation -Intrinsecally accounts for some dynamic effects (p.e. geometry), even if not explicited in the calculation	-NOT yet been used to predict excess pore pressure→but can be adapted! -Only zone under pile tip→OK if interested in excess pore pressure prediction (compression)	-PREFERRED CHOICE

NOTE: There is NO model that completely fullfills our requirements, namely:
Explicitly predict generation of excess pore pressures generated in saturated sand due to pseudostatic loading. Then:

The CONE model of Wolf will be adapted

Figure 3.10: Available analytical models evaluation

Part I

Experimental testing

Chapter 4

Test set-up and regime

4.1 Introduction

The experimental research is focused to determine the effect of excess pore water pressures generated during pseudostatic loading in the pile bearing capacity. To get a reliable experimental answer to the topic, a series of tests in *fully saturated sand* have been performed in the Geotechniek Laboratory of TU Delft. The chosen model is the calibration chamber one, previously used by Broere [16]. The test-set up was designed by J. Dijkstra [5] as part of his master thesis on evaluation of loading rate-effects in pseudostatic loading of piles embedded in unsaturated sand. Therefore, for the results of this research to be comparable with Dijkstra's ones (comparison of dry and saturated situation) the same testing equipment is used. If any differences with his procedure, those will be explained and justified in the following sections.

4.2 The calibration chamber

The experimental tests are performed in a *calibration chamber*, that approximately represents the in-situ case at a scale 1:10. As presented on the literature study, calibration chambers have been widely used over the years to correlate between soil properties and cone resistance. Therefore, the soil properties are regarded as a known input, good insight and reliable data about the soil sample should be obtained. However, though many aspects of the soil sample in the calibration chamber tests can be controlled, the test set-up itself strongly influences the results. Parkin [17] studied the influence parameters on calibration chamber testing and concluded that, part from the preparation method of the sample, the boundary conditions are influential. The different chamber types based on the boundary conditions have been previously presented, as well as the fact that the extent to which the boundaries may effect the measurements depends mainly on the ratio diameter of the chamber-to-diameter of the cone. The placement of the tests in the chamber has been elected in order to neglect those effects.

The calibration chamber at Geotechniek is the same as previously used by Broere [16] and Dijkstra [5]. Consists in a 1.9m diameter rigid wall tank as shown in the plot. The total depth is of 3.23 m and of these, 2.5m approximately (depends on each vibration time, hence, sample density) are filled with sand. At the bottom of the chamber there are a certain number of drains embedded in a filter bed and connected to a pumping installation, they are used to saturate the sand bed from below and fluidize the sand.
  After the sand bed is fluidized, while the water table is higher than the sand top level, two vibrators fixed at the tank walls are used to vibrate the sand while draining water to a fixed phreatic level chosen 30cm below the surface of the sand to guaranty the fully
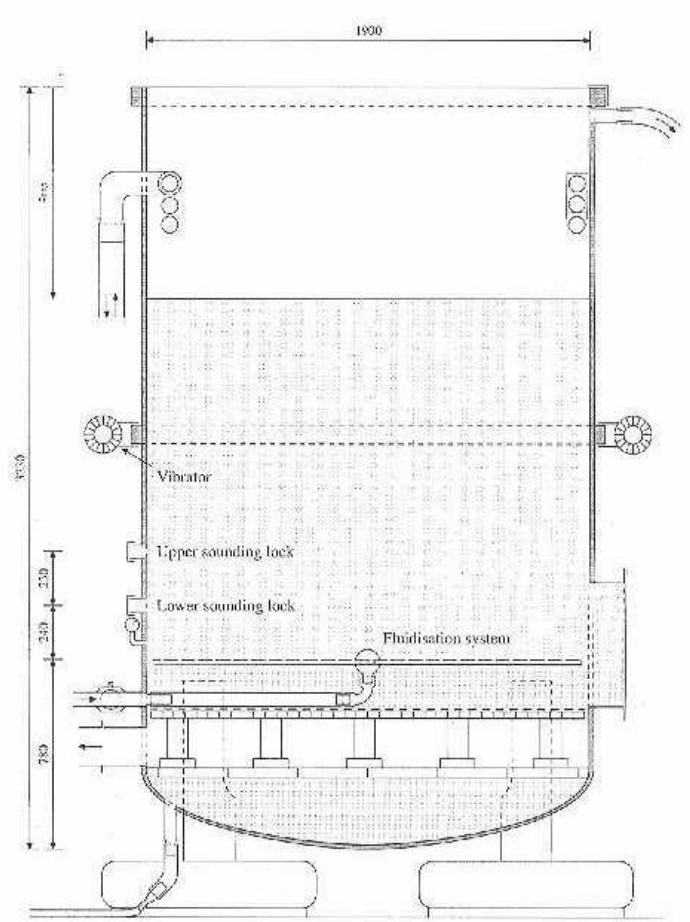
Figure 4.1: Calibration chamber

saturation of the pile tip area. In coming sections the sample preparation is described in more detail.

It can be seen that this calibration chamber does not fit in one of the groups defined by Parkin [17]. instead, it lies somewhere between type BC2 and BC3; it has rigid walls and rigid bottom and the top is a free surface which has not been loaded in any of the tests. The fact that it is a rigid wall calibration chamber makes it special in comparison to most of the calibration chambers used in general research. The boundary effect induced by the rigid walls is larger than for flexible walls, the chamber diameter-to-cone diameter ratio should exceed 56 for those to be negligible.

4.3 The sand

4.3.1 Sand properties

The sand is the same as Dijkstra [5] used and it was already in the calibration chamber. Although in the tank preparation testing normally sand is regarded as an homogeneous sample with reliable knowledge of its properties, some unknown sand was added to the original used by Broere [16]. Therefore, it is important to keep in mid that it is probably

not an homogeneous samples and that the input properties are not fully known. A sieve analysis to get a general idea was carried out and the results are hereby presented. It can be qualified as a moderately coarse sand. More detailed properties cannot be obtained with confidence due to the inhomogeneity of the sample, standard values that agree with the type of soil determined by the granulometric curve will be used when needed.
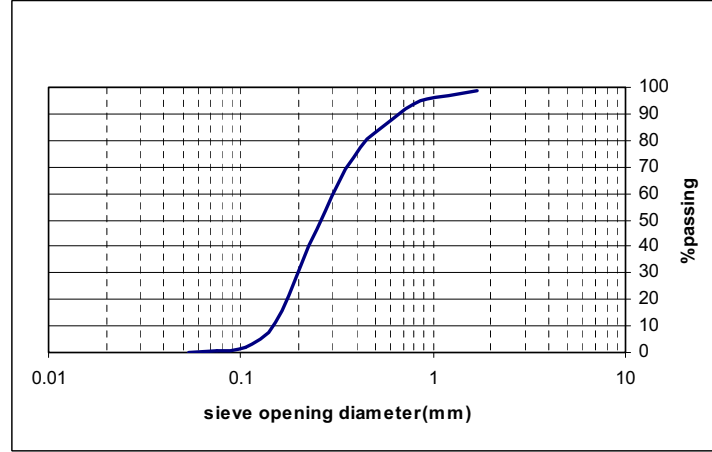
Figure 4.2: Granulometric curve

Some characteristic soil definitions:

- Characteristic soil effective size: $D_{10} = 0.135mm$

- Coefficient of uniformity: $C_u = \frac{D_{60}}{D_{10}} = 2.22$

- Coefficient of concavity: $C_c = \frac{D^2 - 30}{D_{10}D_{60}} = 0.89$

4.3.2   Preparation of the soil

Within each test series the sand used is the same only the density, i.e. preparation, changes.Calibration chamber samples have been normally prepared by means of the pluviation method by most researchers worldwide. This is not the one used in this research: the preparation consists in fluidizing the sand during 1,5h and then vibrating it. Introducing variations in the vibration time, the density of the sample can be changed. Logically, longer vibration periods will produce denser packages than shorter ones. Mainly three different vibration times have been used: 5, 10 and 15 min. To complete the density range, also tests in non-vibrated sand and 30 min vibrated sand have been performed. Broere [16] carried out some experiments in the same tank and listed a relationship vibration time-relative density. The sand he used is still in the tank but some more was added before this thesis started and with no knowledge of its nature. Comparing the sieve curves for his and our sand it can be concluded that they are really similar, the sand added after Broere must have been of a similar kind. Thus, Broere's table can be used, if not to get the exact value of density, yes to get an idea.
The procedure to prepare the samples can be schematized in 3 steps:

1. Fluidization: 1,5h.

2. Vibration:0, 5, 10, 15 and 30 min. Changes in vibration time change the density of the sample.While vibrating the sand is kept under water, making the process more effective.

3. Drainage: Phreatic level is set at 30 cm below the surface.

However, this sample preparation procedure introduces some problems but, on the other hand, requires less time and manpower to prepare the soil. The main handicaps introduced by this method are:

- Leads to less uniformly densified samples. Broere noted that this density variations may be responsible for uncertainty in relative density of 10% or less.

- There are vertical deviations in stratification after each tank preparation

4.4 Overview of the test series

4.4.1 Test regime

The 'piles' used in the research are standard sounding rots of 3.33cm of diameter and 1,2m long each. They are pushed into the soil with a sounding device at a standard CPT speed to reach a depth of 60 cm below the surface,then the properly called tests are started.
It has been pointed out above that the test regime is the same one as used by Dijkstra [5] owing to the fact that one of the purposes of this research is to compare dry and saturated tests in order to quantify the effects induced by the pore pressures. This regime was designed to reproduce different loading rates, mainly, static and pseudostatic. A total of 3 different loading rates, corresponding to different test types, are used. Each test series consists of 4 tests of 3 different types:

1. CPT (installation test)

2. Static 1

3. Pseudostatic

4. Static 2

In total, 6 quantities are measured:

1. Tip resistance

2. Shaft friction

3. Pile acceleration (only pseudostatic)

4. Displacement (only static and pseudostatic)

5. Force on the pile head

6. Pore pressures$\Rightarrow$ Note:we are measuring total pore pressures, this is to say, hydrostatic plus excess pore pressures. For the analysis we will have to subtract the hydrostatic value to the measured one, to see how much water pressure the pseudostatic test generates.

Two static tests, before and after the pseudostatic are carried out. The purpose is to evaluate the changes in the soil that have been generated because of the pseudostatic test.

Hereby these tests are described:

CPT

Consists on the installation of the pile at a certain depth (60cm) into the soil, hence, it is a strain controlled test. It is performed with a standard sounding machine, thus, the velocity can be also perfectly controlled and kept constant at 20mm/s.

Static tests

The proper static test would consist in charging the pile top 2 or 3 times its bearing capacity really slowly, taking the test more than 1 day. Static tests are expensive in both economical and temporal terms, for this Dijkstra [5] designed a mechanism to reproduce the static loading. He carried out the test with the same sounding device but keeping it under a very low loading rate of 1mm/s. The main drawback of this way to proceed is that the test and the velocity are controlled manually, making it almost impossible to assure a constant and really low loading velocity. Again it is a strain controlled test: only 2cm axial displacement are allowed, then the test is stopped.

Pseudostatic test

Commercially, pseudostatic tests are performed with the *STATNAMIC* device. Here the pseudostatic loading rates are reproduced (as large as 250mm/s). Consists on dropping a known mass (63.9 kg) with 6 springs (in total 69 kg) on the pile head. A protection cap is placed on top of the pile to avoid damage. The dropping takes place into a steel tube to maintain the loading axially and prevent the generation of bending stresses. The falling height is of 30 cm, thus the initial velocity is 2.4 m/s. Contrarily to the static and CPT tests, this is a stress controlled test. The pile acts statically (this is one of the key assumptions of the pseudostatic tests) but there is no reason to expect the soil to act statically. This will be discussed in the result evaluation.

4.4.2 Equipment

Loading mechanism

The different loading mechanisms and loading rates were presented in the test descriptions. To sum up, there are two different mechanisms used, one for (a) CPT and static tests and one for (b) pseudostatic tests.

- **Hydraulic actuator**: Constant rate penetration test equipment. Consists in a loading frame fixed to two beams that provide the reaction force when the actuator pushed the pile into the soil. Two level arms control the speed of the penetration, one for the standard CPT velocity ($20mm/s$) and a slower one.

- **Pseudostatic loading**: Dijkstra designed as system composed of [1]:drop mass, aluminum guiding tube, springs and trigger bar. The aluminum tube is meant to guide the dropping mass when falling towards the pile head. The trigger consisted in an aluminum bar and an aluminum rod to hold the ram and launch it to hit the pile.

Measuring tools

For the CPT the equipment consisted in: piezocone, personal computer, software and amplifiers. For the static and pseudostatic tests we also want to measure the force at the pile head, acceleration and displacement, so other electronic equipment is needed.

- **Piezocone**:In order to measure pore pressures, the cone used by Dijkstra has been substituted by a standard piezocone, hence, it would be more appropriate to talk about CPTU than CPT. The cone used has a shoulder placed piezometer. The different types of piezometers have been presented in the literature study.In our case we have type 2,that consists in an electrical cone with a pore pressure sensor located between the tip and the friction sleeve. Smits [46] prefers this kind of cone as it protects the porous element against damage during penetration, it is easy to change its components and the measured pore pressures are not too sensitive

---

[1]see Dijkstra [5] for detailed description and reasoning of the mechanism

to stress variations in the porous element. This position not only measures the compression induced pore pressures but also slightly registers the effects of localized shear deformation.

- **Strain gauge**: It was used to measure the force at the pile head. Has a bandwidth of $20kHtz$ and measures with a time step of $0.05ms$.

- **Acceleration transducer**: It was only used in the pseudostatic test. Recording the acceleration it is possible to quantify the dynamic component of the test and the behavior of the soil. Besides, integrating the acceleration over time it provides the velocity. The frequency was $20kHtz$. It was installed outside the cone, mounted on a steel plate.

- **Displacement gauge**: It consisted on a linear stroke potentiometer. It measured the movement of the rod, as it was mounted on one of the fixed beams. The measuring pinpoint was placed on the same steel plate as the acceleration transducer, providing that displacement and velocity data had no time differences.

4.4.3 Test location

The penetration tests cannot be randomly located. Dijkstra [5] performed three tests per tank preparation. In this research, only one test per preparation, located 'in the center' is carried out. After one test, the soil is already disturbed and a new preparation has to be made. According to this, tests were performed in the morning and in the afternoon the tank was prepared again. The exact location of the tests is shown in the picture; it could not be located exactly in the center due to problems in fixing the sounding apparatus to the beams that support the test devices.

The reasons why only one test, and not three as Dijkstra, was performed for each preparation are:

1. Allow the soil to freely develop its failure shape, without interference of previous failures.

2. Neglect boundary effects.

The key difference between Dijkstra's research and this one is that now the sand is saturated. The waves will propagate faster and larger areas of the soil will be under the effects of the tests.

Wesley [18] proposed that the ratio chamber diameter-to-cone diameter needs to be in excess of about 35 for loose sands ($D_r \approx 30\%$) and 60 for dense sands ($D_r \approx 90\%$). The ratio in this experiments, with the Geotechniek calibration chamber and the standard cone of 3,33cm of diameter, is of 52,77, approximately 60. From here it can be concluded that the best option is to place just one test in the middle of the chamber, although it is more time-consuming and generates more scatter among individual tests due to variations in the preparation of the sand bed, it will give the best and more reliable results. Also this placement is the best to guarranty soil's freedom to develop its own shape every time.

Chapter 5

Experimental results and evaluation

5.1 Introduction

5.1.1 Verification of testing procedure

[1] The test set-up and procedure were designed by Dijkstra [5] in his study of loading rate effects in unsaturated sand. For we are using the same equipment and performing the same tests, and for the interest in comparing the current results with Dijsktra's (dry vs saturated), firstly a calibration test was performed. The test was done under the same conditions as Dijkstra (i.e. unsaturated sand), 1.5h fluidization followed by 10min vibration. Results showed good agreement with Dijkstra's, corroborating the acceptance of the on-going research methodology.

Date	CPT		Static1			Pseudostatic			Static2		
	Tip	Sleeve	Force	Tip	Sleeve	Force	Tip	Sleeve	Force	Tip	Sleeve
	MPa	MPa	kN	MPa	MPa	kN	MPa	MPa	kN	MPa	MPa
20-Jul-04	19.9	0.11	25.0	17.7	0.11	21.0	15.7	0.1	21.0	15.7	0.1
26-Jul-04	22.0	0.1	26.0	19.0	0.12	25.0	18.0	0.1	31.0	16.4	0.09
29-Jul-04	16.9	0.09	23.0	15.0	0.08	22.5	14.4	0.1	22.5	15.7	0.08
verific.	17.5	0.1	22.3	15.6	-	22.1	14.9	0.1	20.5	14.7	0.08

Table 5.1: Verification test results

5.1.2 Failure criteria

Of the available failure criteria for piles, the 10% criteria is the most popular, and the Dutch NEN 6347 code for instance uses it. This criteria defines the ultimate pile capacity as that force that corresponds to pile displacement of 10% the pile diameter. This criteria is not implemented here, though. Instead:

Failure criteria:Failure will be defined to occur when the displacement is 2cm, 50% of the pile diameter.

---

[1]The experimental tests were done in cooperation with another student from Unesco-IHE, E.Archeewa. His thesis consisted in analyzing the experimental results. Therefore, part of the coming evaluation is based on Archeewa's [47] work and the reader is referred to his report for further details.
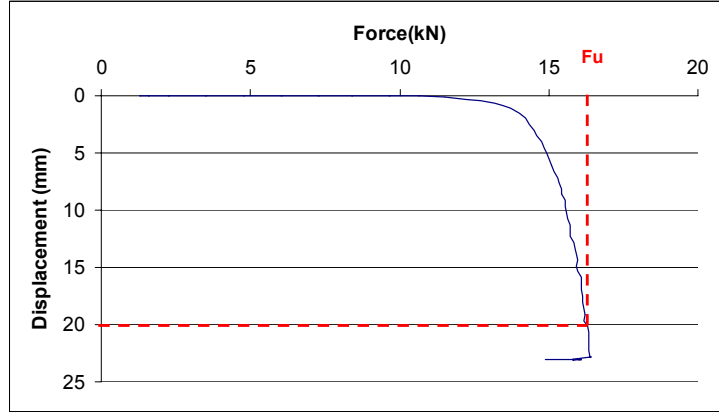
Figure 5.1: Failure criteria

The reason is that the standard load-displacement curves that are obtained with this test set-up do not show a clearly determined inflexion point for which plastification occurs but it is more gradual, force still increases smoothly after 10% pile diameter displacement.

5.2 Results presentation

5.2.1 CPT results

From the figures it can be seen that both tip and sleeve resistance increase with the penetration until this is stopped. Once it is stopped, there is an almost instantaneous relaxation for which there is a sudden decrease in tip resistance and a sudden increase in sleeve friction. Afterwards, both values decrease slowly. The relaxation behavior cannot be seen in the pore pressures, these reach a maximum when penetration stops and then dissipate.
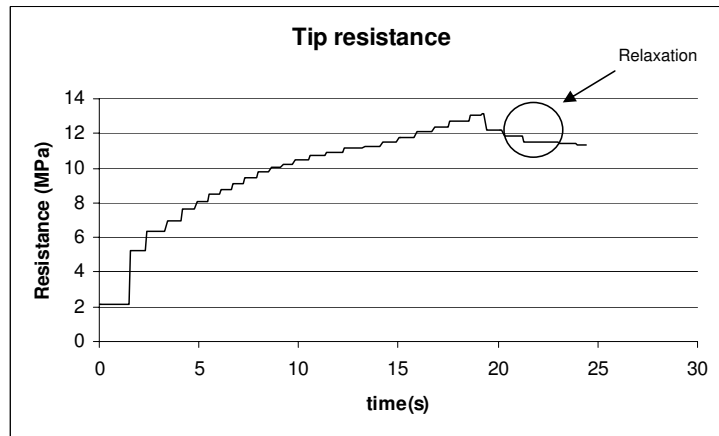
Figure 5.2: Tip resistance for CPT
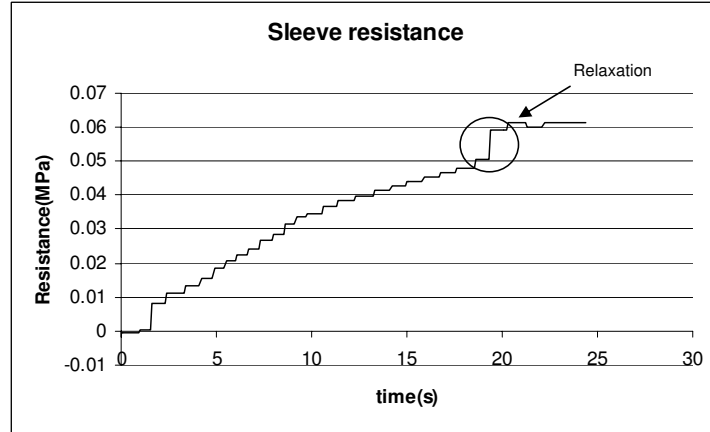
Figure 5.3: Sleeve resistance for CPT
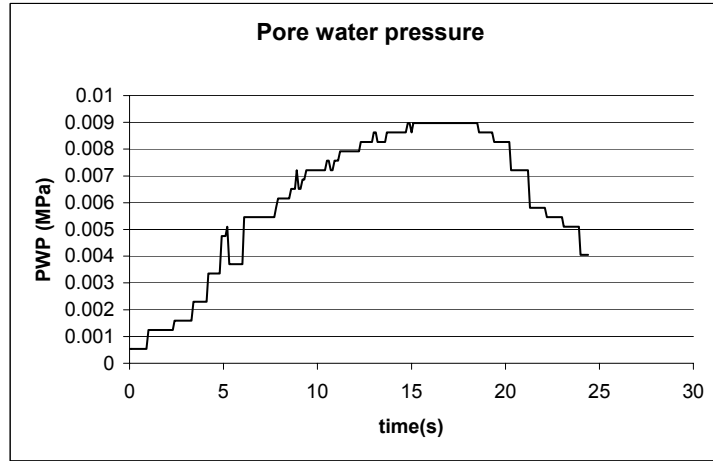
Figure 5.4: Pore pressures for CPT

5.2.2 Static results

For the static test, the plots shapes are quite different. The increase in both tip and sleeve resistance and also the force on the pile head are not gradually as for the CPT but present an abrupt increase, almost reaching the maximum, at the beginning of the test, in a time span of milliseconds, and then there is a slight increase during the rest of the test until the prove is finished. Also pore pressures increase instantly after start, reaching in this case a maximum, and then they decrease to a lower but constant value.

5.2.3 Pseudostatic results

The loading system of the pseudostatic test is absolutely different to the one used in the CPT or static tests, and this is reflected in the recorded data. Archeewa [47] plotted force, tip resistance, sleeve resistance and pore pressures versus time and displacements and also derived the curve for the total pile resistance as the result of adding the contributions of tip and sleeve.

For the force diagram, there is a first peak that can be related to slippage of the pile
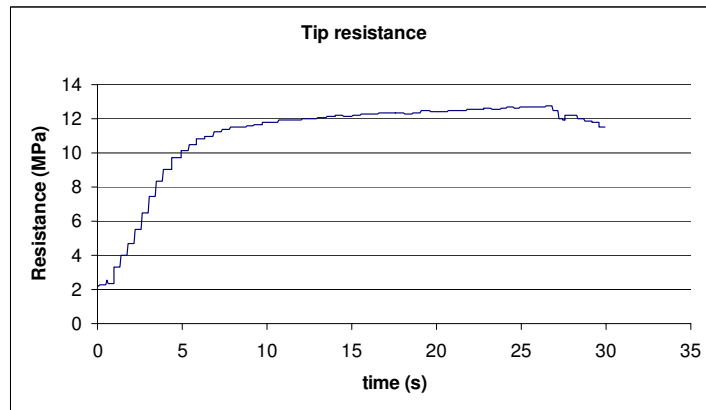
Figure 5.5: Tip resistance for Static test
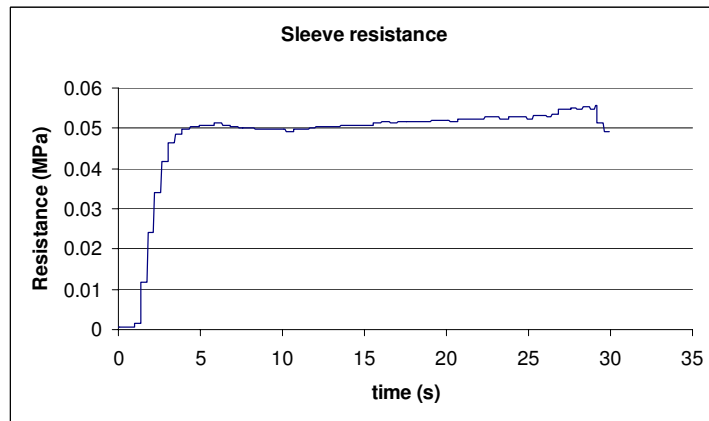
Figure 5.6: Sleeve resistance for Static test
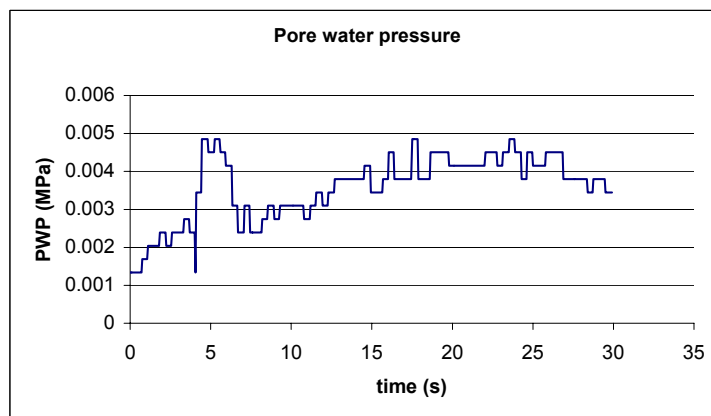
Figure 5.7: Pore pressures for Static test

to the adjacent soil. In fact, the same peak, even more brusque, is found also for the
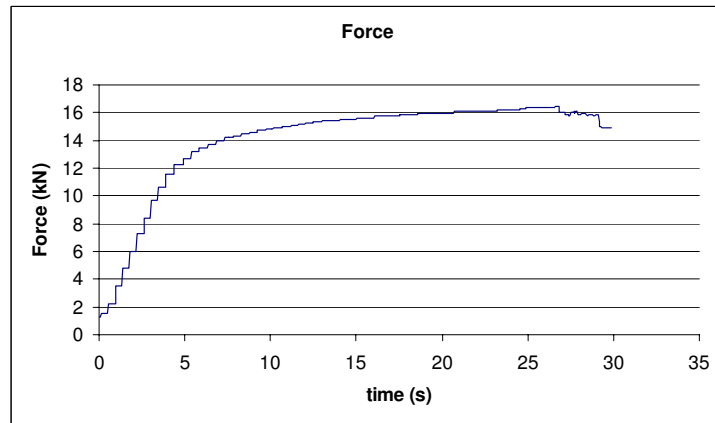
Figure 5.8: Force for Static test
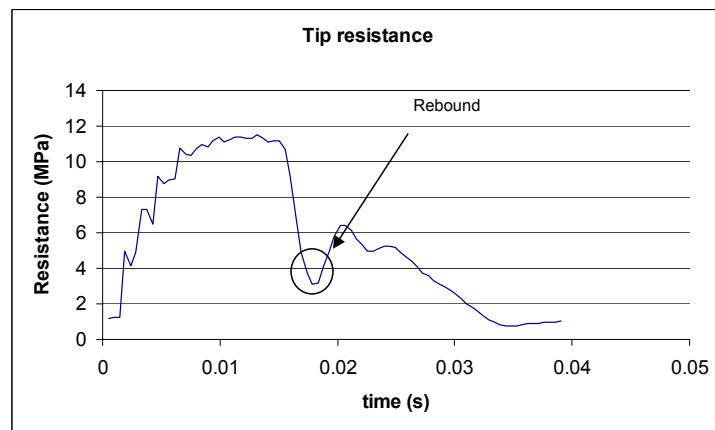
Figure 5.9: Tip resistance for Pseudostatic test
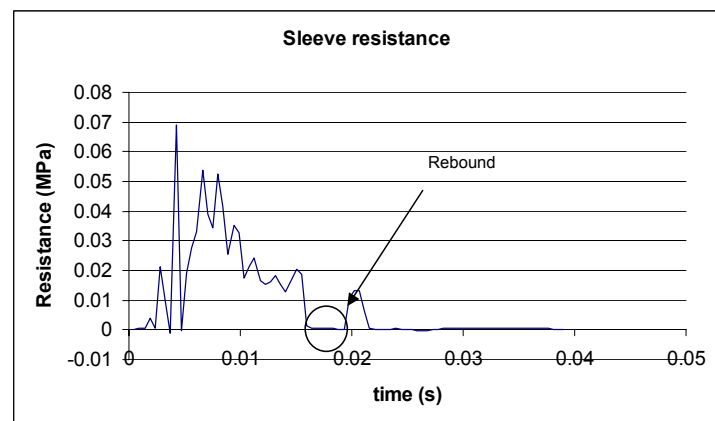
Figure 5.10: Sleeve resistance for Pseudostatic test
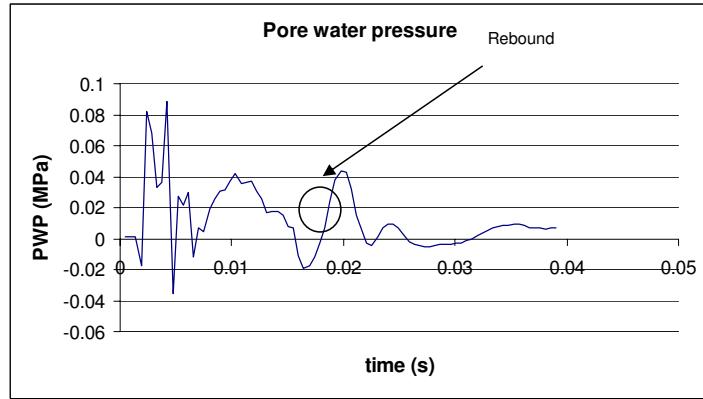
Figure 5.11: Pore pressures for Pseudostatic test
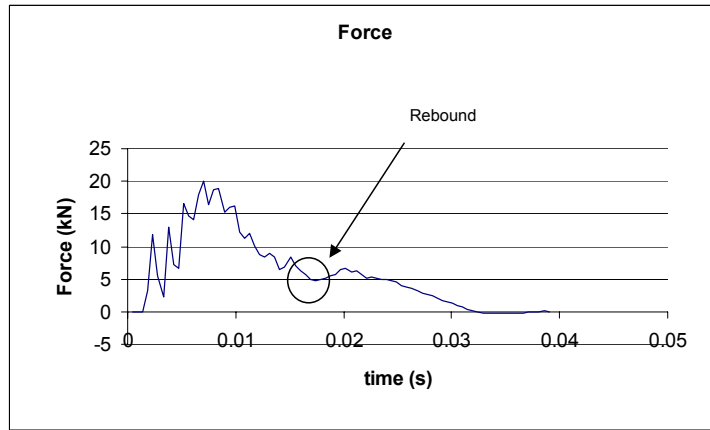
Figure 5.12: Force for Pseudostatic test

sleeve friction. It seems that immediately after dropping the mass on the pile there is a mobilization of the adherence between the lateral pile walls and the sand, that causes this maximum to appear. After this first instant behavior, the force increases again, reaching the maximum for a displacement slightly inferior to 2mm. As the displacement keeps increasing, the force is already decreasing. The same happens for the sleeve resistance. The maximum is reached when the displacement is about 2mm and from then on it decreases. Note that for the pile rebound no sleeve resistance is recorded, no skin friction is measured during tensional behavior. The tip resistance and the derived pile resistance, however, increase immediately after the pile starts to displace and keeps on increasing smoothly until the maximum displacement of 10mm is reached. As the pile rebounds, both values decrease almost instantly.

The plot for the pore pressures is specially interesting. As soon as the pile is started being pushed into the soil, positive values are recorded. Yet, the pore pressures drop even reaching negative values just when the maximum displacement is achieved and suddenly increase again as the pile rebounds. The on-going rebounding can also be distinguished in the pore pressures. The behavior may be interpreted as follows: When penetration starts, sand under the pile tip is being compressed by the pile, expelling the water in the pores and leading to positive values of the pore pressures. The penetration goes on densifying

(a) 5min

(b) 15min
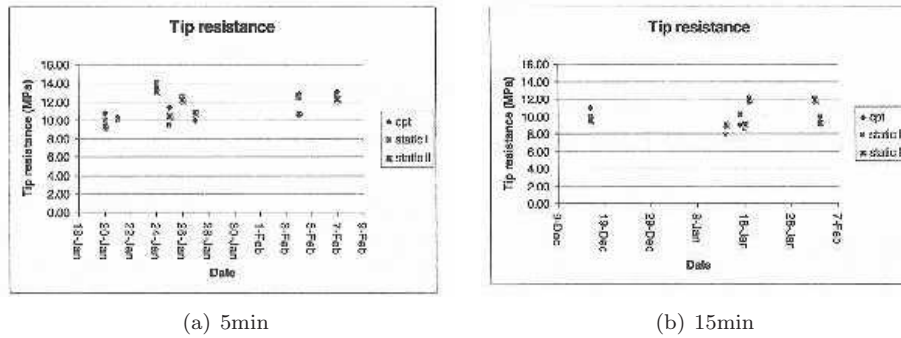
Figure 5.13: Tip resistance values for CPT and Static tests

(a) 5min

(b) 15min
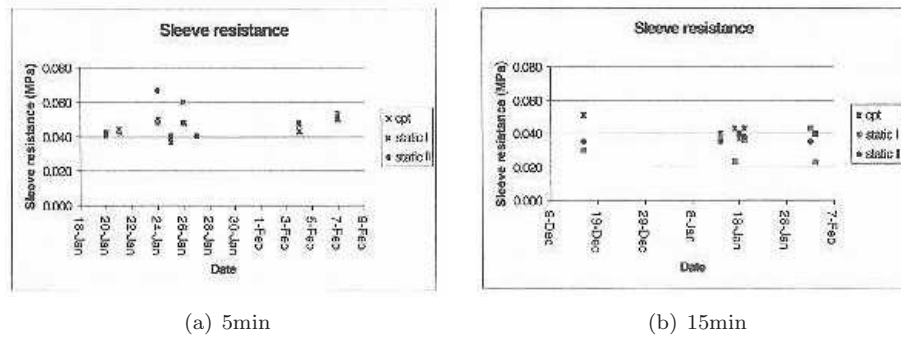
Figure 5.14: Sleeve resistance values for CPT and Static tests

the sand until the maximum density is reached. In this moment dilatancy starts to occur and increasing compression from the pile results in a rearrangement of the granular package, grains slide against each other, increasing the volume and the free pore space. As water comes back to the pore space, negative values are recorded. Negative values go on until the pile rebounds, thus is compresses the soil again, producing positive pore pressures once more.

5.3   Results analysis

5.3.1   CPT and Static tests

The coming charts show some representative recorded values for the different measured properties for CPT, Static 1 and Static 2 tests. Some conclusions can be derived:

1. For both static tests, before and after the pseudostatic test, similar values were recorded⇒It seems to indicate that the pseudostatic test did not significantly affect the soil properties or did not introduce significant residual stresses into the soil.

2. While tip and sleeve resistance for CPT and static tests fall more or less in the same range of values, this is not the case for excess pore pressures. Indeed, the recorded values for CPT are larger than ones for the static tests⇒It seems to indicate that the loading rate does not significantly affect the pile resistance but does affect the excess pore pressures generated.
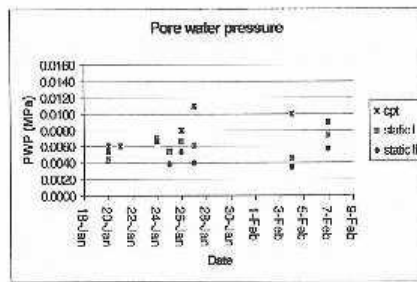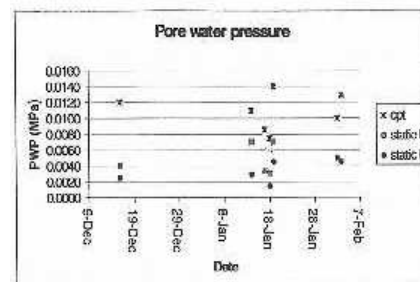
(a) 5min   (b) 15min

Figure 5.15: Pore pressure values for CPT and Static tests
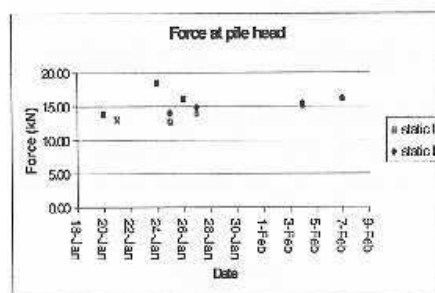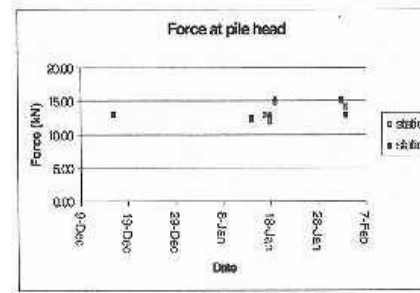
(a) 5min   (b) 15min

Figure 5.16: Force at pile head values for Static tests

3. Samples prepared with different vibration times do not show different recorded values⇒It seems to indicate that the vibration time does not affect the density, hence, the preparation system is not efficient enough.

Some possible conclusions have already been derived, but before definitely stating them, some more insight is needed and will be explained below.

Effect of the pseudostatic test on the soil properties

The results from both static tests can be tabulated (see table 5.2) and used to derived the correspondent pile resistances. Then, the resistances for static tests pre-pseudostatic and post-pseudostatic can be compared and we can evaluate to which extent the dynamics of the pseudostatic test affected the soil conditions.

sample	date	Static 1			Static 2			Pile resist. ratio(1/2)
		Force kN	Tip MPa	Sleeve MPa	Force kN	Tip MPa	Sleeve MPa	
	20-Jan-05	13.8	10	0.04	13.9	9.3	0.041	1.05
	21-Jan-05	13.1	10.04	0.044	-	-	-	-
	24-Jan-05	18.4	14.0	0.048	18.5	13.11	0.067	0.99
f=1.5h	25-Jan-05	12.7	9.5	0.04	14.0	10.44	0.04	0.93
v=5min	26-Jan-05	16.0	12.5	0.06	16.1	12.24	0.048	1.06
	27-Jan-05	14.0	10.7	0.04	14.87	10.8	0.04	0.99
	4-Feb-05	15.3	12.44	0.047	15.37	10.7	0.048	1.12
	7-Feb-05	16.2	12.78	0.054	16.2	12.3	0.051	1.04
average								**1.03**
	16-Jan-05	13.0	10.04	0.03	13.0	9.5	0.035	1.02
	14-Jan-05	12.3	7.9	0.037	12.5	9.0	0.035	0.91
f=1.5h	17-Jan-05	13.0	10.17	0.023	-	-	-	-
v=15min	18-Jan-05	11.9	8.5	0.04	12.8	9.1	0.04	0.95
	19-Jan-05	14.8	12.0	0.043	15.3	11.8	0.035	1.01
	2-Feb-05	15.0	12.0	0.043	15.3	11.8	0.035	1.05
	3-Feb-05	14.1	10.0	0.023	13.0	9.3	0.04	0.98
average								**0.99**

Table 5.2: Effect of pseudostatic test on soil properties and stresses

The average ratios are 1.03 and 0.99, aproximately 1; in other words, the derived pile resistances are the same for the static tests before and after the pseudostatic. Now yes, we can conclude that the pseudostatic test does not introduce changes in the soil properties or any residual stresses.
Archeewa [47] performed a t-test statistical analysis in his report and concluded that certainly the results of the two static tests can be considered one same data set.

Loading rate effect on pore water pressures

The three commonly measured values for CPT and static, namely, tip resistance, sleeve friction and excess pore pressure, can be compared (table 5.3) to discern whether or not there is a palpable effect of CPT's larger loading velocity.

From the table it can be seen that the results for tip and sleeve resistance are slightly higher for the CPT, but not significantly. However, the pore pressures of the CPT are more than twice the static ones; therefore, there is a loading rate effect on the pore pressure generation: higher rates of loading produce higher pore pressures.

sample	Tip		ratio	Sleeve		ratio	Pore pressure		ratio
	CPT	Static		CPT	Static		CPT	Static	
	10.7	10.0	1.07	0.042	0.04	1.05	0.006	0.0044	1.36
	10.3	10.04	1.03	0.043	0.044	0.98	0.006	-	-
	13.65	14.0	0.97	0.05	0.048	1.04	0.0067	0.007	0.96
f=1.5h	11.37	9.5	1.2	0.037	0.04	0.92	0.0054	0.0054	1
v=5min	11.98	12.5	0.96	0.048	0.06	0.8	0.008	0.0067	1.2
	10.0	10.7	0.93	0.04	0.04	1	0.011	0.006	1.83
	12.9	12.44	1.04	0.043	0.047	0.92	0.01	0.0045	2.22
	13.11	12.78	1.03	0.05	0.054	0.93	0.009	0.0074	1.22
Average	11.75	11.49	1.03	0.044	0.046	0.95	0.0078	0.0059	1.4
	11.0	10.04	1.1	0.051	0.03	1.7	0.012	0.004	3
	8.9	7.9	1.13	0.04	0.037	1.07	0.011	0.007	1.58
	9.0	10.17	0.88	0.043	0.023	1.87	0.0085	0.0033	2.54
f=1.5h	9.0	8.5	1.06	0.037	0.04	0.92	0.0075	0.0031	2.44
v=15min	12.2	12	1.02	0.043	0.036	1.19	0.014	0.007	2.01
	12.04	12.0	1.0	0.043	0.043	1.0	0.01	0.005	2.0
	10.0	10.0	1.0	0.04	0.023	1.76	0.013	0.0045	2.89
Average	10.31	10.08	1.03	0.042	0.033	1.36	0.0078	0.0048	2.35

Table 5.3: Comparison CPT and Static

(a) 5min   (b) 15min
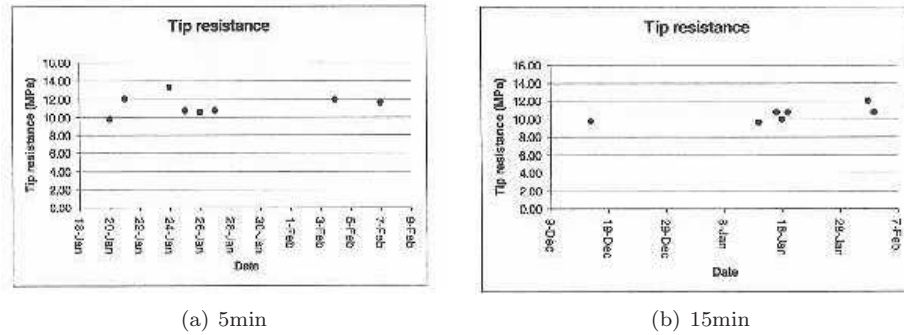
Figure 5.17: Tip resistance values for Pseudostatic test

Influence of the density

Also from the last table one can see that there is no difference in the values for different vibration times. A statistical study by Archeewa [47] confirmed this idea. This means that changes in vibration time cannot modify soil's density. The sample preparation system was inefficient, in practice, all the tests were performed with the same sample. Consequently, one of the objectives that was defined, to evaluate the influence of the soil strength, will remain unfulfilled.

5.3.2 Pseudostatic test

The charts present the maximum recorded values for tip resistance, sleeve resistance, pore pressures and force at the pile head recorded for the pseudostatic tests. Once more no difference between different vibration times can be appreciated.
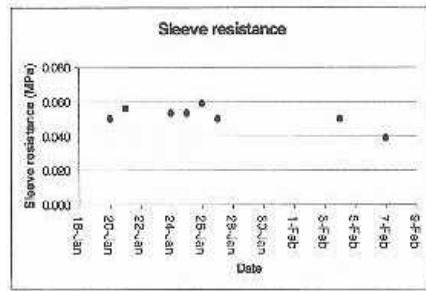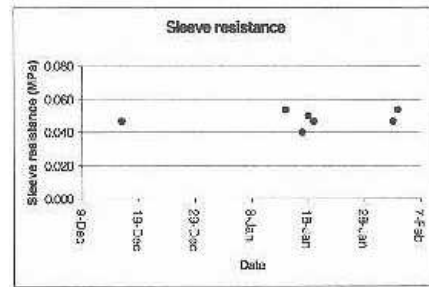
(a) 5min   (b) 15min

Figure 5.18: Sleeve resistance values for Pseudostatic test
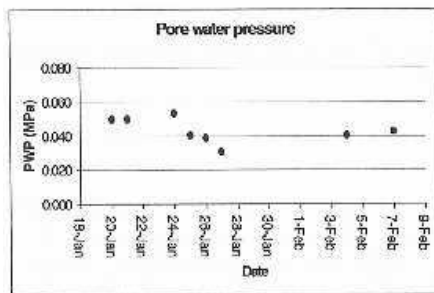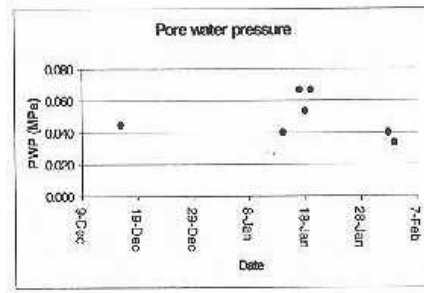
(a) 5min   (b) 15min

Figure 5.19: Pore pressure values for Pseudostatic test
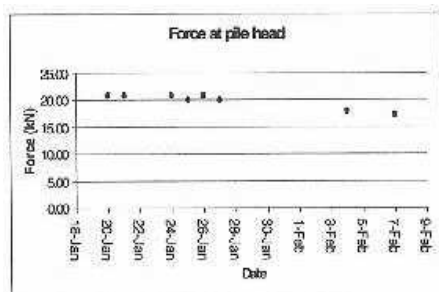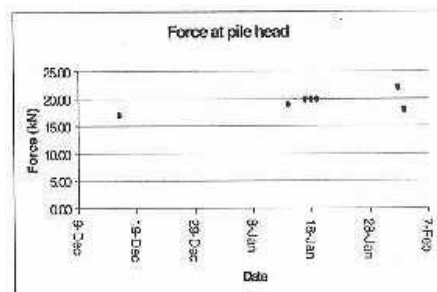
(a) 5min   (b) 15min

Figure 5.20: Force at pile head values for Pseudostatic test
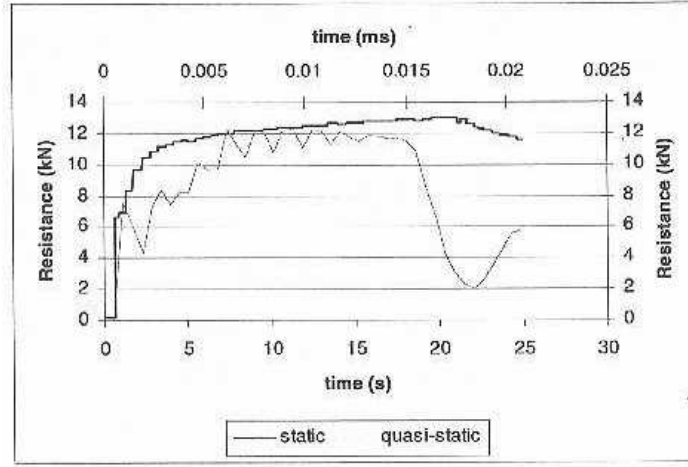
Figure 5.21: Comparison between total pile resistance for static and pseudostatic test

Pseudostatic vs Static (a): Loading rate effect on bearing capacity

Comparing the recorded maximums for pseudostatic and static tests and calculating the derived pile bearing capacities (table 5.4) we can see that there is no decisive rate effect in tip resistance, sleeve resistance and even ultimate pile capacity. This results are in accordance to Dijkstra's[5] for dry case, hence, for the pseudostatic test it can be concluded that there is no rate effect on the pile capacity.

sample	Force		ratio	Tip		ratio	Sleeve		ratio	Pile res.
	pseudo	static		pseudo	static		pseudo	static		ratio
	21.0	13.8	1.52	9.8	10.0	0.98	0.05	0.04	1.25	1.03
	21.0	13.1	1.6	12.05	10.04	1.2	0.056	0.044	1.28	1.22
	21.0	18.4	1.14	13.38	14.0	0.96	0.054	0.048	1.12	0.98
f=1.5h	20.0	12.7	1.57	10.7	9.5	1.13	0.054	0.04	1.33	1.17
v=5min	21.0	16.0	1.31	10.57	12.5	0.85	0.059	0.06	0.98	0.87
	20.0	14.0	1.43	10.70	10.70	1	0.05	0.04	1.25	1.04
	18.11	15.3	1.18	12.0	12.44	0.96	0.05	0.047	1.07	0.98
	17.3	16.2	1.07	11.67	12.78	0.91	0.039	0.054	0.73	0.88
Average	19.92	14.94	1.35	11.36	11.49	0.99	0.051	0.046	1.12	1.02
	17.0	13.0	1.31	9.7	10.04	0.97	0.047	0.03	1.56	1.05
	19.0	12.3	1.54	9.63	7.9	1.22	0.054	0.037	1.43	1.26
	20.0	13.0	1.54	10.7	10.17	1.05	0.04	0.023	1.74	1.13
f=1.5h	20.0	11.9	1.68	10.0	8.5	1.18	0.05	0.04	1.25	1.19
v=15min	20.0	14.8	1.35	10.7	12.0	0.89	0.047	0.036	1.3	0.95
	22.0	15.0	1.47	12.04	12.0	1	0.047	0.043	1.09	1.02
	18.0	14.1	1.28	10.7	10.0	1.07	0.054	0.023	2.35	1.22
Average	19.43	13.44	1.45	10.5	10.08	1.05	0.048	0.033	1.53	1.12

Table 5.4: Comparison Pseudostatic and Static

Pseudostatic vs Static (b): Loading rate effect on pore pressures

The most graphic way to evaluate the loading rate effect in saturated soil is to compare the values of the pore pressures generated by pseudostatic and static tests:

sample	Pore pressure		ratio
	pseudost	static	
	0.05	0.0044	11.32
	0.05	-	-
	0.054	0.007	7.65
f=1.5h	0.04	0.0054	7.5
v=5min	0.039	0.0067	5.8
	0.031	0.006	5.13
	0.04	0.0045	8.92
	0.043	0.0074	5.82
Average	0.043	0.0059	7.44
	0.045	0.004	11.25
	0.04	0.007	5.77
	0.067	0.0033	20.0
f=1.5h	0.054	0.0031	17.39
v=15min	0.0667	0.007	9.62
	0.04	0.005	8.0
	0.033	0.0045	7.43
Average	0.049	0.0048	11.35

Table 5.5: Pore pressure generation for Pseudostatic and Static tests

The pore pressures recorded for the pseudostatic tests are very high. Pseudostatic testing on saturated granular soil does indeed generate high excess pore pressures. Even though, they do not affect the pile capacity.

Saturated vs Dry (a): Influence of excess pore pressures on the pile resistance

Table (5.5) showed that the pseudostatic test generated up to 5 times larger pore pressures than the static one. The pile capacities can be calculated for the different type of tests and conditions and compared with the measured for on the pile top to check the effect of the excess pore pressures on the pile capacity:

test type	condition	Force(F) (kN)	Tip (MPa)	Sleeve (MPa)	Pore prs. (MPa)	Pile rest.(R) (kN)	ratio F/R
static	dry	24.67	17.25	0.104	-	23.07	1.07
test	saturated	14.49	10.97	0.041	0.005	13.26	1.09

Table 5.6: Influence of pore pressures on pile resistance 1

For the dry case Dijkstra[5] measured a force at the pile head a 7% larger than the calculated pile resistance from sleeve and tip values. For the saturated case, the percentage is almost the same, hence, despite the fact that excess pore pressured do occur, they do not change the measured force-calculated resistance ratio. Besides, from table 5.7 it can be derived that excess pore pressures for the pseudostatic case are definitively much higher than the static ones, but the calculated pile resistances are the same. The conclusion is then that excess pore pressures do not affect the bearing capacity.

condition	test type	Force(F) (kN)	Tip (MPa)	Sleeve (MPa)	Pore prs. (MPa)	Pile rest.(R) (kN)	ratio F/R
saturated	static	14.49	10.97	0.041	0.005	13.27	1.09
	pseust	19.75	11.0	0.05	0.044	13.8	1.43
ratio pseud/stat		1.36	1.0	1.22	8.8	1.04	

Table 5.7: Influence of pore pressures on pile resistance 2
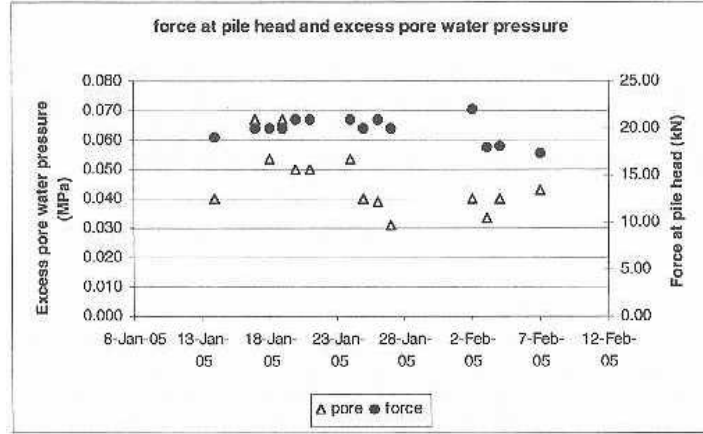
Figure 5.22: Force at pile head and pore pressures for pseudostatic test

Saturated vs Dry (b): Influence of excess pore pressures on the force on the pile head

What does change significantly between static and pseudostatic tests is the measured force at the top of the pile. Plotting pore pressures and force for different pseudostatic tests no correlation can be found, hence, the generated pore pressures are not to be held responsible for the increase in force.

The increase in force has to be then due to the dynamics of the pseudostatic test. Archeewa [47] analyzed the dynamic resistance with a simple Smith model and could determine that the damping force was not influential but instead what played a determinant role was the inertia force.

5.4   Conclusions

The experimental results have been presented and evaluated. From the previous considerations, and related to the objectives that had been defined in the problem analysis it can be concluded:

- **Relationship loading rate-excess pore pressure**: Indeed, the loading rate does have an effect in the generation of excess pore pressures. Higher loading rates generate higher values of excess pore pressures; pseudostatic tests create pore pressures almost a ten times the static ones.

- **Relationship excess pore pressure-bearing capacity**:The generation of excess pore pressures does not, however, affect the pile bearing capacity. In accordance to
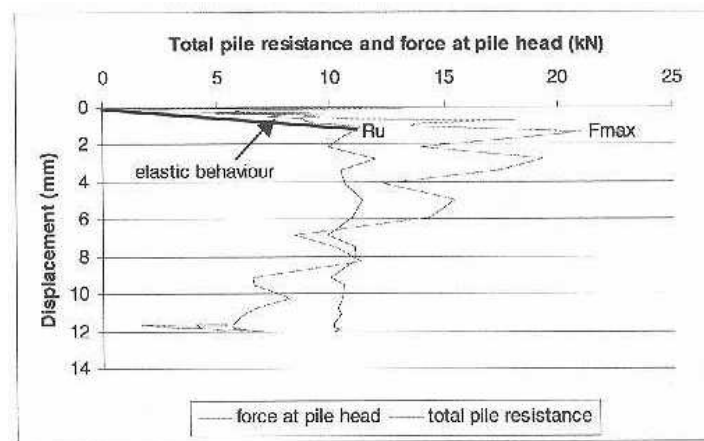
Figure 5.23: Force at pile head and computed pile resistance for pseudostatic test

Dijkstra's results for dry sand, pseudostatic testing does not introduce a loading rate effect on the pile bearing capacity,neither for dry nor for saturated sand.

- **Relationship soil strength-excess pore pressure**: Due to inefficiency of the sample preparation system, this could not be evaluated, the third sub-objective could not be fulfilled.

Some considerations about the conclusions: the first conclusion could have been expected on beforehand. The second conclusion, though, is quite more striking. If the generation of excess pore pressures does take place, then inevitably the effective stresses in the soil must be decreased. It would seem logical to expect lower bearing capacities for saturated pseudostatic tests when compared to (a) saturated static tests and (b) dry pseudostatic tests. Results show that excess pore pressures do not affect pile bearing capacity, this is true, but just leaving this statement in the air may seem illogical and incongruent from a geotechnical point of view. More understanding on not the value itself, but the generation and dissipation of pore pressures is needed. What results are implicitly showing is that the loading process is of course not drained, but probably neither is it fully undrained. We may be in the case of coupled loading and drainage, thus, partial drainage, with pore pressures starting to dissipate while the load is still being applied. Pore pressures generated are mainly posisitve due to compression of the soil under the pile tip. Looking back at the plots tip resistance versus time and pore pressures versus time it can be seen that, leaving apart the first instantaneous peak, excess pore pressures reach the maximum value for 0.0125s approximately and decrease from then on at the end of the penetration they are exactly 0, whereas tip resistance keeps increasing, reaching its maximum at the end of the penetration. Therefore, Archeewa [47] proposed the explanation of the dilatancy and this is a good explanation but not the only one. In my opinion, the fact that excess pore pressures start dissipating during the loading process is even more determining. It is not the case of undrained loading. So, finally, another conclusion, that explains the second one, could be written down:

- **Drainage**: Contrary to what was initially supposed, the loading process is not fully undrained. Instead, we are in a case of partial drainage.

Part II

Analytical modeling

Chapter 6

The elastoplastic saturated static cone model

It has been argued in the conclusions of chapter 3 that the cone model of Wolf [31], [32], [33], [34] would be adapted for the analytical modeling. This chapter is intended to clearly define this analytical model. To be certain that a model is genuinely suitable for a potential real application, one must be aware of the limitations of the model as well as its inherent assumptions. Also the load conditions and the geometry of the problem are defined. No further calculations are performed in this chapter. The complete calculations of the model can be will be explained in chapter 7.

6.1 Model definition

6.1.1 Main features

As presented in the literature study, the core concept of the cone model rests in the idealization of the zone beneath the pile toe as a truncated cone with geometry easy to determine. In the simplest case of a cone in an homogeneous half-space its geometry may be defined quite straightforward if the pile characteristics and soil properties are known. In this case the last infinitesimal layer of the pile can be idealized as a massless disk supported on a free-space with a load applied in its center that will lead to stresses in the soil half-space and that act on an area that increases linearly with depth. In the cone theory axisymmetry is considered. Moreover, the cone is regarded as a rod (bar) with the displacement pattern over the cross section determined by the corresponding value on the axis of the cone. Strength of materials is applied, namely, plane sections remain plane. The domain of the soil half-space outside the cone is disregarded.

The principal idea of the analytical model can then be summarized:

> It is an axisymmetrical plane model that deals with the soil under the pile tip. It has the shape of a truncated cone. On top of it, the pile is neglected and only the last layer is assimilated to a massless loaded disk. The soil outside the cone and above it are not considered, as well as the shaft of the pile.

Note that in every defining feature intrinsic limitations are being introduced. By now the main one is the fact that the shaft of the pile and consequently the soil around it are neglected. This may be questioned when considering failure of the pile, thus the ultimate

capacity, as the shaft resistance is left out of the model. Still, the model has been developed to reproduce the generation of excess pore pressures. As the most significant part of the excess pore pressures are generated under the tip due to compression, the assumption can be accepted.

6.1.2   Assumptions and limitations

Once the principal idea of the model has been defined, it is time to look more in-depth to its characteristics. The current analytical model is a simplification of the real case. Hence, some assumptions are made and will probably introduce a strong limitation in the results applicability. The most remarkable ones are:

- Static problem. No dynamics are considered.

- The soil is considered as an homogeneous fully saturated perfectly linear elastic-plastic material.

- Excess pore pressures are only generated in the plastified area.

- Fully undrained loading. Once the loading process is finished, consolidation starts.

- Unidimensional axial deformation

The main limitations introduced by assumptions are related below as well as other hypothesis:

- The dynamics of the pseudostatic test are neglected. The cone model of Wolf was developed for elasticity and dynamics. However, plasticity and dynamics is too complicated. As the dynamics in the pseudostatic test are low-frequency and, if it is true that the results can be directly assimilated to the static ones, it can be a good first approach a static analysis. No wave theory is introduced by now. Precisely the best fit to this would have been a translational cone in vertical motion. Besides, the force is supposed to act as a single pulse whereas experimentally reboundings have been seen to occur when it's dropped on the pile head.

- It is assumed fully undrainend loading. Sand, as a granular material, is mostly supposed to behave as drained. Nevertheless, as the pseudostatic is a fast test, it is possibly the case, and actually experimentally it has been so, that excess pore pressures are generated. Thus, the behavior will be assumed to be fully undrained. Further in the calculations chapter, the correctness or not of this hypothesis will be discussed. By now, the excess pore pressures can be estimated assuming that, in undrained conditions, the mean effective stress remains constant. The excess pore pressure is equal to the change in mean total stress in the plastified zone. Outside the plastified zone, the hypothesis states fully elastic behavior and no permanent deformation, and so excess pore pressures, if generated there, are immediately dissipated and not taken into account.

- The cone is in a half-space, the soil domain is infinite. This is not true, the bottom of the tank acts like an underlying rigid rock. In addition to the decay of amplitudes as the wave propagates in the simple cone, we should include the reflections at rock interface and on the free surface, presenting the echo constants.

- The last layer of the pile is simulated as a massless disk on the surface of a half-space. In reality this disk is embedded in a full-space,double-cones should be used

with Green's function analysis.It is not possible to extend the concept of a single semi-infinite truncated cone to an embedded foundation, the concept of the double cone needs to be preferred.

- Considering only the last infinitesimal layer of the pile is not exact. The pile should be modeled as a sandwich of embedded disks

- In the case of saturated soil analyzed as a single-phase medium, the Poisson's ratio is essentially 1/2 due to the near incompressibility of the water filling the pores. Vertical motions with this ranges of Poisson's ratio might need to introduce two special features:

    1. The appropriate wave velocity dominating the radiation damping is twice the shear-wave velocity and not the dilatational-wave velocity.

    2. A trapped mass $\Delta M = \mu \rho r_0^3$ with $\mu = 2.4\pi(\nu - 1/3)$ is introduced.

    . As a first approach we will not take into account this observations.

If any other assumptions are made while calculating the model, these will be explained in the next chapter and the limitations introduced will be evaluated.

6.1.3   Procedure

In general terms, any analytical model that pretends to simulate the generation of excess pore pressures and its effect in the pile bearing capacity, if the loading is undrained, is meant to have three objectives, and steps in the calculation:

1. Determine excess pore pressure generated during loading

2. Evaluate the consolidation process after loading. Hence, in principle it is assumed that there is no consolidation during loading and it only occurs once the loading process is finished

3. Study how the generation of excess pore pressures affects the pile bearing capacity.

A particular model has been defined, though. To achieve the three main purposes, the steps to perform in more detail are enumerated below. The coming chapter includes all the calculations of the model:

1. Calculate the extent of the plastic zone. It needs two sub-steps:

    (a) Model of an elastic cone
    (b) Model of an elastoplastic cone

2. Calculate the generated excess pore pressure

3. Generate a consolidation model and calculate it

4. Check the results and the hypothesis of undrained loading

5. Estimate pile bearing capacity under current conditions.

Before starting the calculations, the model need to be defined quantitatively. The next sections explain the stresses that will be used as input and the geometry.
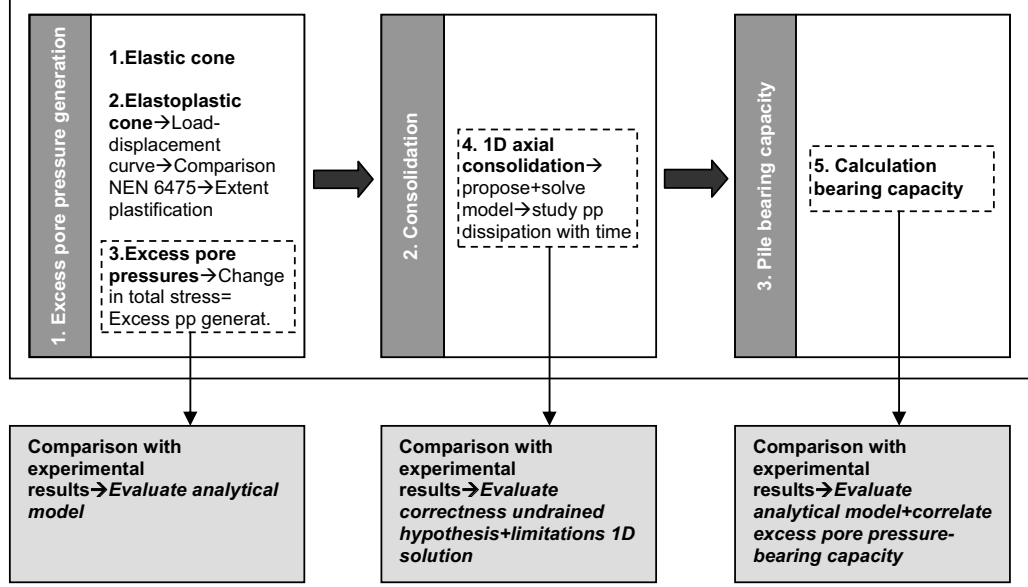
Figure 6.1: Steps to perform in analytical model

6.2 Force that reaches the soil

The dropping mass on the pile head is known. Using dynamics theory the force on the pile head can be obtained and how it propagates through the pile, including dissipation due to shaft friction. Finally, the force that reaches the soil can be calculated.
In fact, one can represent the loading device with the following rheological model. Take into consideration that the pile acts as a damper.

Dijkstra[5] estimated for the same pile and sand a force that reached the pile toe, and so the soil of **12 kN**. This value will be used for the calculations.

6.3 Construction of the cone

In the case of a semi-truncated cone in an homogeneous half-space, the defining features are:

1. Top radius:it is the radius of the pile

2. Cone height: determined by the embeddement depth and the tank depth

3. Aspect ratio: determines the opening angle of the cone. It is a function of the soil properties.

The two first properties are known. Just remains undetermined the opening angle. Generally it has been seen to range between 12° for failure and 45°.The (apex) aspect ratio (z_0/r_0) follows for each degree of freedom from matching the static-stiffness coefficient of the disk with radius equal to the pile radius to that of the corresponding cone. For the translational disk in vertical motion, the static stiffness is defined:

$$k_s = \frac{4Gr_0}{1 - \nu} \tag{6.1}$$

And for the translational cone:

$$K = \rho c^2 A_0 / z_0 \tag{6.2}$$

This leads to an aspect ratio:

$$\frac{z_0}{r_0} = \frac{\pi}{4}\left(1 - \nu\right)\left(\frac{c}{c_s}\right)^2 \tag{6.3}$$

Note that z_o/r_0 depends only on ν. For translational cone in vertical motion deformation occurs axially and the waves propagate with the velocity of a dilatational wave ($c = c_p$). This velocity is a function of the properties of the soil:

$$c = c_p = \sqrt{\frac{E}{\rho}} = \sqrt{2\frac{G}{\rho}\frac{1-\nu}{1-2\nu}} \tag{6.4}$$

Similarly, the velocity of the shear waves:

$$c_s = \sqrt{\frac{E}{\rho}\frac{1-2\nu}{1-\nu}} = \sqrt{\frac{G}{\rho}} \tag{6.5}$$

Properly substituting these values into the expressions one could end up with the definition of the cone's geometry.

6.4   Conclusion

The analytical model can be summarized with the following figure. where α is the opening
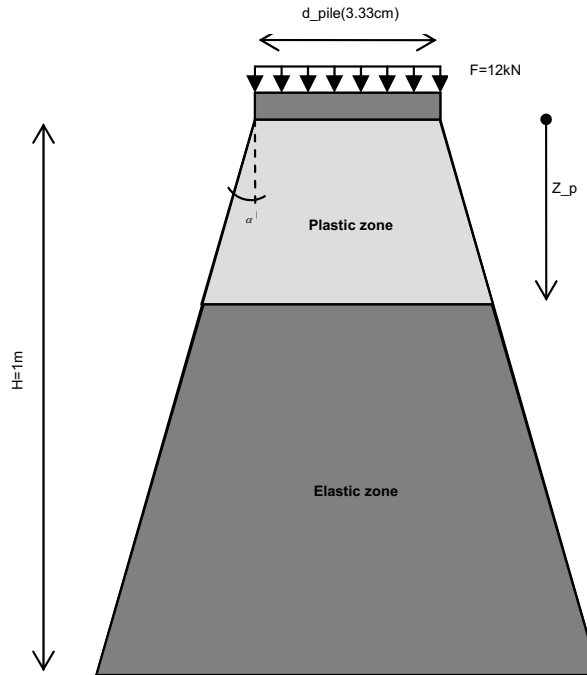
Figure 6.2: Analytical model geometry

angle. It depends only on the Poisson ratio. Yet, there is a lack of reliable soil properties data. A standard value of 40° will be assumed. z_p is the extent of the plastification. It has to be determined to be able to calculate the generated excess pore pressure. The other parameters are inputs derived from the experimental tests in the calibration chamber.

Chapter 7

Cone calculation

7.1 Introduction

The soil is assumed to be a linear perfectly elastoplastic material. Only in the plastic zone pore pressures will be generated, hence, the first step is to determine the extent (depth) of the plastic zone.

The known parameters are:

- Cone's geometry: height H, opening angle α, pile radius (disk radius) R_0.

- Force applied F

- Soil properties: elastic E_e and plastic E_p moduli.
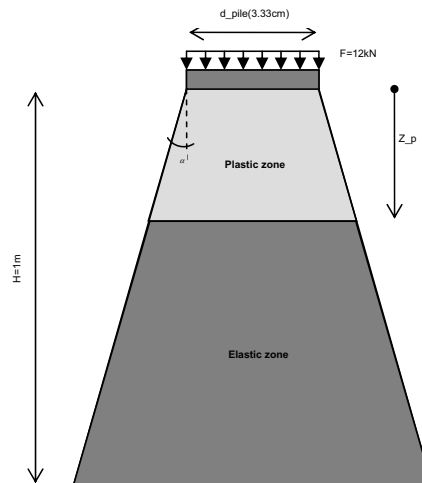
Figure 7.1: Cone geometry

The elastic and plastic lines intersect at the *elastic limit of the soil, σ_e*. This limiting stress will define the extent of the plastification. As the cone expands in depth, the stresses will progressively diminish (the same applied force but over larger areas); the area for which the corresponding stress is σ_e indicates the limit depth between plastified and elastic domains.

The the procedure will be in the coming order:
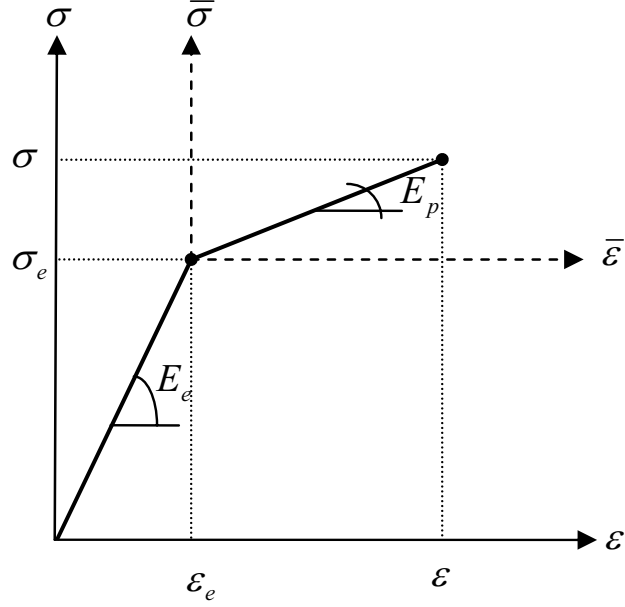
Figure 7.2: Elastoplasticity

1. Model of an **elastic cone** (before plasticity starts to occur, the full cone is elastic).
   Derivation of the expression for the vertical displacement of the elastic cone.

2. Model of a **elastoplastic cone**. When the applied stress exceeds the elastic limit,
   plastification will begin in the top of the cone. As the loading process goes on, the
   plastified section of the cone increases, therefore the elastic limit is progressively
   found at larger depths. When the full test load is applied, find out the depth at
   which the stress level corresponds to the elastic limit. This depth is the limit of the
   plastic zone.

3. When the full load is applied, find out at which depth corresponds the elastic limit

7.2   Elastic cone

7.2.1   Model definition

The deformation of the cone follows from fig (7.3). Hence, to define the cone model, one
needs to consider an infinitesimal slice of the cone (fig.7.4). The model is defined by three
equations:

1. **Equilibrium of the infinitesimal slice**:

$$N = N + \frac{\partial N}{\partial z}\Delta z \Rightarrow \frac{\partial N}{\partial z}\Delta z = 0 \tag{7.1}$$

2. **Constitutive equation: Elasticity**:

$$\sigma = E\epsilon \tag{7.2}$$
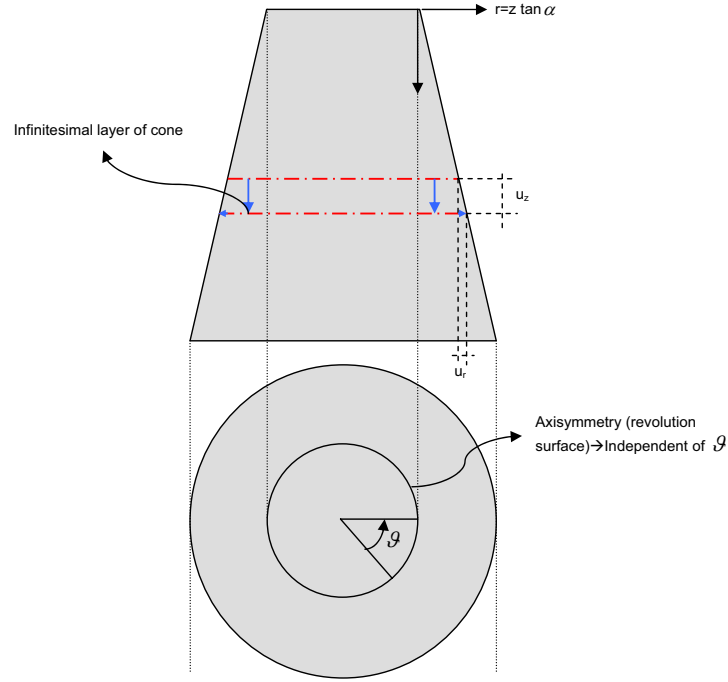
Figure 7.3: Cone deformation

3. **Geometric equation**:

$$\epsilon = \frac{\partial u}{\partial z} \tag{7.3}$$

Rewriting (7.1) as a function of the cross-section of the cone ($N(z) = A(z)\sigma(z)$), it can be obtained:

$$\frac{\partial A}{\partial z}\sigma + A\frac{\partial \sigma}{\partial z} = 0 \tag{7.4}$$

The derivative of σ with respect to z can be found from eq. (2):

$$\frac{\partial \sigma}{\partial z} = E\frac{\partial \epsilon}{\partial z} \tag{7.5}$$

with eq. (7.3):

$$\frac{\partial \sigma}{\partial z} = E\frac{\partial^2 u}{\partial z^2} \tag{7.6}$$

Finally the governing differential equation of the static cone model in elasticity to solve is:

$$A\frac{\partial^2 u}{\partial z^2} + \frac{\partial A}{\partial z}\frac{\partial u}{\partial z} = 0 \tag{7.7}$$

One can explicitly express it as a function only of z. The cone has a circular cross-section:

$$A = \pi r^2 = \pi(R_0 + z\tan\alpha)^2 \tag{7.8}$$

and consequently:

$$\frac{\partial A}{\partial z} = 2\pi\tan\alpha(R_0 + z\tan\alpha) \tag{7.9}$$
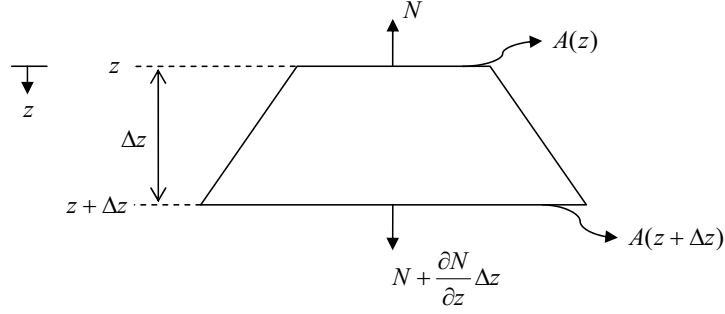
Figure 7.4: Infinitesimal cone slice

where R_0 is the radius of the pile and α is the opening angle of the cone, that is only function of the Poisson ratio of the soil.

Substituting into eq.(7.7):

$$\pi(R_0 + z\tan\alpha)^2\frac{\partial^2 u}{\partial z^2} + 2\pi\tan\alpha(R_0 + z\tan\alpha)\frac{\partial u}{\partial z} = 0 \qquad (7.10)$$

7.2.2 Solution of the differential equation

Eq.(7.7) is a second order differential equation. It is derived only as a function of z, so the partial derivatives can be turned into total derivatives. It can be rewritten:

$$\frac{d}{dz}(A\frac{du}{dz}) = 0 \qquad (7.11)$$

This equation has a solution of the shape:

$$A\frac{du}{dz} = K \qquad (7.12)$$

where K is a constant to be determined and $A = \pi(R_0 + \tan\alpha)^2$. Eq.(7.12) is the new equation to be solved. It is now a first order differential equation. With a change of variable it can be obtained a function of linear coefficients.
Define the following change of variable:

$$u = \frac{X(z)}{C_0 + C_1 z + C_2 z^2} \qquad (7.13)$$

$$\frac{du}{dz} = \frac{-C_1 - 2C_2}{(C_0 + C_1 z + C_2 z^2)^2}X(z) + \frac{1}{C_0 + C_1 z + C_2 z^2}\frac{dX(z)}{dz} \qquad (7.14)$$

with:

$$\begin{cases} C_0 = R_0 \\ C_1 = \tan\alpha \\ C_2 = 0 \end{cases}$$

Substituting into eq.(7.12) follows:

$$-\pi\tan\alpha X(z) + \pi(R_0 + z\tan\alpha)\frac{dX(z)}{dz} = K \qquad (7.15)$$

Eq.(7.15) is a linear first order differential equation with non-constant coefficients of the form:

$$aX(z) + b(z)\frac{dX(z)}{dz} = K \qquad (7.16)$$

or, in a more general shape:

$$\frac{dX}{dz} + p(z)X = g(z) \qquad (7.17)$$

with the coefficients:

$$\begin{cases} p(z) = \frac{a}{b(z)} = \frac{-\pi \tan\alpha}{\pi(R_0 + z\tan\alpha)} = \frac{-\tan\alpha}{R_0 + z\tan\alpha} \\ g(z) = \frac{K}{b(z)} = \frac{K}{\pi(R_0 + \tan\alpha)} \end{cases}$$

Once the standard shape has been achieved, the next step is to convert it into an integrable equation. For this, eq(7.17) must be multiplied by an integration factor. The next developments will show how this factor can be found.
Eq.(7.17) can be rewritten:

$$\mu(z)X' + \mu(z)p(z)X = \mu(z)g(z) \qquad (7.18)$$

The left term of eq.(7.18) shall be recognized as the derivative of some function; the most general approach is to consider it to be the derivative of a function of style $\mu(z)X$. Then the second part of the left term can be associated:

$$\mu(z)p(z)X = \mu'(z)X \Rightarrow \mu'(z) = p(z)\mu(z) \qquad (7.19)$$

Assuming $\mu(z) > 0$:

$$\frac{\mu'(z)}{\mu(z)} = p(z) \Rightarrow \frac{d}{dz}ln\mu(z) = p(z) \qquad (7.20)$$

Integrating,

$$ln\mu(z) = \int p(z)dz + Y \qquad (7.21)$$

Choosing the integration constant Y to be 0, the integration factor may be expressed:

$$\mu(z) = exp\int p(z)dz \qquad (7.22)$$

Once the integration factor is known, eq.(7.19) can be rewritten:

$$[\mu(z)X]' = \mu(z)g(z) \qquad (7.23)$$

Integrating the former expression:

$$\mu(z)X = \int \mu(z)g(z)dz + C \qquad (7.24)$$

And the solution of our differential equation is the quotient:

$$X = \frac{\int \mu(z)g(z)dz + C}{\mu(z)} \qquad (7.25)$$

To get the exact form our our particular case we only need to substitute the notation previously defined:

$$g(z) = \frac{K}{\pi(R_0 + \tan\alpha)} \qquad (7.26)$$

The integration factor is:

$$\mu(z) = exp \int p(z)dz = exp \int \frac{a}{b(z)}dz = exp \int \frac{-\tan\alpha}{R_0 + z\tan\alpha}dz$$

$$= exp[-\ln(R_0 + z\tan\alpha)] = \frac{1}{exp[\ln(R_0 + z\tan\alpha)]} = \frac{1}{R_0 + z\tan\alpha} \qquad (7.27)$$

Then:

$$\mu(z) = \frac{1}{R_0 + z\tan\alpha} \qquad (7.28)$$

And the product $\mu(z)g(z)$ is expressed:

$$\mu(z)g(z) = \frac{K}{\pi(R_0 + z\tan\alpha)^2} \qquad (7.29)$$

Integrating:

$$\int \mu(z)g(z)dz = \frac{K}{\pi}\int \frac{dz}{(R_0 + z\tan\alpha)^2} = \frac{-K}{\pi\tan\alpha(R_0 + z\tan\alpha)} + C \qquad (7.30)$$

The first solution for the modified differential equation is:

$$X = \frac{-K + C\pi\tan\alpha(R_0 + z\tan\alpha)}{\pi\tan\alpha} \qquad (7.31)$$

were C is an integration constant to be determined from the boundary conditions, like K.

Finally one has to undo the change of variable to get the expression for the displacement. Substituting expression (7.31) into eq.(7.13) we get the definitive solution:

$$u(z) = C - \frac{K}{\pi\tan\alpha(R_0 + z\tan\alpha)} \qquad (7.32)$$

7.2.3   Demonstration of the correctness of the solution

If the expression (7.32) is a correct solution it should be possible to put it back in eq.(7.7) and satisfy this equation. Eq.(7.7) was:

$$A\frac{\partial^2 u}{\partial z^2} + \frac{\partial A}{\partial z}\frac{\partial u}{\partial z} = 0 \qquad (7.33)$$

First the derivatives of the solution need to be calculated:

$$\frac{du}{dz} = \frac{K}{\pi(R_0 + z\tan\alpha)^2} \qquad (7.34)$$

$$\frac{d^2u}{dz^2} = \frac{-2k\tan\alpha}{\pi(R_0 + z\tan\alpha)^3} \qquad (7.35)$$

The area of the circular cone:

$$A = \pi(R_0 + z\tan\alpha)^2 \qquad (7.36)$$

And its derivative:

$$\frac{dA}{dz} = 2\pi\tan\alpha(R_0 + z\tan\alpha) \qquad (7.37)$$

The first part of the left term is expressed then:

$$A\frac{d^2u}{dz^2} = \frac{-2K\tan\alpha}{(R_0 + z\tan\alpha)} \qquad (7.38)$$

And the second part of the left term:

$$\frac{dA}{dz}\frac{du}{dz} = \frac{2K\tan\alpha}{(R_0 + z\tan\alpha)} \tag{7.39}$$

That is exactly the same as the first part of the left term but with opposite sign, they cancel one another. It has been shown that eq.(7.32) is a solution of eq.(7.7).

NOTE: The equation $X' + p(z)X = g(z)$ does indeed have a solution. Since $p(z)$ is continuous for a general interval $\alpha < X < \beta$, μ is defined in this interval and is a nonzero differentiable function. Both μ and g are continuous, then the function μg is integrable and the integral of the function is differentiable, so the solution for X in the shape of equation (7.25) does exist and is differentiable throughout the interval $\alpha < X < \beta$. That the solution verifies the differential equation has been demonstrated. Moreover, the boundary conditions will define constant C uniquely, so there is only one solution of the problem. In other words, the solution of the problem is characterized both by its *existence* and *uniqueness*.

7.2.4   Boundary conditions

The constants K, C can be determined with the boundary conditions. The boundary conditions of the cone problem are two:

1. The bottom of the cone corresponds to the bottom of the calibration chamber, thus it is fixed and fully rigid and no displacement is possible there:

$$z = H \Rightarrow u(H) = 0 \tag{7.40}$$

2. At the top of the cone a force is applied over a circular area in an elastic material, so the force-displacement relationship may be expressed:

$$z = 0 \Rightarrow EA\frac{du}{dz} = F \tag{7.41}$$

From boundary condition [1]:

$$C = \frac{K}{\pi\tan\alpha(R_0 + H\tan\alpha)} \tag{7.42}$$

Applying boundary condition [2] and substituting the result obtained above one can define the two constants as a function only known inputs of the problem:

$$K = \frac{F}{E} \tag{7.43}$$

and

$$C = \frac{F}{E\pi\tan\alpha(R_0 + H\tan\alpha)} \tag{7.44}$$

Finally, the definitive solution for the displacement of the cone as a function of depth can be achieved substituting the expressions (7.43) and (7.44) for the constants into eq.(7.32):

$$u(z) = \frac{F(z - H)}{E\pi(R_0 + z\tan\alpha)(R_0 + H\tan\alpha)} \tag{7.45}$$

where everything is known except the parameter z. Eq.(7.45) defines the displacement in an axially loaded elastic cone.

NOTE: According to Fig.(7.4), the normal force that generates the displacement of eq.(7.32) and (7.49) goes in the upward direction, the negative one, while the displacement follows the positive z direction. Keeping this idea in mind, one can expect that if the force applied is positive the displacement computed shall be negative or, the other way around, if to be coherent with fig.4, one can use as input $F = -N$, negative force and the result should be the same value but now a positive displacement.

7.3 Elastoplastic cone

It has been argued previously that if the loading process continues so that the stresses are larger than the elastic or yield stress, the soil will plastify. Plastification will initially take place at the top of the cone, this is the area where the load is imposed. However, the plastification will propagate downwards, increasing the plastified area (or volume in 3d) inside the cone. Logically, the test load will largely exceed the yield criteria and a the cone deformation will follow the pattern shown in fig.1. It is then of crucial importance to determine the extent of the plastification as it is in this area where the excess pore pressures will generate. First, an expression equivalent to eq. (7.45) must be obtained for the case of an elastoplastic cone.

7.3.1 Elastoplastic modeling

Roughly defined, plasticity introduces two transcendental modifications with respect to the previous elastic case:

1. Loss of linearity: tensions are no longer proportional to deformations

2. Introduction of the *permanent deformation* concept; part of the deformations generated during loading are not recovered during the unloading process.

In this case, the constitutive equation:

$$\sigma - \sigma_e = E_p(\epsilon - \epsilon_e) \tag{7.46}$$

where σ_e and ϵ_e are the elastic limit and the correspondent deformation. These values are properties of a determined soil or material type, this meaning that they are given constants.

The total deformation after an elastoplastic loading process is then:

$$\epsilon(z) = \frac{\sigma(z) - \sigma_e}{E_p} + \epsilon_e \tag{7.47}$$

Considering the cone geometry it can also be expressed:

$$\epsilon(z) = \epsilon_e(1 - E_e/E_p) + \frac{F}{\pi E_p(R_o + z\tan\alpha)^2} \tag{7.48}$$

The total displacement caused by the application of the external force in the plastified zone may be derived integrating the deformation over the extent of the plastic zone:

$$u_p = \int_0^{z_p} \epsilon(z)dz = \left[\epsilon_e(1 - E_e/E_p)z + \frac{-F}{\pi E_p \tan\alpha(R_0 + z\tan\alpha)}\right]\Bigg|_0^{z_p} \tag{7.49}$$

The total displacement of an elastoplastic cone comes from the contribution of both the displacement in the plastic area (given by eq.(7.49)) and the displacement in the elastic area. The displacement in the elastic area is the displacement of an elastic cone of height

$\bar{H} = H - z_p$. Note that eq.(7.45) is always applied on the top of the cone, thus, the following variables need to be introduced:

$$\begin{cases} \bar{H} = H - z_p \\ \bar{R}_0 = R_0 + z_p \tan \alpha \\ \bar{z} = z - z_p \end{cases}$$

$$u_e = \frac{F(\bar{z} - \bar{H})}{E_e \pi (\bar{R}_0 + \bar{z} \tan \alpha)(\bar{R}_0 + \bar{H} \tan \alpha)} \tag{7.50}$$

Undoing the change of variable the expression for the elastic displacement, for $z = z_p$:

$$u_e = \frac{F(z_p - H)}{E_e \pi (R_0 + z_p \tan \alpha)(R_0 + H \tan \alpha)} \tag{7.51}$$

Finally, if equation (7.45) was the total displacement of an elastic cone, the equivalent expression for an elastoplastic cone follows:

$$u(z) = u_e(z) + u_p(z) = \frac{F(z_p - H)}{E_e \pi (R_0 + z_p \tan \alpha)(R_0 + H \tan \alpha)} +$$

$$+ \frac{F}{\pi E_p \tan \alpha} \left[\frac{1}{R_0} - \frac{1}{R_0 + z_p \tan \alpha} \right] - \epsilon_e z_p \left(\frac{E_e}{E_p} - 1 \right) \tag{7.52}$$

7.3.2   Load-displacement curve

After the calculations, the load-displacement curve for the cone can be plotted. However, the calculations up to now have been derived for a linear elastoplasticity. In reality soil does not behave linearly, for sure not once plastified. The Dutch code presents load-displacement curves without linearity. To be able to compare the obtained one with the standardized, an extrapolation must be made: suppose the load-displacement curve obtained for the cone is also non-linear for plasticity. For the derived equations, i.e. (7.52) to be suitable, the hypothesis that all the plastic history and non-linearity is recorded in the plastic modulus E_p must be made. Then the same equations derived can be used even taking into consideration that were derived for a linear case, just supposing E_p records the translation into non-linear.

Then, the coordinates for point 1 are ($z = 0$ for the top of the elastic cone):

$$\begin{cases} F_1 = \sigma_e \pi R_0^2 \\ u_1 = \frac{F_1(-H)}{E_e \pi R_0 (R_0 + H \tan \alpha)} \end{cases}$$

And the coordinates for point 2 are (in this case the top of the elastic cone is at $z = z_p$):

$$\begin{cases} F_2 : \text{any input force larger than } F_1 \\ u_2 = \frac{F(z_p - H)}{E_e \pi (R_0 + z_p \tan \alpha)(R_0 + H \tan \alpha)} + \frac{F}{\pi E_p \tan \alpha} \left[\frac{1}{R_0} - \frac{1}{R_0 + z_p \tan \alpha} \right] - \epsilon_e z_p \left(\frac{E_e}{E_p} - 1 \right) \end{cases}$$

7.3.3   Extent of the plastic zone

This load-displacement curve that has been obtained for the cone model can now be compared to the NEN 6473 code (see fig.(7.6)). The maximum displacement at the top of an elastic cone is $0.04R_0$ and occurs when the stress level at the top is equal to the elastic limit (yield stress). When the total force is applied, there still exists an elastic cone as it has been derived above, however, its top is placed at a certain depth z_p. This is expressed:

$$0.04R_0 = \frac{-F(z_p - H)}{E_e \pi (R_0 + z_p \tan \alpha)(R_0 + H \tan \alpha)} \tag{7.53}$$
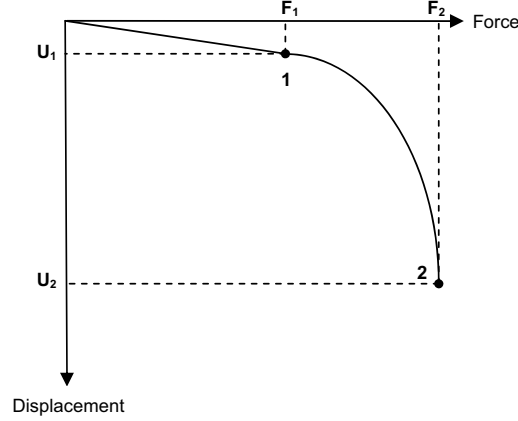
Figure 7.5: Cone load-displacement curve

This defines the extent of the plastic zone at a depth:

$$\boxed{z_p = 12cm} \tag{7.54}$$

According to the cone geometry, this corresponds to a yield stress:

$$\boxed{\sigma_e = 300kN} \tag{7.55}$$

7.4 Excess pore pressures generated

The main assumption is that excess pore pressures are only generated within the plastified area; outside it, at the elastic part, no generation takes place. With this approach, pore pressures don not dissipate instantly after removing the load because they are related to plastic deformation, but instead they will suffer consolidation with time.

As a first approach, let's evaluate which excess pore pressures would be generated if the loading process was fast enough as not to let drain at all and considering completely incompressible water filling the pores. In this case the generated excess pore pressure equals the given load. The explanation is that in the case of an incompressible pore fluid there can be no immediate volume change. Therefore there can be no vertical strain, if considering only 1D axial deformation (and later 1D axial pore water flow), without any lateral deformation. In this case, there can be no vertical strain at the moment of application of the load, and consequently the effective stress can not increase instantly. This is a situation where all the entire load is carried by the water in the pores.

$$\epsilon^T = \epsilon^p + \epsilon^e \tag{7.56}$$

The stresses are known and so are the total and elastic deformations:

$$\begin{cases} \epsilon^T = \frac{(\sigma - \sigma_e)}{E_p} \\ \epsilon^e = \frac{(\sigma - \sigma_e)}{E_e} \end{cases}$$

And the plastic deformation is:

$$\epsilon_p = \frac{(\sigma - \sigma_e)(E_e - E_p)}{E_e E_p} \tag{7.57}$$
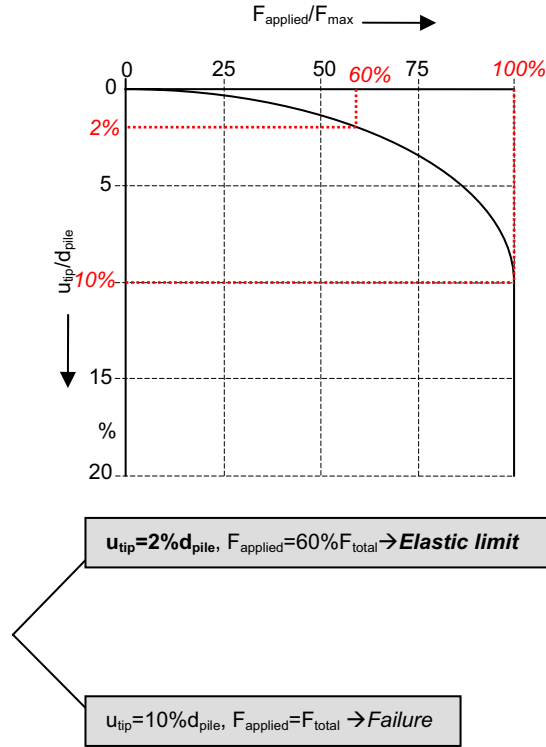
Figure 7.6: NEN 6473, load-displacement curve for displacement piles

This value of deformation corresponds to a certain stress level σ_p. This stress level is the pore pressures at that depth:

$$\sigma_p = E_p \epsilon^p = \frac{(\sigma(z) - \sigma_e)(E_e - E_p)}{E_e} \tag{7.58}$$

Finally, the generated excess pore pressures follow the distribution:

$$\bar{u} = \begin{cases} (\sigma - \sigma_e)(1 - \frac{E_p}{E_e}) & \text{if } z \leq z_p \\ 0 & \text{if } z > z_p \end{cases}$$

This would lead to a value of the excess pore pressures of:

$$\bar{u} = 5,2 MPa \tag{7.59}$$

Which is exaggeratedly large compared to the experimental values (around $0.002 MPa$ for static and $0.03 MPa$ for pseudostatic). The difference between values may be understood recapitulating the main simplification made: unidimensional deformation and flow in the direction of loading. However, in reality it is a three-dimensional case, where lateral deformations can occur and, in fact, do occur; thus, an immediate deformation is possible, although the volume must remain constant if the water is still considered incompressible. In reality then, there can be immediate change in effective stresses. It has been demonstrated that not all the load is sustained by the pore water in the tests. More insight will be

provided in the consolidation analysis. First, according to the developed cone model, 1D axial consolidation will be evaluated and the results will be discuss as well as the suitability to take into account radial and even 3D consolidation or coupled loading and consolidation.

Instead, the excess pore pressures may be more correctly estimated when relating them to the volumetric strain:

$$\bar{u} = k_f \Delta\epsilon_{vol} \tag{7.60}$$

where k_f is the compressibility of the fluid and $\Delta\epsilon_{vol}$ is the volumetric strain defined as:

$$\Delta\epsilon_{vol} = \int_0^{z_p} \epsilon_p(z)A(z)dz = \int_0^{z_p} \epsilon_p(z)\pi(R_0 + z\tan\alpha)^2 dz \tag{7.61}$$

The plastic deformation has been found in the previous subsection(see eq.(7.48)). Integrating eq.(7.61) and approximating $k_f \approx E_p$, the excess pore pressures:

$$\boxed{\Delta P_w = 0.003 MPa} \tag{7.62}$$

Which fits perfectly into the range of excess pore pressures generated for the static test.

7.5 Consolidation

7.5.1 Introduction

[1] *'A decrease of water content of a saturated soil without replacement of the water by air is called a process of* consolidation*'(Terzaghi, 1943)*

In the first instance it has been considered that the loading process is fully undrained and only after the load has been removed the excess pore pressures start to dissipate and consolidation take place. To sum up, the key assumption in the development of the analytical model is that there are two differentiate steps:

1. **Undrained loading process**: It is that process in which the variation of the load or of the boundary conditions takes place in a time frame very small compared to that necessary for the dissipation of the excess pore pressures. Hence, when saturated low permeability soil is subjected to compressional stress, the pore pressures will increase immediately but they will not dissipate immediately because of the low permeability. It can even be the case that at $t = 0$ all stress increase is taken by the pore pressure and none by the soil skeleton, taking into account water incompressibility.

   It was previously assumed that this was the case to model analytically, eventhough this study deals with sand, as it is certainly what happens under fully dynamical loading (one of the main risks of earthquakes for example is that of sand liquefaction). Despite the fact that the pseudostatic methodology is not supposed to introduce stress-waves into the soil, it still is a rapid load test, thus it seems logical to expect the loading process to be undrained, even the relatively high permeability of the soil.

2. **Consolidation**: Once the loading process is finished, the water will start to flow due to the gradient in excess pore pressures and there will be a variation in the volume of the soil. Namely, during consolidation it occurs simultaneous deformation of the porous material and flow of pore fluid.

---

[1]Theoretical concepts extracted from Lambe [48], Verruijt [49], Das [50] and Atkinson [51].

There will be an increase in bearing capacity of the pile controlled by the dissipation of excess pore pressures and the increase in effective stresses. Note that as the excess pore pressures diminishes, the hydraulic gradients and the rates of flow also diminish, so that the volume changes and effective stress increments continue at reducing rates.

7.5.2 Certainty or uncertainty of the hypothesis of undrained loading

It has been argued that when first thinking of the problem it seems justified to expect the loading process to be undrained. However, still from a theoretical point of view there are two ideas that should make the reader be doubtful:

- **Loading rate**: A previous study by J.Dijkstra [5] in dry sand did not recod a remarkable loading rate effect while comparison pseudostatic-static results. May this mean that the pseudostatic test is fast enough as to be a thrilling economical option but, on the other hand, its rate of loading is not large enough as to produce different results from the static ones? Hence, may it be the case that the soil behaves almost as in the static test and so the loading process may not be fully undrained, nor fully drained?

- **Soil type**: Not to forget the material in question is sand not clay. Sand is always considered in the literature to drain under loading, although it has been pointed out the shortcoming in the available literature when related to saturated sand under pseudostatic loading conditions. Besides, some authors have noted that very rapid loading of coarse-grained material is likely to be undrained.

For more consistency, this study consists also in a numerical model and experimental tests in a calibration chamber. Two results should attract our attention:

- **Experimental testing**: The results of the tests done with E.Archeewa demonstrated the certainty about the excess pore pressure generation. For the rapid test, excess pore pressures up to 10 times larger than found in static results were generated. Surely then the loading process is not drained and there is some effect of the loading rate in the saturated material behavior. However, the same test series showed no difference is found in the bearing capacity values when using pseudostatic test or static one, which is an accordance with Dijkstra's results for dry sand. If the loading process was fully undrained it should be reflected in lower bearing capacities for the pseudostatic test, as the excess pore pressures reduce the effective stresses acting on the pile. However, experimental results prove the fully undrained loading hypothesis wrong.

- **Numerical results**: The analytical modeling has been carried out simultaneously with a numerical one. It will be presented later in this report that a fully undrained calculation in PLAXIS gives soil failure for too low loads when compared to the experimental values. Once more, results are not precisely pointing towards the case of undrained loading process.

The available results seem to indicate that the loading process is not fully undrained, nor fully drained. It is probably the case of coupled loading and consolidation, partial drainage.

It seems logical to finally check analytically the accuracy of the above statement. Some more theoretical considerations related to drainage and consolidation will follow in the next lines.

It is crucial to make clear that when distinguishing between drained and undrained loading

it is the relative rates of loading and seepage that are important and not the absolute rate of loading. In pseudostatic tests loading rates as high as $250mm/s$ occur. Besides, the flow rate is determined by Darcy's law, with the permeability as a key governing parameter. The value of k (permeability) is the seepage velocity of water through soil with unit hydraulic gradient and this value for sands typically falls into the range $10^{-1} - 10^{-5}(m/s)$. Hence, loading rate and seepage rate are probably of the same order; it is coherent to expect the dissipation of excess pore pressures to start while loading process is going on.

Another crucial concept to introduce is that of the *coefficient of consolidation*.It is defined:

$$c_v = \frac{k}{\gamma_w m_v} \tag{7.63}$$

where k is the coefficient of permeability, γ_w is the water specific weight and m_v is the coeffcent of volumetric variation ($m_v = \Delta\epsilon_v/\Delta\sigma_v$). The coefficient of consolidation can be determined performing an eodometric test.
Related to the coefficient of consolidation a *time factor* can be introduced as the ratio:

$$T_v = \frac{c_v t}{h^2} \tag{7.64}$$

where c_v is the coefficient of consolidation, t is a characteristic time and h is the average draining length. Note that we are considering 1D consolidation. To know whether we need to take into account consolidation or not we need to evaluate this time factor. For $T > 1$ the process can be considered fully drained, thus consolidation can be disregarded. In general, the time necessary for fully complete consolidation is proportional to $\frac{h^2 m_v}{k}$ although according to Verruijt [49] the consolidation can be considered finished when:

$$T_v = \frac{c_v t}{h^2} > 2 \tag{7.65}$$

Then, the time required for the consolidation process to be finished can be calculated:

$$t_{99\%} = \frac{2h^2}{c_v} \tag{7.66}$$

Note that the consolidation process is governed by the factor $c_v t/h^2$ so its duration can be shortened considerably reducing the drainage length.

Moreover a *degree of consolidation* can be presented, which indicates how far the consolidation process has reached at a certain time, hence, relates the current excess pore pressure to the original one:

$$U = 1 - \frac{\bar{u}}{u_0} \tag{7.67}$$

where $\bar{u}$ is the excess pore pressure at that given time and u_0 is the maximum initial excess pore pressure. It can be expressed as well as a function of the time factor, for small values of time:

$$U = \frac{2}{\sqrt{\pi}}\sqrt{\frac{c_v t}{h^2}} \tag{7.68}$$

From eq.() it can be estimated how short must be the loading time to be considered instantaneous.

$$t_{1\%} = 10^{-4}\frac{h^2}{c_v} \tag{7.69}$$

A load that is applied faster than this $t_{1\%}$ can be considered an instantaneous load.

No oedometric results are available. Any further investigation on this topic should have good soil data avaiable. If the following approximation is made:

$$m_v \approx 1/E \qquad (7.70)$$

and taking average sand permeability values, the coefficient of consolidation is around $0.3m^2/s$. The pseudostatic tests took some $0.04 - 0.06s$. Therefore, if the consolidation started at the same time as the load application -which does not- by the end of the test $T_v \approx 0.85$, in 1D axial consolidation in a 12cm thick draining stratum. For T_v values larger than 1 it is the fully drained case, so 0.85 should correspond to partial drainage, for sure not undrained case. Of course the consolidation does not start immediately when the load is applied, there must be a time lapse. This is maybe the most remarkable unknown question: it will be proved that the consolidation process does take place when loading, not after as would correspond to the undrained case, but, when does the consolidation process start. Surely the fact that is starts later in the loading time should make it also finish later, but one must remember all these calculations are for 1D and in reality there would be 3D consolidation which would occur naturally much faster.

7.5.3 Consolidation model

Problem definition

In the previous subsection it has been demonstrated that the loading process is not fully undrained but instead the loading and the consolidation processes take place simultaneously. Also it has been seen that not all the load is carried by the water instantly, as it corresponds to a more complicated multidimensional deformation and consolidation problem. By now, two of the principal assumptions of the model, namely 1D case (for simplification reasons) and undrained loading (due to the rapid load application it could have been expected), have been demonstrated to be wrong.

However, to model analytically loading, generation of excess pore pressures and consolidation all almost in the same time frame and 2 or 3D is complex. What interests the engineer is to obtain a simple and straightforward manner to model analytically the pseudostatic test or, at least, give insight in the behavior of the soil under those conditions. Then, to account for the generation of excess pore pressures the simplest available approach is that of undrained loading and subsequent consolidation, as it was the original idea. The calculations for this model are be computed despite the previous statements, and in the end the correctness and suitability of the results is to be discussed. It can be interesting to see which results the first idea of the problem may give, keeping in mind which error we might me introducing and why. Further on more attention to the coupled loading-consolidation equation can be paid if necessary.

The next step is then to model the consolidation process. Remember the another of the key assumptions: excess pore pressures are only generated in the plastic zone. Thus, the flow will be towards the elastic area below and also to the laterals of the cone. It would be a 2D consolidation problem. This is a difficult situation to model analytically and even numerical models seem more suitable. Besides, one of the definition statements of Wolf's cone model is that the soil outside the cone can be neglected. Nevertheless, different authors have studied excess pore pressures generated during pile driving and have explained the flow to be mainly radial (Randolph, Wroth [41]). To sum up: it is a very complicated problem to solve analytically with high accuracy. It is very important to understand this difficulties and why they arise. Once this is understood, some assumptions will require to be made in order to propose a simplified model. Again, it is important to understand the shortcomings and limitations this assumptions may introduce. In the end, this considerations should introduce a degree of perspective and relativity in whatever the

results are and their application and correctness.

They main problems to face in the consolidation modelling are:

1. It is not really an undrained loading process but instead a coupled loading-consolidation one.
   Even separating the processes of loading and consolidation, to make the model more simple, one finds new trouble in the consolidation modelling:

2. Consolidation, and deformation, will be 2-dimensional, this is, axially and radially. Even more, in practice it should be 3D, but axisymmetry can simplificate it to 2D. Even considering only 1D consolidation, either axial or radial, one finds new trouble in the consolidation modelling:

3. Excess pore pressure variation with radius has not been obtained in the previous cone model.
   Even considering only 1D axial consolidation, one finds new trouble in the consolidation modelling:

4. Excess pore pressure distribution not constant, not even linear within the plastic zone. The initial condition is coupled with the boundary condition.

5. Area of the cone not constant with depth.

6. Boundary condition in the plastic-elastic boundary: in $t = 0$, $\bar{u} = 0$. However once the consolidation process starts for $t > 0$, $\bar{u} \neq 0$ until the consolidation has finished. To put it in words, it is not really a fully drained boundary.

To define the problem in a simple way, the following assumptions may be made:

1. Undrained loading process + consolidation after the load has been removed.

2. 1D consolidation only in the direction of the application of the load (axially).

3. Soil behaves elastically during consolidation.

4. Plastic-elastic limit is a full drained boundary for any time.

Assumption (1) solves problem (1); assumption (2) solves problems (2) and (3). Assumption (3) allows for the application of Terzaghi's equation and the classical consolidation theory. Besides it has been proved not to be so inaccurate as during consolidation soil mainly moves backward toward the pile, undergoing an unloading process in shear (Randolph, Wroth [41]). Thanks to assumption (3) problem (5) can be disregarded as the area does not appear in the consolidation equation of Terzaghi, it disappeared when combining volume variation with Darcy's law. Last assumption (4) solves problem (6). Just problem (4) remains unsolved by now, but it will be dealt with during the calculations.

Finally, the consolidation problem to analyze is:
The equation to solve:

$$\frac{\partial \bar{u}}{\partial t} = c_v \frac{\partial^2 \bar{u}}{\partial z^2} \tag{7.71}$$

which is the equation of consolidation of Terzaghi.

Two boundary conditions:

1. At the lower limit of the drainage area (plastic-elastic limit) the excess pore pressure is always 0 (fully drained boundary):

$$z = z_p \Rightarrow \bar{u}(z_p) = 0 \tag{7.72}$$

2. At the upper limit of the drainage area there is the pile and this one is not removed after the test and is impermeable (fully undrained boundary):

$$z = 0 \Rightarrow \frac{\partial \bar{u}}{\partial z} = 0 \qquad (7.73)$$

And one initial condition:

1. At the time of loading an immediate increase in excess pore pressure is generated, which has been discussed before. It follows:

$$t = 0 \Rightarrow \bar{u} = \bar{u}(z) \qquad (7.74)$$
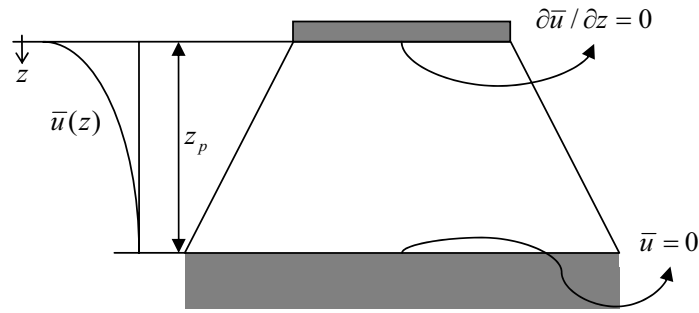
Figure 7.7: 1D Axial consolidation

Equation solution

The consolidation equation is a 2nd order partial differential equation that can be solved by means of separation of variables or Laplace transform. Here the first procedure will be considered.

The separation of variables technique makes one defining assumption and that is that the solution $\bar{u}$ is a product of two functions, one in z and one in t:

$$\bar{u} = Z(z)T(t) \qquad (7.75)$$

The partial derivatives follow:

$$\begin{cases} \frac{\partial \bar{u}}{\partial t} = Z(z)T'(t) \\ \frac{\partial^2 \bar{u}}{\partial z^2} = Z''(z)T(t) \end{cases}$$

and then the equation of consolidation can be rewritten:

$$Z(z)T'(t) = c_v Z''(z)T'(t) \qquad (7.76)$$

or also:

$$\frac{Z''(z)}{Z(z)} = \frac{1}{c_v}\frac{T'(t)}{T(t)} \qquad (7.77)$$

where the left side term is independent of t and the right-hand one is independent of z. Then, the derivatives and original functions can be related to each other by a constant:

$$\begin{cases} Z''(z) = -B^2 Z(z) \\ T'(t) = -B^2 c_v T(t) \end{cases}$$

These two equations have respectively solutions of the shape:

$$\begin{cases} Z(z) = A_1 \cos Bz + A_2 \sin Bz \\ \quad T(t) = A_3 exp(-B^2 c_v t) \end{cases}$$

And combining the solutions that of the main equation can be found:

$$\bar{u} = Z(z)T(t) = (A_4 \cos Bz + A_5 \sin Bz)exp(-B^2 c_v t) \tag{7.78}$$

with $A_4 = A_1 A_3$ and $A_5 = A_2 A_3$. The constants have to be determined with the boundary conditions. From the second boundary condition:

$$\frac{\partial \bar{u}}{\partial z} = (-A_4 B \sin 0 + A_5 B \cos 0)exp(-B^2 c_v t) = 0 \Rightarrow A_5 = 0 \tag{7.79}$$

From the first boundary condition:

$$0 = A_4 \cos Bz_p exp(-B^2 c_v t) \tag{7.80}$$

which only has two possible solutions for all t, $A_4 = 0$ or $Bz_p = n\frac{\pi}{2}$ that would mean:

$$B = \frac{n\pi}{2z_p} \tag{7.81}$$

Substituting into (7.65):

$$\bar{u} = \sum_{n=1}^{n=\infty} A_n \cos(\frac{n\pi}{2z_p}z)exp\Big(-\frac{n^2\pi^2}{z_p^2}c_v t\Big) \tag{7.82}$$

According to Das [50], it can also be rewritten:

$$\bar{u} = \sum_{n=1}^{n=\infty} A_n \cos(\frac{n\pi}{2z_p}z)exp\Big(-\frac{n^2\pi^2 T_v}{4}\Big) \tag{7.83}$$

where T_v is an adimensional factor equal to $c_v t/H^2$ and H is half the total thickness in a two-way drainage condition. In this case there is only a one way drainage condition, hence, the longest drainage path possible equals the thickness of the draining layer, namely, the plastic zone, thus $H = z_p$. Applying the initial condition ($t = 0 \Rightarrow u = u_i$):

$$u_i = \sum_{n=1}^{n=\infty} A_n \cos(\frac{n\pi}{2z_p}z) \tag{7.84}$$

Eq.(7.78) is a Fourier cosine series, then A:

$$A_n = \frac{1}{z_p} \int_0^{z_p} u_i \cos(\frac{n\pi z}{2z_p})dz \tag{7.85}$$

Combining eq.(7.77) and eq.(7.79):

$$\bar{u} = \sum_{n=1}^{n=\infty} \left[\frac{1}{z_p} \int_0^{z_p} u_i \cos(\frac{n\pi z}{2z_p})dz\right] \cos(\frac{n\pi}{2z_p}z)exp\Big(-\frac{n^2\pi^2 T_v}{4}\Big) \tag{7.86}$$

In his book Das [50] developed achieved an equivalent expression to (7.80) but for a two-way drainage ($H = z/2$); the only difference between his solution and (7.80) is due to the different boundary condition at the top of the layer. This leads to finding sin where the current solution has a cos. He developed the solution to his consolidation problem for several cases, among them:

- **Linear variation of u_i:** $u_i = u_0 - u_1 \frac{H-z}{H}$:

$$\bar{u} = \sum_{n=1}^{n=\infty} \left[\frac{1}{H} \int_0^{2H} \left(u_0 - u_1 \frac{H-z}{H} \right) \sin(\frac{n\pi z}{2H}) dz \right] \sin(\frac{n\pi}{2H}z) exp\left(-\frac{n^2\pi^2 T_v}{4} \right) \quad (7.87)$$

- **Sinusoidal variation of u_i:** $u_i = u_0 \sin \frac{\pi z}{2H}$

$$\bar{u} = \sum_{n=1}^{n=\infty} \left[\frac{1}{H} \int_0^{2H} u_0 \sin(\frac{\pi z}{2H}) \sin(\frac{n\pi z}{2H}) dz \right] \sin(\frac{n\pi}{2H}z) exp\left(-\frac{n^2\pi^2 T_v}{4} \right) \quad (7.88)$$

Parallely, in the one-way drainage equation for the cone consolidation we can express:

- **Linear variation of u_i:** $u_i = u_0 - u_1 \frac{z_p - z}{z_p}$:

$$\bar{u} = \sum_{n=1}^{n=\infty} \left[\frac{1}{z_p} \int_0^{z_p} \left(u_0 - u_1 \frac{z_p - z}{z_p} \right) \cos(\frac{n\pi z}{2z_p}) dz \right] \cos(\frac{n\pi}{2z_p}z) exp\left(-\frac{n^2\pi^2 T_v}{4} \right) \quad (7.89)$$

- **Sinusoidal variation of u_i:** $u_i = u_0 \sin \frac{\pi z}{z_p}$

$$\bar{u} = \sum_{n=1}^{n=\infty} \left[\frac{1}{z_p} \int_0^{z_p} u_0 \sin(\frac{\pi z}{z_p}) \cos(\frac{n\pi z}{2z_p}) dz \right] \cos(\frac{n\pi}{2z_p}z) exp\left(-\frac{n^2\pi^2 T_v}{4} \right) \quad (7.90)$$
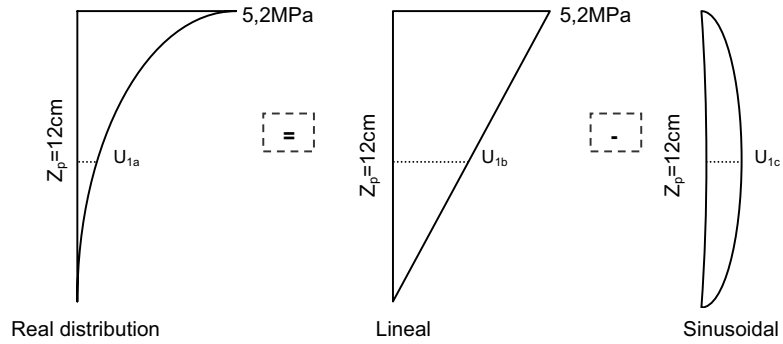
Figure 7.8: Pore pressure diagram approximation

According to the figure, the excess pore pressure distribution in the plastic area can be approximated as the difference between a linear function and a sinusoidal one, thus, subtracting (7.84) to (7.83). This solves the last remaining problem of how to apply the initial excess pore pressure non-linear distribution with depth.

$$\bar{u} = \sum_{n=1}^{n=\infty} \left[\frac{1}{z_p} \int_0^{z_p} \left(u_0 - u_1 \frac{z_p - z}{z_p} - u_0 \sin(\frac{\pi z}{z_p}) \right) \cos(\frac{n\pi z}{2z_p}) dz \right] \cos(\frac{n\pi}{2z_p}z) exp\left(-\frac{n^2\pi^2 T_v}{4} \right)$$
$$(7.91)$$

Eq.(7.88) may be easier solved considering first the two separate components (linear and sinusoidal distributions). The linear distribution follows:

$$u_i(z) = u_0 - \frac{u_0}{z_p}z \quad (7.92)$$

where u_0 is the maximum excess pore pressure, located at the top of the cone. Substituting into eq.(7.83) for the two-way drained cone and performing the required calculations:

$$\bar{u}_{lin}(z,t) = \frac{4u_0}{\pi^2} \cos(\frac{\pi z}{2z_p}) \exp(\frac{-\pi^2 T_v}{4}) \tag{7.93}$$

On the other hand, the sinusoidal distribution for the cone case would be:

$$u_i(z) = u_{1c} \sin(\frac{\pi z}{z_p}) \tag{7.94}$$

where $u_{1c} = u_{1b} - u_{1a}$ (see figure (7.8)). Substituting into the general sinusoidal equation (7.84) and integrating:

$$\bar{u}_{sin}(z,t) = \frac{4u_{1c}}{3\pi} \cos(\frac{\pi z}{2z_p}) \exp(\frac{-\pi^2 T_v}{4}) \tag{7.95}$$

Finally, the solution to the axial consolidation in the cone is the combination of the two obtained expressions eq.(7.89)-eq.(7.87).

$$\boxed{\bar{u}(z,t) = \frac{4}{\pi} \left(\frac{u_0}{\pi} - \frac{u_{1c}}{3} \right) \cos\left(\frac{\pi z}{2z_p} \right) \exp\left(\frac{-\pi^2 T_v}{4} \right)} \tag{7.96}$$

Degree of consolidation

Pore pressures are directly linked to deformations. To describe the deformation as a function of time, the *degree of consolidation* proves useful. The degree of consolidation, at any time and at any depth, was defined as the relation between the excess pore pressure that has been dissipated and the initial excess pore pressure, this is, how far the consolidation has progressed. It may be the case that what is of interest is the average degree of consolidation over an entire layer, that can be expressed according to Das [50]:

$$U_{av} = \frac{(1/H_t) \int_0^{H_t} u_i dz - (1/H_t) \int_0^{H_t} \bar{u} dz}{(1/H_t) \int_0^{H_t} u_i dz} \tag{7.97}$$

where H_t is the total thickness of the layer, u_t the initial excess pore pressure and u the actual excess pore pressure. In the cone model case it is interesting to see the evolution in time of the degree of consolidation of the plastic zone, that acts as the layer in question. Once more Das [50] proposed some solutions for general cases:

- **Linear variation of u_i:**

$$U_{av} = 1 - \sum_{m=0}^{m=\infty} \frac{2}{M^2} exp(-M^2 T_v) \tag{7.98}$$

  where $M = (2m + 1)\pi/2$.

- **Sinusoidal variation of u_i:**

$$U_{av} = 1 - exp(\frac{-\pi^2 T_v}{4}) \tag{7.99}$$

Following the approximation of the initial excess pore pressure distribution as the difference between a linear one and a sinusoidal one, the average degree of consolidation in the plastic zone may be estimated:

$$U_{av}(T_v) = \frac{U_{av}^{linear}(T_v)A_1 - U_{av}^{sin}(T_v)A_2}{A_1 - A_2} \tag{7.100}$$

where A_1 and A_2 are respectively the areas of the linear and the sinusoidal diagrams.

$$\begin{cases} A_1 = \frac{1}{2}z_p u_0 = 312 kN/m^2 \\ A_2 = \sum_{z=0}^{z=z_p} u_{1c} sin(\frac{\pi z}{z_p})dz = \int_{z=0}^{z=z_p} u_{1c} sin(\frac{\pi z}{z_p})dz = 181.8 kN/m^2 \end{cases}$$

The values of the degree of consolidation for both linear and sinusoidal distributions are tabulated for different time factors. It is especially interesting to evaluate the case for $t = t_{test} \approx 0.04s$. The corresponding T_v is $Tv = c_v t/z_p^2 = 0.85$. It can be seen that, mainly due to the large permeability of sand, $U_{av}(T_v = 0.85) = 92.23\%$, this is, the consolidation process is almost finished by the end of the loading process.

7.5.4 Radial consolidation

Problem definition

The equation for radial consolidation was derived by Scott in 1963:

$$c_r\left(\frac{\partial^2 u}{\partial r^2} + \frac{1}{r}\frac{\partial u}{\partial r}\right) = \frac{\partial u}{\partial t} \tag{7.101}$$

Radial consolidation normally occurs in axisymmetrical problems where there is radial transitory flux but the axial flux is nil. In the case we are studying it seems logical to expect consolidation to happen both radially and axially. Up to now, the evaluation of a simplified case where only axial consolidation takes place has been developed. The next step is, still in the 1D assumption, to consider the fluid to flow radially from the center of the cone outwards, neglecting the axial flux toward the elastic part.

The problem is fully defined with the boundary and initial conditions and the radial consolidation equation. Two boundary conditions are required:

1. There is no flow between the two symmetrical halves of the cone, the axis of symmetry may be modeled as a fully undrained boundary:$r = 0 \Rightarrow \frac{\partial \bar{u}}{\partial r} = 0$

2. At the lateral boundary of the cone the excess pore pressure is always kept to zero. By definition, in the cone model of Wolf, the soil outside the cone can be neglected. Now this soil is supposed to act as a fully drained boundary: $r = \bar{r} = R_0 + z\tan\alpha \Rightarrow \bar{u} = 0$

And one initial condition. The problem of defining the initial excess pore pressure distribution as a function of the radius arises due to the fact that the excess pore pressures in the cone have only been obtained as a function of depth. The deformation of the cone has been derived only in z, the excess pore pressures are directly related to the plastic deformation. Therefore, it should be possible to approximate the radial distribution by relating the horizontal deformation to the vertical one by means of the Poisson ratio ($\epsilon_r = \nu\epsilon_z$). However, looking more into the geometry one could expect the radial excess pore pressures to be constant, for a certain given depth, throughout the pile section and then start to decrease as the cone expands as shown in the figure. This gives complicated expressions to work with. As a simplification, the radial excess pore pressures will be assumed to be constant with the radius.In this way, the calculations, when related to the Bessel functions are easier. Then, the initial condition:

1. $t = 0 \Rightarrow \bar{u} = \bar{u}, \forall r$

where $\bar{u}$ is a constant value.

Equation solution

Eq.(7.101) is more difficult to solve than the equation for axial consolidation. Randolph and Wroth [41] proposed an analytical solution for the consolidation around a driven pile,

where the gradients were mainly radial. By means of separation of variables and Bessel functions, the solution has the general form:

$$\bar{u} = Be^{-\alpha^2 t}[J_0(\lambda r) + \mu Y_0)(\lambda r)] \tag{7.102}$$

where $-\alpha^2$ is a separation constant.J_0 and Y_0 are Bessel functions of first and second kind. The linear combination of $J_0(\lambda r) + \mu Y_0(\lambda r)$ is a cylinder function $C_0(\lambda r)$. Boundary condition [1] implies that:

$$C_1(0) = J_1(0) + \mu Y_1(0) = 0 \tag{7.103}$$

The Bessel function of second order and second kind $(Y_1(x))$ presents a singularity for $(x = 0)$. Hence, the only option remaining is:$\mu = 0$.
Form boundary condition [2]:

$$C_0(\lambda\bar{r}) = J_0(\lambda\bar{r}) = 0 \tag{7.104}$$

The values of $\lambda\bar{r}$ such that they make the Bessel function of first order and first kind equal to zero are tabulated.
In the end, what we get is:

$$\bar{u} = Be^{-\alpha^2 t}J_0(\lambda r) \tag{7.105}$$

Also applying the initial condition:

$$u_0 = \sum_{n=1}^{\infty} B_n J_0(\lambda_n r) \tag{7.106}$$

and then:

$$\int_0^{\bar{r}} u_o r J_o(\lambda_n r) dr = \frac{B_n}{2}[\bar{r}^2 J_1^2(\lambda_n \bar{r})] \tag{7.107}$$

Integrating the left term of eq.(98), according to the rules of integration of the Bessel functions the formal solution for the radial consolidation problem can be obtained. First, the values of the constant B_n can be expressed:

$$B_n = \frac{2u_0}{\lambda_n^2} \frac{[\lambda_n/2 J_1(\lambda_n\bar{r}) + J_0(\lambda_n\bar{r}) - 1]}{\bar{r}^2 J_1^2(\lambda_n\bar{r})} \tag{7.108}$$

So the formal solution for the radial consolidation:

$$\bar{u}(r,t) = \frac{2u_0}{\lambda_n^2} \frac{[\lambda_n/2 J_1(\lambda_n\bar{r}) + J_0(\lambda_n\bar{r}) - 1]}{\bar{r}^2 J_1^2(\lambda_n\bar{r})} e^{-\alpha^2 t} J_0(\lambda_n r) \tag{7.109}$$

What follows is a very complicated evaluation to do by hand and is best computed numerically. No more detail is provided here.

7.5.5 Coupled loading and pseudodimensional consolidation

The reasons for the incorrectness of the undrained loading followed by a consolidation process have been explained in detail and supported by analytical results. It has been justified why in reality what takes place is both loading and consolidation simultaneously. Besides, this consolidation is not unidimensional but both radial and axial. Therefore, it can be stated that pseudostatic tests in saturated sand generate instantly excess pore pressures that dissipate during the time lapse in which the load is applied; the loading-consolidation for a pseudostatic test in saturated sand is governed by the equation:

$$c_v\Big(\frac{\partial^2 u}{\partial z^2} + \frac{\partial^2 u}{\partial r^2}\Big) = \frac{\partial u}{\partial t} - \frac{\partial \sigma}{\partial t} \tag{7.110}$$

Eq.(7.110) has to be solved numerically, however this falls beyond the scope of this thesis. Nevertheless, the effects could be roughly appreciated with a pseudobidimensional analysis.

Considering the total degree of consolidation it is possible to picture out an idea of the rate of dissipation of excess pore pressures. The results from the unidimensional analysis in z and r may be combined to finally estimate which would the degree of consolidation be if the radial problem was solved:

$$U_{zr} = 1 - (1 - U_z)(1 - U_r) \tag{7.111}$$

Chapter 8

Analytical results and evaluation

8.1 Results presentation and analysis

8.1.1 Solution evaluation

The most straightforward way to understand and evaluate eq.(7.93) is to plot it. It can
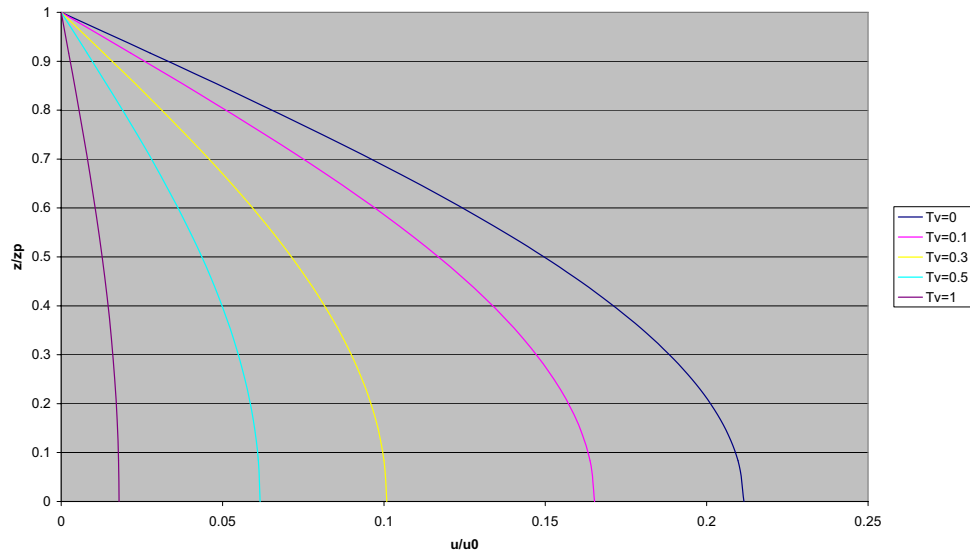
Figure 8.1: 1D consolidation analytical solution

be seen that for $z = z_p$ the excess pore pressure is always zero because the $\cos(n\pi/2) = 0$ which satisfies the boundary condition (7.69). The boundary condition (7.70) is also satisfied. It can be checked differentiating eq.(7.98) with respect to z, a factor $sin(...z)$ appears and it is always zero for $z = 0$. To check the initial condition it is more difficult. However, looking into eq.(7.98) with more detail, the first constant factor $\frac{4}{\pi}(\frac{u_0}{\pi} - \frac{u_{1c}}{3})$ should strike the reader's attention. It is certainly derived from the approximation of the initial condition as a difference of a linear and a sinusoidal functions. Verruijt [49] solved a consolidation problem with the same boundary conditions but the initial condition stated constant excess pore pressure all over the domain at $t = 0$. For large time values he

simplified it:

$$\frac{c_v t}{h^2} >> 0.1 : \frac{\bar{u}}{u_0} \approx \frac{4}{\pi} \cos(\frac{\pi}{2}\frac{z}{h}) exp(-\frac{\pi^2}{4}\frac{c_v t}{h^2}) \tag{8.1}$$

which is exactly as the derived eq.(7.98) with the exception of the constant factor $\frac{4}{\pi}$. Hence, the initial condition is the key element determining this constant value. For Verruijt's [49] solution one can see that instantly when t and z equal 0, the cosine and exponential terms equal 1 and $\bar{u}(0,0) = \frac{4}{\pi}u_0$. It is characteristic of the coupled consolidation solutions to present an instantly increase in the excess pore pressure at the start of the process. This is the Mandel-Cryer effect. However, in our case it is the opposite:

$$\bar{u}(0,0) = \frac{4}{\pi}(\frac{u_0}{\pi} - \frac{u_{1c}}{3}) \tag{8.2}$$

which is notably smaller than u_0. It seems instead of an instantly increase the derived solution presents and instantly decrease in the value of the pore pressure. It may be explained looking back at the initial condition. The approximation itself, linear minus sinusoidal,is not bad, it could even be considered good enough. The problem is the combination with boundary condition (7.70). Eq.(7.70) states there is no flow in $z = 0$ which is a correct way of indicating the presence of an impermeable boundary. Nevertheless, the inital condition seems to contradict it as the linear distribution leaves an area in the shape of a triangle which means that large gradients exist around $z = 0$. This somehow inconsistency is the reason of the awkward initial value of the problem, as if eq.(7.98) could not account for the initial large gradients. It is not that the problem is wrongly defined, the boundary and initial conditions are true (obviously the steel pile is impermeable and the maximum initial excess water pressure will be found at its contact with the soil), the complication is that of combining the non-linear pressure distribution with the boundary conditions. Eq.(7.98) is an exact analytical solution to an analytical problem and this process is correct; but it can not be considered an exact analytical solution to the *real* problem.

8.1.2   Derived results

The analytical solution for the consolidation equation can be plotted without taking into consideration the first constant factor, that was discussed on the previously, and the graphical solution is in accordance to available ones in the literature. It is plotted against Tv. If the coefficient of consolidation is estimated, the same plot could be done in function of time in absolute terms. The coefficient was estimated in the previous chapter to corroborate the hypothesis of partial drainage, so it could be easily done. Still it was a very rough estimation and besides the initial consolidation time is unknown, for these reasons the plots are left in function of T_v. It would show that, due to the high permeability of the sand, combined with the relatively long duration of the pseudostatic test, the dissipation is completed, or almost completed (degree of consolidation almost 1)when the application of the load finishes. This supports the idea derived from the experimental tests that the loading process is not fully undrained. Besides, the excess maximum pore pressure calculated for fully undrained case was $5, 2MPa$, far more larger than the one recorded in the tests. Therefore no there was no effect of the generated excess pore pressures in the bearing capacity.

The solution can also be presented graphically by plotting the variation of excess pore pressure with depth at certain times; the resulting family of curves are called *isochrones*. They start almost perpendicular to the x-axis for $z = 0$, at the surface of the cone, indicating there is an impermeable boundary there, and converge at $z = 12cm$, the end of the plastified area, where the excess pore pressure is always zero as indicated by the fully drained boundary condition. The gradient of an isochrone is related to the hydraulic gradient by:

$$\frac{\partial \bar{u}}{\partial z} = -\gamma_w i \tag{8.3}$$
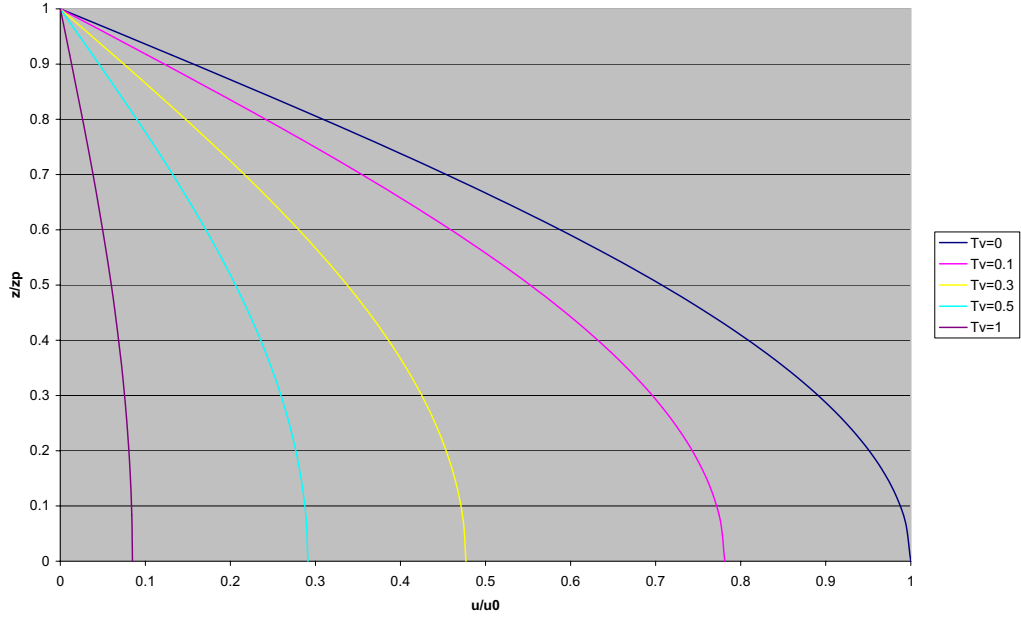
Figure 8.2: Analytical solution for 1D axial consolidation(without constant term)

and from Darcy's law, the seepage velocity is:

$$V = -\frac{k}{\gamma_w}\frac{\partial \bar{u}}{\partial z} \tag{8.4}$$

At the surface of the cone there is no seepage flow, because the boundary was defined to be impermeable. But just a little deeper into the soil, for depths as 2cm, the gradient for small values of time increases abruptly and remains kind of constant for the rest of the stratum, once more explaining the large flow that occur. Isochrones normally show increasing gradients, thus increasing seepage velocities, towards the drain, in this case, because of the way the initial condition was defined, large gradients also occur close to the impermeable boundary.

The shape of the isochrones, even for $Tv = 0$ displays an interesting feature: immediately when consolidation starts even the top of the cone starts to drain. In 1D consolidation, it is common for isochrones properties in general to find that for small times (i.e. $t = Tv = 0$) consolidation is limited to a certain depth of the layer while the for the rest pore pressures have not yet start to fall. In this cases, a critical time t_c can be defined when excess pore pressures start to decrease also at the other boundary, the non-draining one. However it seems in this case the solution starts directly at this critical time and the whole stratum drains from the beginning. This can be corroborated looking at the dissipation plot. Even for $z = 0$, at the top, pore pressures start to decrease as soon as consolidation begins. This large gradients can explain why the excess pore pressures dissipate so fast and do not affect pile's bearing capacity. The figure of the dissipation also shows that the initial value at the top of the cone according to the derived consolidation solution is not the $5.2MPa$ that had been estimated, $\bar{u}(0,0) \neq u_0$. This feature of the solution was previously discussed.

The movement of the isochrones represents the changes in excess pore pressures and effective stress. Again, large changes occur in for really small values of time, logical if one keeps in mind that the soil type is sand. The values of permeability and compressiblity of
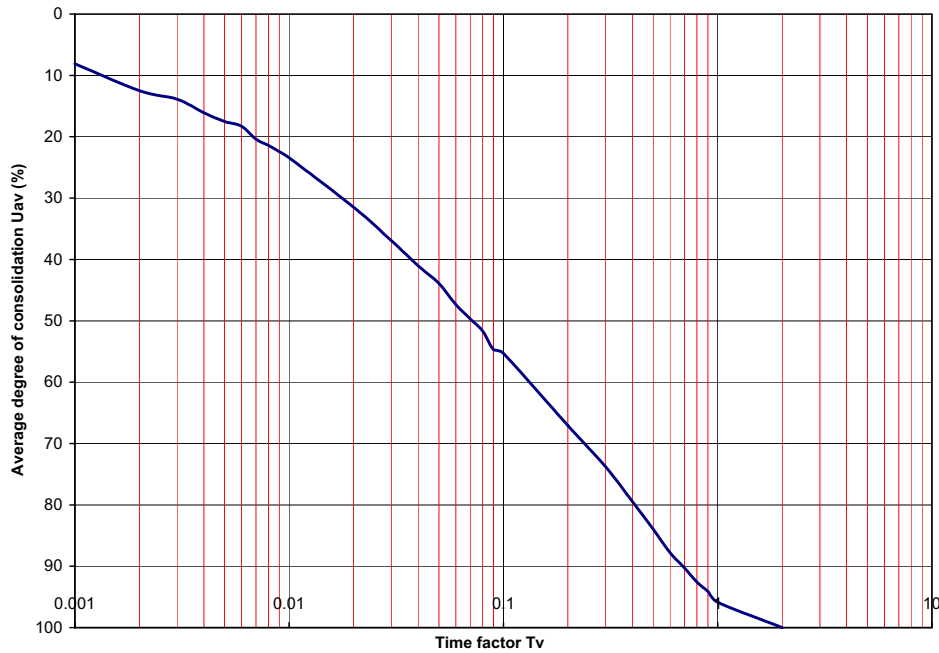
Figure 8.3: Degree of consolidation

the soil determine these variations.

8.2   Model evaluation

Despite all the limitations and assumptions that were made in the definition of the analytical model, it has been useful to corroborate the conclusions of the experimental tests. The amount of simplifications made much limits the application of the model as a predicting tool or quantitative evaluation. However, it was designed to check the experimental results, not to predict them, and, qualitatively, this has succeeded. It proves useful to achieve better scientific insight into the problem and further understand the conclusions that had been derived in the first part and why they have been so. Some questions, though, remain unanswered, among them:

- Lack of quality data from the soil properties⇒the coefficient of consolidation c_v can be only roughly estimated. It is decisive to determine the degree of drainage/undrainage of the problem. Right now one can only state that it is a case of 'partial drainage', nothing else.

- It remains unknown when drainage starts. From the experimental plots it was argued that there was a time lapse between the maximum pore pressure recorded and the maximum bearing capacity. It is indeed a problem in time, more analytical detail and understanding should be obtained.

- Dynamics, even if it is only low-frequency, occur. It would be interesting to incorporate them to the model. Information about inertia and damping should be contrasted with the static approach.
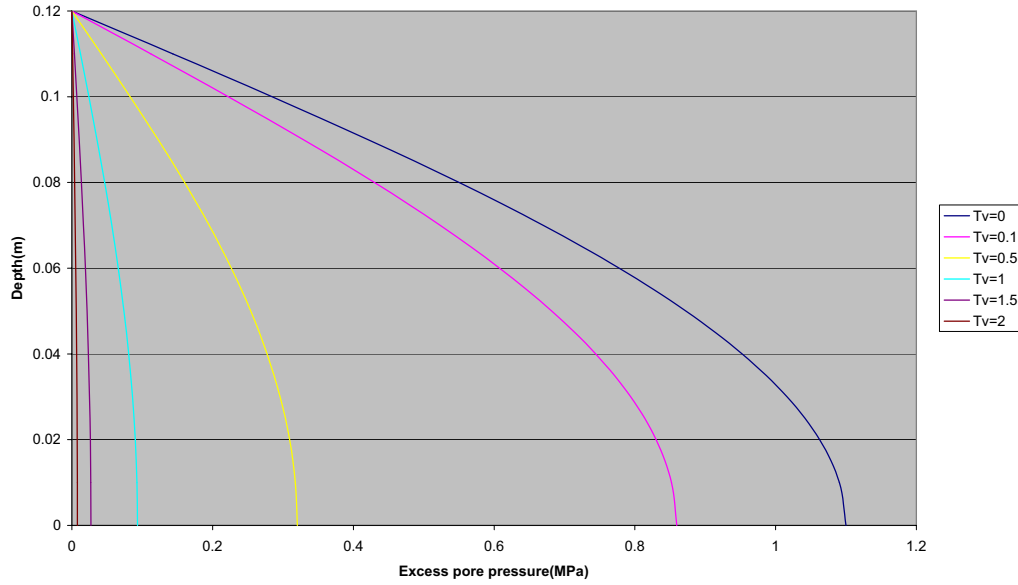
Figure 8.4: Isochrones

8.3 Conclusions

The analytical results support the experimental ones in the extent that:

- The loading process is not fully undrained.

- Consolidation during loading can explain the fact that excess pore pressures experimentally occur but they do not affect ultimate pile bearing capacity.

- No dynamics were taken into consideration in the analytical model. Yet, the model accordance with experimental results is good enough as to support Middendorp, Bermingham and Kuiper's [4] concept for which this kind of pile testing at this loading rates can be directly correlated with the static test, no need for calibration tests.

- More detail on the time-factor (i.e. when consolidation starts to take place exactly) is needed.

- The analytical model can not be used to predict or estimate the behavior of a pile test. Yet, it is a good approach to represent the experiments carried out and gain understanding.
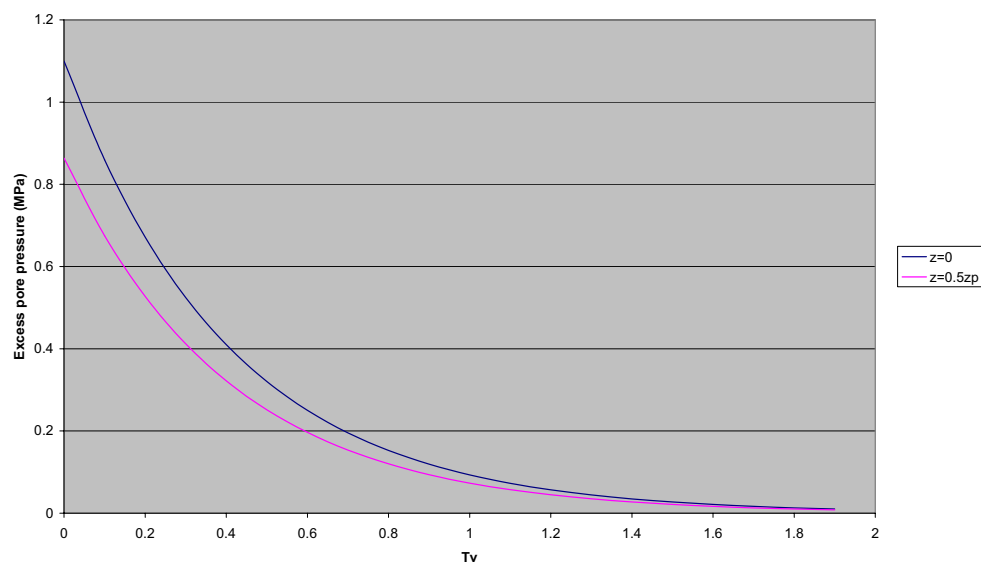
Figure 8.5: Dissipation of excess pore pressures

Part III

Numerical modeling

Chapter 9

The hardening soil model

9.1 Reasons for the election of the model

9.1.1 Introduction

The numerical modeling is going to be carried out by means of the finite-element method as it allows for modeling complicated nonlinear soil behavior and various interface conditions, with different geometries and soil properties.
PLAXIS program will be used, this program has a series of advantages:

- **Excess pore pressure**:Ability to deal with excess pore-pressure phenomena. Excess pore pressures are computed during plastic calculations in undrained soil.

- **Soil-pile interaction**: Interfaces can be used to simulate intensely shearing zone in contact with the pile, with values of friction angle and adhesion different to the friction angle and cohesion of the soil. Better insight into soil-structure interaction.

- **Automatic load stepping**: The program can run in an automatic step-size and an automatic time step selection mode, providing this way robust results.

- **Dynamic analysis**: Possibility to analyze vibrations and wave propagations in the soil.

- **Soil model**: It can reproduce advanced constitutive soil models for simulation of non-linear behavior.

9.1.2 Model election: soil, pile and interface

The available soil models are (PLAXIS Version 8):

1 LINEAR ELASTIC MODEL: it is the simplest available stress-strain relationship. According to the Hooke law, it only provides two input parameters, i.e. Young's modulus E and Poisson's ratio ν. It is NOT suitable because soil under load behaves strongly inelastically.*However, this will be used to model the pile*

2 MOHR-COULOMB MODEL: it is a perfectly elastoplastic model of general scope, thus, has a fixed yield surface. It involves five input parameters, i.e. E and ν for soil elasticity, the friction angle φ and the cohesion c for soil plasticity, and the angle of dilatancy ψ. It is a good first-order model, reliable to provide us with a trustful first insight into the problem.

   Advantages:

- For each layer one estimates a constant average stiffness. Due to this constant stiffness computations are quite fast and give a good first impression of the problem.

Shortcomings:

- It can be too simple

Interfaces are normally modeled with this model

3 JOINTED ROCK MODEL: it is thought to model rock, NOT suitable.

4 HARDENING-SOIL MODEL: it is an advanced hyperbolic soil model. The main difference with the Mohr-Coulomb model is the stiffness approach. Here, the soil is described much more accurately by using three different input stiffness:triaxial loading stiffness E_{50}, triaxial unloading stiffness E_{ur} and the oedometer loading stiffness E_{oed}. Apart from that, it accounts for stress-dependency of the stiffness moduli, all stiffnesses increase with pressure (all three inputs relate to reference stress, $100kPa$).
Advantages:

- More accurate stiffness definition than the Mohr-Coulomb model (stress-dependent stiffness)
- Takes into consideration soil dilatancy
- The yield surface can expand due to plastic straining

Shortcomings:

- Higher computational costs
- Does not include viscous effects
- Does not include softening

5 SOFT-SOIL-CREEP MODEL: for soft soil (normally consolidated clays, silt or peat). NOT suitable.

6 SOFT SOIL MODEL: for soft soil (normally consolidated clays, silt or peat). NOT suitable.

> For all the reasons presented above, **Hardening soil model** is the most appropriate to model the soil.

More complex models can be implemented but then the user has to define them, and this falls beyond the scope of this research.
Finally we conclude:

9.2   Theoretical background

The Hardening Soil model has been presented before as an hyperbolic model. Often hyperbolic soil models have been used to describe the nonlinear behavior; this is also a suitable application in this research as sand usually behaves as a linear elastic material with shear modulus G for shear strains up to $\approx 10^{-5}$, and afterward the stress-strain relationship is strongly non-linear (Lee, Salgado, 1999). The background of this kind of models is the hyperbolic relationship between vertical strain and deviatoric stress in primary triaxial loading. However, the Hardening-soil model is far better than the original hyperbolic model (Duncan and Chang, 1970) as it uses theory of plasticity instead of theory of elasticity and because it includes soil dilatancy and a yield cap. In contrast to an
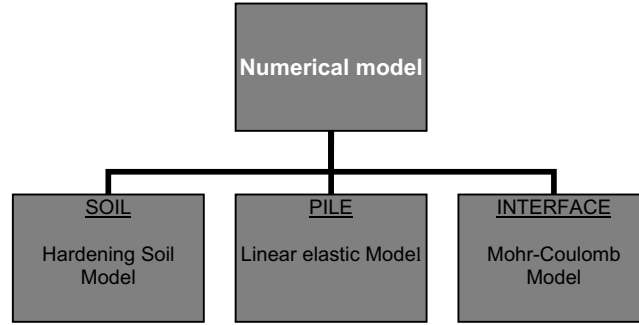
Figure 9.1: Chosen models for numerical analysis with PLAXIS

elastic perfectly-plastic model like Mohr-Coulomb, now the yield surface is not fixed but can expand due to plastic straining.

The main characteristics of the model are:

- Stress dependent stiffness according to power law (m)

- Plastic straining due to primary deviatoric stress (E_{50}^{ref})

- Plastic straining due to primary compression (E_{oed}^{ref})

- Elastic unloading/reloading (E_{ur}^{ref},ν_{ur})

- Failure according to the Mohr-Coulomb model (c,φ,ψ)

As any plasticity model it has an associated flow rule, namely, a relationship between rates of plastic shear strain γ^p and plastic volumetric strain ϵ_v^p; it has the linear form:

$$\epsilon_v^p = \sin \psi_m \gamma^p \tag{9.1}$$

where

$$\sin \psi_m = \frac{\sin \varphi_m - \sin \varphi_{cv}}{1 - \sin \varphi_m \sin \varphi_{cv}} \tag{9.2}$$

with φ_{cv} the critical state friction angle, constant for a certain material, independent of the density, and φ_m the mobilized friction angle that can be calculated:

$$\sin \varphi_m = \frac{\sigma_1' - \sigma_3'}{\sigma_1' + \sigma_3' - 2c \cos \varphi} \tag{9.3}$$

According to Rowe's stress-dilatancy theory (1962), material contracts for small stress ratios ($\varphi_m < \varphi_{cv}$) and dilates for high stress-ratios ($\varphi_m > \varphi_{cv}$). At failure, the mobilized friction angle equals the failure one and:

$$\sin \psi = \frac{\sin \varphi - \sin \varphi_{cv}}{1 - \sin \varphi \sin \varphi_{cv}} \tag{9.4}$$

$$\sin \varphi_{cv} = \frac{\sin \varphi - \sin \psi}{1 - \sin \varphi \sin \psi} \tag{9.5}$$

The parameters of the model are those of Mohr-Coulomb for the failure criteria (c,φ,ψ); in addition other parameters are introduced.

- Secant stiffness in standard drained triaxial test:E_{50}^{ref}

- Tangent stiffness for primary oedometer loading:E_{oed}^{ref}

- Power for stress-level dependency of stiffness:m

- Unloading/reloading stiffness:E_{ur}^{ref}(default: $E_{ur}^{ref} = 3E_{50}^{ref}$)

- Poisson's ratio for unloading/reloading:ν_{ur}(default: $\nu_{ur} = 0.2$)

- Reference stress for stiffness:p^{ref} (default: $p^{ref} = 100$ stress units)

- K_0 value for normal consolidation:K_0^{nc} (default:$K_0^{nc} = 1 - \sin\varphi$)

- Failure ratio: $R_f = q_f/q_a$ (default: $R_f = 0.9$)

- Tensile strength: $\sigma_{tension}$ (default: $\sigma_{tension} = 0$)

Also it defines the oedometer stiffness:

$$E_{oed} = E_{oed}^{ref}\left(\frac{c\cos\varphi - \sigma_3'\sin\varphi}{c\cos\varphi + p^{ref}\sin\varphi}\right)^m \tag{9.6}$$

To explain the plastic volumetric strain in isotropic compression, a second yield surface closes the elastic region in the direction of the p-axis. While the shear yield surface is mainly controlled by the triaxial modulus, the oedometer modulus controls the cap yield surface. This can be defined:

$$f^c = \frac{\beta}{1-m}\left(\frac{p_p}{p_{ref}}\right)^{1-m} \tag{9.7}$$

The volumetric cap strain is the plastic volumetric strain in isotropic compression. Another constant, β, is introduced. The following relationships are used in PLAXIS to get the input parameters:

$$\alpha \leftrightarrow K_0^{nc}$$
$$\beta \leftrightarrow E_{oed}^{ref}$$

The cap has the shape of an ellipse in the $p - \tilde{q}$ plane. p_p determines the magnitude of the ellipse and α its aspect ratio; high values of α lead to steep caps underneath the Mohr-Coulomb line, and small values generate much more pointed caps. This ellipse is also a plastic potential and it still has the hexagonal shape of the Mohr-Coulomb criteria.

(a) 2D yield surface   (b) CAP surface
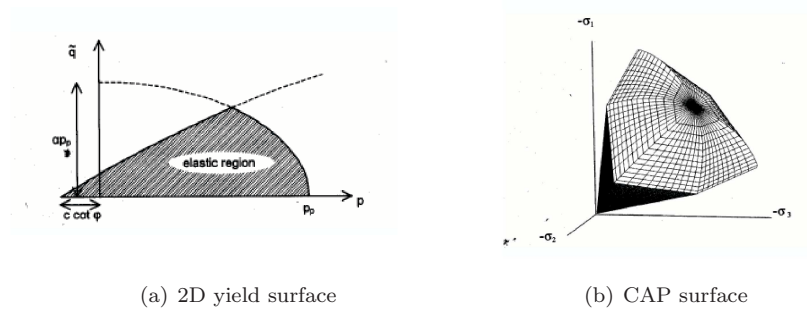
Figure 9.2: Hardening Soil model

Chapter 10

Model definition

10.1 Main features

10.1.1 Introduction

Any analysis, static or dynamic, in a FEM follows a standard procedure: The experimental
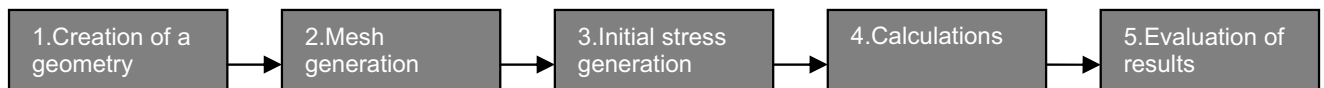
Figure 10.1: Phases in Finite Element Modeling

sequence to perform in the calibration chamber is as follows:

1. CPT (installation test)

2. Static test 1

3. Quasistatic test

4. Static test 2

The ideal model would be that one that reproduced the exact experimental sequence. CPT and Static tests are strain controlled tests, an input displacement is imposed and the force is then the output. Prescribed displacements can be defined in PLAXIS. However, the program does not allow large strains. CPT imposes 70 cm displacement, consequently, CPT-installation test can not be modeled. The second test, the static, imposes 2cm displacement. According to NEN 6745 code a pile fails for a displacement equal to $10\%d_{pile}$, so 2cm in our 3,33cm diameter rot largely exceeds this value and it is to expect that the model of the static test will give soil failure as output. A numerical analysis cannot be continued from a previous failed phase. This implies that, if it is the case that failure is achieved while static test, the pseudostatic one could not be reproduced. To recapitulate, it is NOT possible to reproduce the experimental sequence, the static and pseudostatic tests will be modelled on their own and later compared. Of course, the input of this problem will be defined according to the experimental reality, this is to say, accounting for the effects of CPT and static (namely, displacement and stresses on the soil) on the definition of the model.

There is a second main shortcoming in this numerical model:the impossibility to consider explicitly different loading rates. PLAXIS offers the possibility of static and dynamic
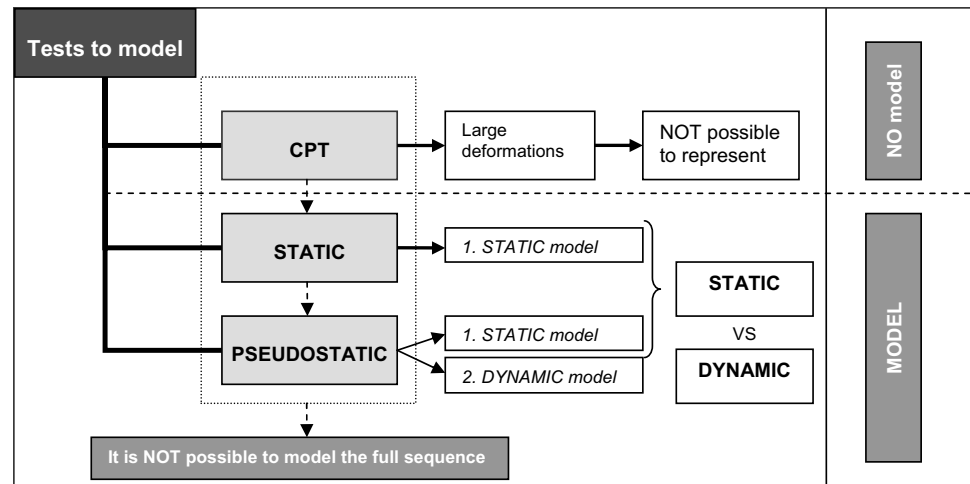
Figure 10.2: Key problems and approaches to the numerical model

models. The only way to account for the loading times will be defining accurately the time frames in the calculation settings. Certainly, PLAXIS offers the possibility to analyze the effects of vibrations into the soil.The effects of vibrations have to be calculated with a dynamic analysis when the frequency of the dynamic load is in the order or higher than the natural frequency of the medium. Low frequency vibrations can be calculated with a static analysis. The pseudostatic test is also a low frequency test; for this, both dynamic and static approaches to it are carried out and compared. An appropriate time frame will be chosen for the dynamic test, the multipliers for the dynamic load will require a precise low frequency definition and a good definition of the loading pulse.In the static modeling there is no time involved.

10.1.2   About dynamic analysis

Hereby some general remarks about dynamical modeling in PLAXIS that may be useful for the model are presented.

Input

- Geometry: Despite the fact that the dynamic phenomena may have 3-D characteristics, in PLAXIS Version 8 the dynamic model is limited to plane strain and axysimmetric conditions. Normally single-source vibration problems are modeled with axisymmetric models, because waves in an axisymmetric system radiate in a manner similar to the 3D case. Energy dissipates leading to wave attenuation with increasing distance form the source, namely, geometric damping.Geometric damping is by definition included in the axisymmetric model. The physical damping due to viscous effects, plasticity or friction can be considered by using the Rayleigh damping.
  15-noded elements are normally used both for pile and soil. The thickness of the interface may be determined previously according to analytical methods.

- Boundary conditions: What requires special attention is the modeling of the boundaries. Although these can be picked up in order to match with the calibration chamber does, in a real in-situ case they have no physical significance. Hence, to

avoid spurious reflection special wave absorbing conditions must be applied. It is also important to place them far enough; as said, these may be at the calibration chamber boundaries but also other criteria can be implemented. Lee and Salgado (1999) proposed that the bottom boundaries of the meshes should be placed at a depth larger than 2 times the pile length measured from the ground surface and the width of the mesh should be equal or larger than the pile length.

- EXTERNAL LOADS: It has been analytically calculated the load that reaches the pile head. This total load must be distributed over the pile section. This load can be created and treated as static or dynamic as follows:

    - Static load: define the load and activate it in the second calculation phase by clicking on it

    - Dynamic load: define the load, set it as dynamic in the loads menu and activate it in the second calculation phase by entering appropriate dynamic load multipliers.

- MODEL PARAMETERSBy entering the characteristic parameters required for the hardening soil model, the wave velocities are automatically generated. Besides, Rayleigh damping could be taken into account defining two coefficients:

$$C = \alpha M + \beta K \tag{10.1}$$

where C represents the damping, M the mass, K the stiffness and α and β are coefficients to be given as input parameters in the material data sets. However, in single source problems with axisymmetric model, it may not be necessary to include Rayleigh damping as most damping occurs due to radial spreading of the waves (geometric damping).

Calculations

The calculations in dynamic analysis always use seconds as time unit. The iterative procedure can be defined manually, different options are available (Newmark alpha and beta,boundary relaxation coefficients); it is especially useful to set manually the dynamic sub steps. If the wave velocities exhibit different values (i.e. between pile and soil) the number of sub-steps automatically set may be too large and it can be appropriate to set it manually.

A dynamic load can consist of a harmonic load, a block load or a user-defined load. In all cases, dynamic loads must be activated setting the appropriate multipliers:

$$Active load = Dynamic multiplier * Input value \tag{10.2}$$

- **Harmonic loads**: In PLAXIS they are defined:

$$F = \hat{M}\hat{F}\sin(\omega t + \varphi_0) \tag{10.3}$$

where $\hat{M}$ is the Amplitude multiplier, $\hat{F}$ is the input load, $\omega = 2\pi f$ with f the frequency and φ_0 is the initial phase angle.

- **Block load**:It is a dynamic load applied suddenly in a single time-step. It can be defined setting the amplitude multiplier equal to the magnitude of the block load, $f = 0$ and $\varphi = 90$, so $F = \hat{M}\hat{F}$; or as a user-defined load.

- **User-defined loads**:A dynamic load can be activated creating an ASCII file containing time and load multiplier in two columns separated by a space.

10.2   Input

10.2.1   General settings

- Axisymmetrical model (axis at the center of the pile), for the reasons presented in previous sections it is the best option for single-source vibrations. Then, only the right-half of the real geometry is represented in the model.

- 15-noded-elements

- Time unit left in days as in the default value because apart from the dynamic test we also are interested in representing the consolidation of the soil.

10.2.2   Geometry and mesh

The geometry has been designed to match with that of the calibration chamber. It should be an appropriate consideration because the experimental tests in the calibration chamber were designed to avoid boundary effects (one test in the center only), hence, matching the numerical model boundaries with that of the chamber we are placing them far enough. It has been argued that the CPT and the static can not be included and only the pseudostatic tests is object of attention. Nevertheless, the effects of the CPT and the static test are taken into consideration by means of placing the pile initially at -72cm below the surface. Besides it is important to generate a proper stress state in the soil. To achieve it, prescribed displacements along the pile and at the tip are imposed even before the pile is created, to 'prestress' the soil, to simulate the installation effects.

- Along the shaft a horizontal displacement of 1cm is imposed.

- At the tip a vertical displacement of 10cm is imposed.

The shoulder point will have both vertical and horizontal coordinates of the prescribed displacement as it belongs to both tip and shaft.

Of special interest is also the interface that generated surrounding the pile, to register
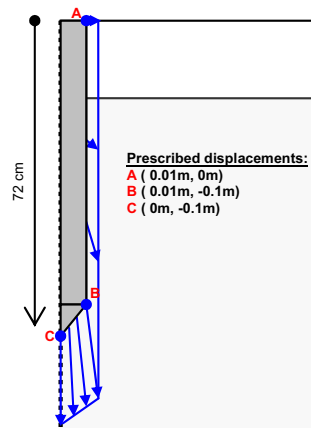

Figure 10.3: Expansion:Prescribed displacements

the pile-soil interaction. The shoulder point of the pile is an extremely difficult point to model. To guaranty the degree of freedom of this point (it is allowed to move but it is difficult to implement that in the program), both tip and shaft interfaces will be extended into the sand.

The mesh is generally set to coarse, with refinements in the pile cluster, along the pile shaft and at the pile tip.

10.2.3 Boundary conditions

The boundaries are placed far enough. In addition, absorbent boundaries are generated at the bottom and right-hand boundaries to absorb increments of stresses caused by the dynamics of the problem and that otherwise would reflect inside the soil. These boundaries are also consolidation limits. Standard fixities are also applied.

10.2.4 Loads and prescribed displacements

We have already discussed the necessity to prescribe displacements along the pile to simulate the installation effects. These displacements have to be activated first of all, then deactivated and the pile can be created and the test modeled.

The tests will be modeled different depending on whether it is static or dynamic:

- **Static**: Experimentally it was a strain controlled test, the pile was pushed exactly 2cm into the soil. The same idea is implemented numerically. A prescribed displacement of 2cm downwards must be defined on the top of the pile and activated by means of staged construction during the calculations. Another option would be to model the pseudostatic test statically, hence, defining a force and applying it statically. In PLAXIS both static calculations should give the same results. Prescribed displacement is less computational expansive so it is preferred.

- **Dynamic**: A unit distributed load system must be defined on the top of the pile and set to dynamic. Its value will be increased to the experimental one in the calculation definition.

10.2.5 Initial conditions

- **Water pressures**: Phreatic level in the tank is at $-15cm$ below surface. Hydrostatic pressures are generated in the whole geometry according to this level. The unit weight of water is set to default value $10kN/m^3$. As shown above, special consolidation limits are placed at the boundaries, meaning that during consolidation process water cannot flow through them.

- **Initial stresses**: PLAXIS generates the initial stresses by default with the formula of Jaky ($k_0 = 1 - \sin\phi$). However this is not the case. The soil is set to overconsolidated with OCR=5 and the horizontal stresses are set to be the double than the vertical ones ($k_0 = 2$). This may need further explanation. As Hanna and Soliman-Saad [52] presented in their study on the effect of compaction duration on the induced stress levels in laboratory prepared sand bed, the in-situ stress levels are often not properly known and aware of. Especially the sand placing technique can drastically influence the stress levels, consequently, the produced sand bed may not be as normally consolidated and homogeneous as assumed in many theories. It is most likely to be an overconsolidated, nonhomogeneous and anisotropic sand (Broms, 1971).We had already discussed the problems that appeared in the experimental test related to the preparation technique. The fluidization-vibration-drainage system did not work appropriately, up to the point that a maximum had been reached and it was no longer possible to loosen the soil, no matter the fluidization time and even without vibration. Thus we were all continuously remolding the same sample, making it denser, re-vibrating it once and again. A very overconsolidated sand is to be
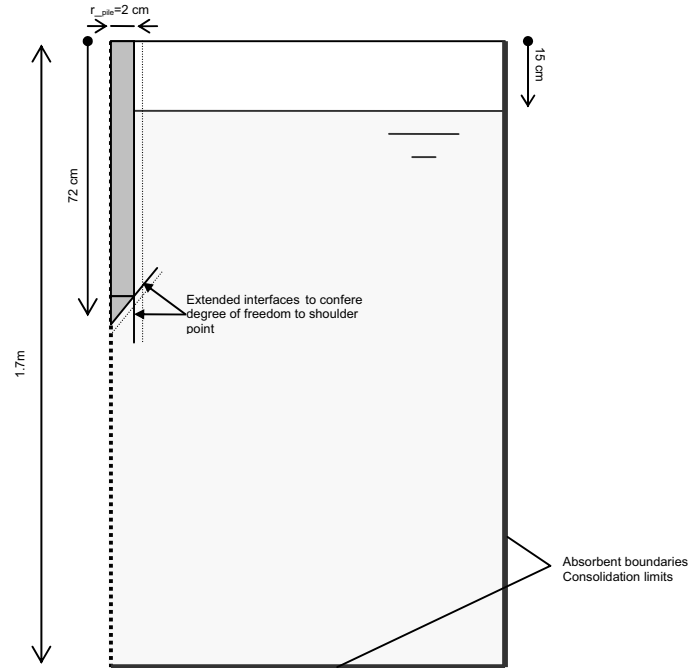
Figure 10.4: Input geometry: axisymmetrical model with pile created at depth defined by CPT+static tests

expected. Moreover, there are the boundary conditions created at the bottom and sides of the calibration chamber. It is not a standard calibration chamber. The rigid walls and bottom, combined with the 2 vibrators adhered to the walls can largely increase the horizontal confining stresses. The waves introduced into the soil for durations up to 30 min can be reflected from at the rigid walls and combined with the inefficient re-preparation of the sample make it expectable to have in-situ horizontal stresses doubling the vertical ones. The numerical results corroborate these hypothesis, as we will see in the next chapter.

10.2.6   Material sets and models

- **Sand**: It is modeled with the hardening soil model to be able to record non-linear deformations below the pile tip. As it is a rapid loading process, the behavior is undrained. Also dry and drained calculations are going to be performed for comparison. The soil is fully saturated by water, hence, almost imcompressible and the Poisson's ratio has to reflect it. We are dealing with quite dense sands, due to problems with the preparation system in the tank. This originates experimental samples with high friction angle and stiffnesses. No dilatancy is taken into consideration.

- **Pile**:The pile is not modeled as a plate but instead it is considered a linear-elastic non-porous material. The Young modulus and the Poisson's ratio are reduced to facilitate the numerical calculation.

- **Interface in sand**: An extra material needs to be defined. The interfaces have been extended inside the sand, but only to allow shoulder point displacement and
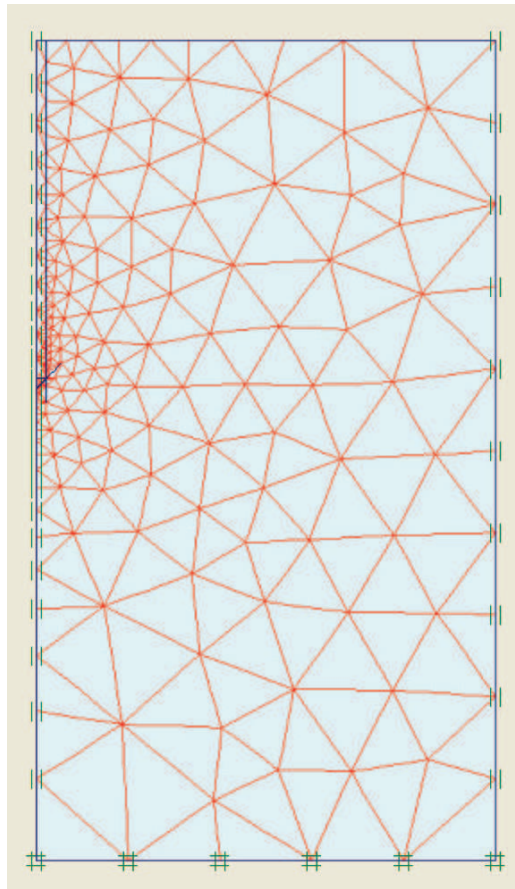
Figure 10.5: Input geometry: axisymmetrical model with pile created at depth defined by CPT+static tests

not to represent any pile-soil interaction, thus, only geometric function, no stress reduction. For this reason, the properties given to the extensions of the interfaces must be the same ones as the sand. The *interface in sand* material is exactly as the sand but without interface strength reduction.

As in axisymmetric models most damping is due to geometry, no Rayleigh damping is included. This also agrees with the assumptions of the analytical cone model that showed that the Rayleigh damping was not significant for our case.

The table summarizes the properties.

10.3 Calculations

The phases carried out for modeling static and dynamic tests are explained below.

1 EXPANSION: Plastic, staged construction. To represent the effects of the installation of the pile (CPT), before even creating the pile, the prescribed displacements previously defined must be activated at the boundaries of the pile cluster. The pile cluster may be deactivated to reduce computational time.

Effective stresses
Extreme effective principal stress -67,76 kN/m ^{2}
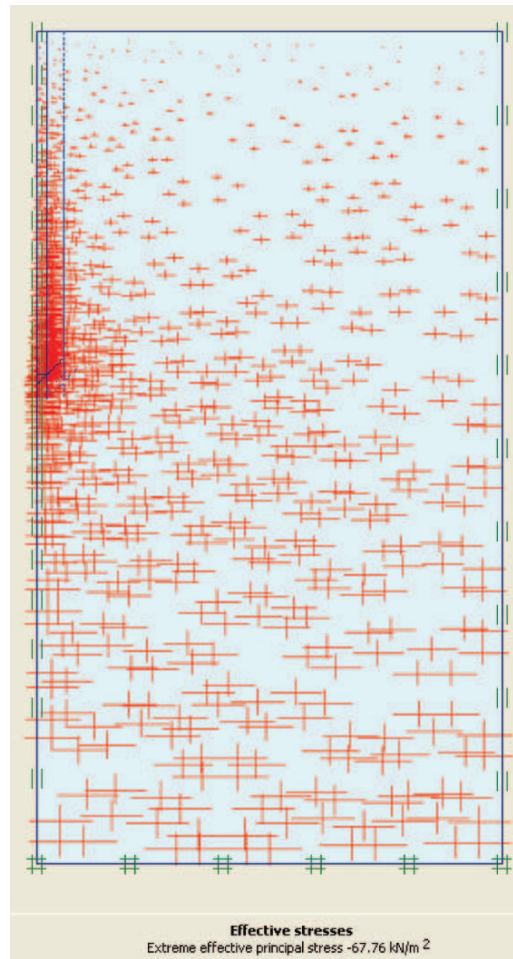
Figure 10.6: Initial effective stresses

2 PILE CREATION: Plastic, staged construction. The prescribed displacements of the expansion are deactivated. the pile cluster has to be activated and pile properties are given to it.

3 TEST:

2.1 **Static**:Plastic analysis, staged construction. It consists in activating the prescribed displacement on the top of the pile by clicking on it in the definition of the staged construction.

2.2 **Dynamic**:Dynamic analysis, harmonic multipliers. In the literature and the experimental results we have seen that the pulse for a pseudostatic test has the shape of half an harmonic cycle (at the end of the test, the phase angle is of 180°). For a duration of 0.06s, the total period would be of 0.12. The frequency is the inverse of the period, thus, 8Hz. The amplitude multiplier is the maximum value of the force at its peak. Experimentally the forces for the pseudostatic test were around 25kN, thus 25000N.

4 RESPONSE: For the dynamic test only it may be interesting to model the free response of the soil after the test. This can be done setting all the harmonic multipliers to zero.

Parameter	Symbol	Sand	Interface in sand	Pile (steel)	Unit
Material model	Model	Hardening soil	Hardening soil	Linear elastic	-
Behavior	Type	Drained/Undrained	Drained/Undrained	Non porous	-
Unit weight above phreatic line	γ_{unsat}	20	20	78.5	kN/m^3
Unit weight below phreatic line	γ_{sat}	23	23	-	kN/m^3
Young's modulus	E_{ref}	60000	60000	$2.1*10^7$	kN/m^2
Oedometer modulus	E_{oed}	80220	80220	-	kN/m^2
Power	m	0.6	0.6	-	-
Unloading modulus	E_{ur}	382500	382500	-	kN/m^2
Poisson's ratio	ν_{ur}	0.15	0.15	0	-
Reference stress	P_{ref}	100	100	-	kN/m^2
Cohesion	c	1	1	-	kN/m^2
Friction angle	φ	39	39	-	Deg
Dilatancy angle	ψ	0	0	-	Deg
Interface strength reduction	R_{int}	0.7	1(rigid)	0.6	-

Figure 10.7: Material properties

5 CONSOLIDATION: For the undrained models, excess pore pressures are generated. A consolidation analysis can be programmed, until a minimum pore pressure (the hydrostatic value) is reached, hence, until all the excess pore pressures have dissipated. The problem arises once more in the fact that is it not possible to go on with the calculation after a failed phase. We will see in the results that commonly failure of the soil or error in the numerical calculation occur, it is quite complex to be able to model the consolidation.
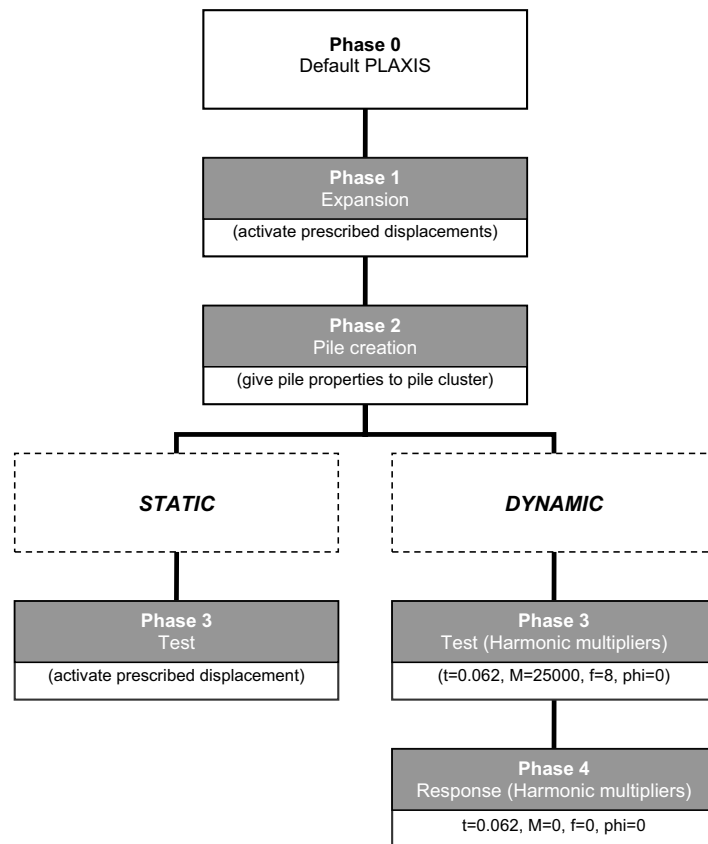
Figure 10.8: Calculation phases

Chapter 11

Numerical results and evaluation

11.1 Results presentation and analysis

Figure (11.1) summarizes the results of the numerical modeling. The obtained load-displacement curves for static and low-frequency dynamic tests, in all three available soil conditions (dry, saturated drained and saturated undrained) are all together in the figure. Note that the y-axis -displacement- has as maximum value 2cm, the force corresponding to this displacement if the failure force, according to the criteria established for the experimental tests.
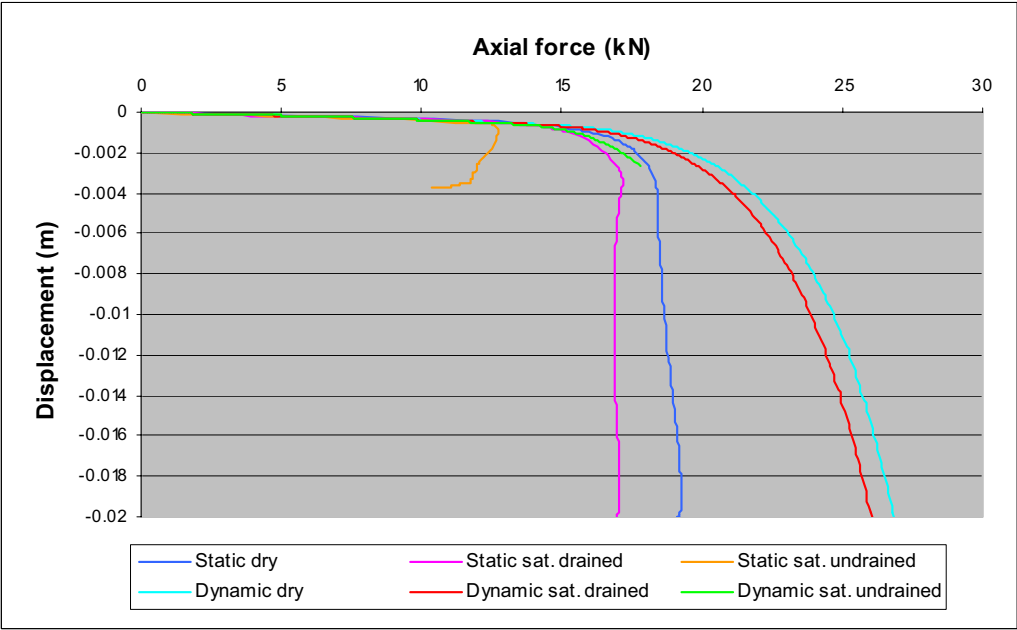
Figure 11.1: Static load-displacement curve

All the calculations were performed with exactly the same model and soil properties, only the definition of the calculation and/or the presence of water changed. A first glimpse at

the load-displacement curves should note that, the difference between static and dynamic calculations turns out not to be only the failure load, but also the shape of the curve. For the static calculation a displacement was imposed, for the dynamic one, a load at the pile top the value of which was increased as half-harmonic cycle. This different, may it be called, loading process implicitly introduced variations in the soil model itself and behavior. For the static case a brusque change in stiffness occurs when the soil plastifies, even with some softening. Softening could perhaps take place in the dense sand package, considering the input parameters used and taking into account that experimentally we kept re-vibrating once and again the same sample due to the preparation system inefficiency. Hardening soil model can not, explicitly, account for softening, thus this shape is not due to any stress or stiffness incorrect input. The experimental curves for static dry tests (see Dijkstra [5]) also showed this sudden failure, but not the saturated curves. On the contrary, the dynamic curves display a much more gradual plastification and hardening is visible. However, the defined pulse clearly represented the pseudostatic pulses as defined in the literature. The different application of the load is the only responsible for the differences. In both type of calculations, for the undrained case, failure of the soil was accompanied by a large numerical divergence making the calculation to stop almost immediately after plastifying the soil. As PLAXIS cannot go on calculating after a failure, it was not possible to model consolidation after the undrained failure.

To check the precision of the results, these have to be compared with the recorded experimental values. Archeewa [47] already calculated the average recorded values and related them to those of Dijkstra [5]. The comparison can be extended to the numerical values in he following table:

Model	Condition		Test	Fail.force(kN)
Experimental	Dry		Static	24.7
			Pseudost.	27
	Saturated		Static	14.5
			Pseudost.	19.75
Numerical	Dry		Static	19.5
			Dynamic	26.8
	Saturated	Drained	Static	17
			Dynamic	26.1
		Undrained	Static	12.5
			Dynamic	17.8

Table 11.1: Comparison between experimental and numerical results

Note that experimentally there is only one result for the 'saturated' case. On the contrary, in PLAXIS, while defining the calculations, it is needed to specify the assumed behavior of the soil, therefore, two options are available for the saturated model, namely, drained and undrained. The conclusions of experimental and analytical models agreed in defining the problem as partially drained, but this intermediate option is not possible in PLAXIS. For these considerations, the best option to check the accuracy of the numerical results is comparing the dry ones.

- The static calculation slightly underpredicts the failure force, however the fit is of a 80% which can be considered good.

- The dynamic calculation result fits surprisingly good the experimental one, 26,8kN versus 27kN, this is a fit of a $99,25\%$.

It can be concluded that the numerical results fit very well the experimental ones. Then, the computed results for saturated conditions can be used to analyze the soil response to the fast load. The coming graphs compare the load-displacement curves for saturated soil under static and pseudostatic loading.
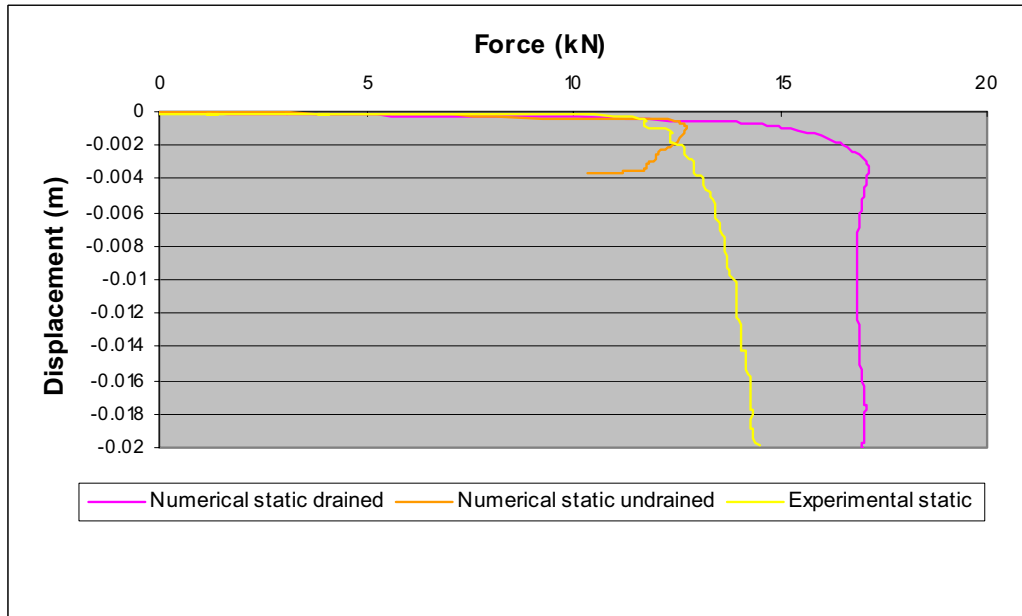

Figure 11.2: Dynamic load-displacement curve

For both cases, the yellow curve is the experimental one and it falls in-between the drained and undrained results of PLAXIS, also for the pseudostatic case. Hence, once more the model corroborates that the experimental tests were not carried out under undrained conditions. Even for the pseudostatic loading, the numerical undrained approach fails for too low loads, whereas the drained loads are too large, demonstrating that it is a partially drained situation.

Also according to the experimental conclusions, the computed failure forces for the dynamic calculation are larger than for the static one. In the evaluation of the experimental results there was information about the tip and shaft resistances and one could calculate the correspondent bearing capacity. Despite the larger forces on pile top for pseudostatic tests, the calculated bearing capacities for static and pseudostatic were almost the same for dry and saturated tests. From that it was concluded that there was no loading rate effect on the pile bearing capacity. There was a rate effect on the pore pressures but the pore pressure generation did not affect the pile bearing capacity. Unfortunately all these reasonings cannot follow from PLAXIS results. The problem is as follows: Some punctual numerical artifacts occur in the values of effective stresses and pore pressures around locations were the gradients are expected to be large (i.e. pile tip, shoulder position of the cone). These anomalies do not affect the general comput of the load-displacement curves, but when evaluating the output and looking for concrete values at concrete points it is more complicated. More understanding on the problem could not be achieved due to the
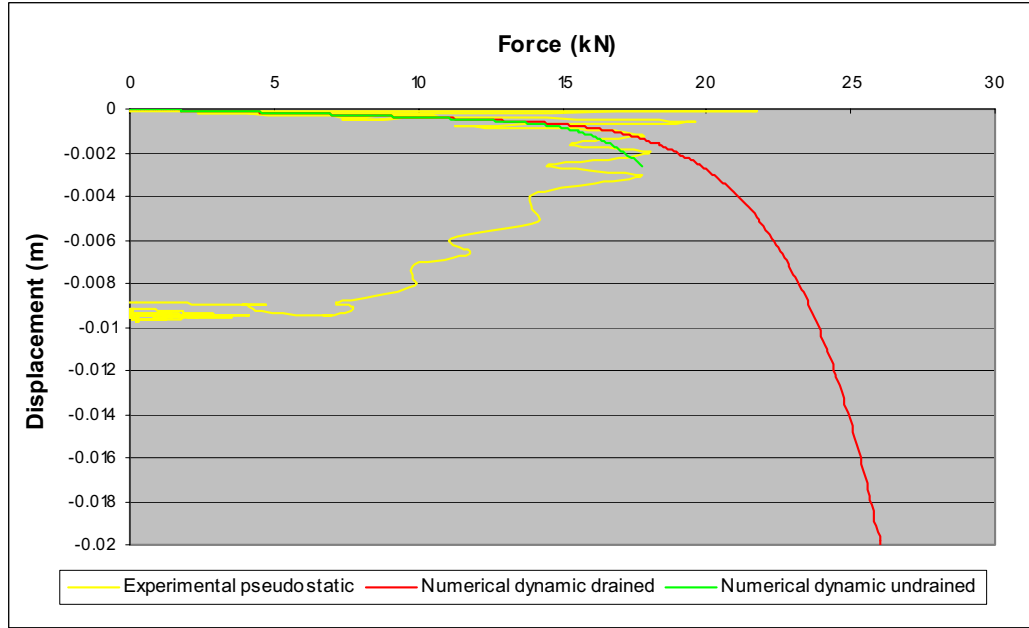
Figure 11.3: Static load-displacement curve

existence of punctual numerical artifacts. Even if the rest of the points in the geometry have reasonably appropriate values of pore pressures or effective stresses, at least one of them is unrealistic and this should be enough to question the reliability of the other points. This problem is common in some finite element discretizations of complex geometries or stress distributions but does not affect the main results as the load-displacement curves. To sum up, the only reliable results are the load-displacement curves and it is not possible to (a) predict the excess pore pressures that generate or (b) separate which part of the resistance is due to shaft friction and which one belongs to the tip resistance, in other words, the corresponding bearing capacity can not be calculated.

The larger values of the force at the pile top, which also occurred experimentally, could be explained as due to the inertia effect. This was the conclusion for the tests and could perfectly be valid here as well. Therefore, that the failure forces for dynamic calculations are larger than for static is not a reason to held responsible for it neither (a) loading rate or (b) excess pore pressures. Yet, be careful: on the other hand, as it is not possible to derive the exact bearing capacity for the numerical case, stating out load there there is no loading-rate or pore pressure effect would be incorrect form a logical point of view. One can just 'suppose' that is the cause but unfortunately no more insight is available.

As mentioned in the beginning, for saturated experimental static the softening product of the numerical model was not observed. A better shape-fit could not be achieved as it would require to manually redefine one of the available soil models or use a fully user-crafted one.

For the dynamic curves, the numerical results would represent the 'theoretical' behavior of a pseudostatic or quasistatically tested soil. The set-up used is not the commercial **stat-namic** and the hitting of the mass onto the pile did not occur so neatly. The irregular shape, especially visible comparing to the numerical results, is produced by the reboundings of the load on the pile head as it is let to fall freely inside the guiding aluminium tube.

11.2   Model evaluation

In the previous chapter, when the model was defined, some of the limitations were already presented, as the impossibility to model large deformations (i.e. CPT/installation of the pile), the lack of an explicit definition of the loading rate as the velocity at which the load is applied, the fact that saturated soil could only be modeled as a drained or undrained material, etc. As happens in the analytical model, or in any model, a model is just a model, an approximation to the reality, that will be more or less precise, but is always a simplification. In reality, either it is in-situ or in the scaled calibration chamber tests, the situation is always much more complicated and there are a large number of factors involved. The aim of the numerical model was to try to represent what took place experimentally and in this it has succeeded quite well. It is true that it failed to provide detailed information of the behavior of the soil resistance but, on its favor, the achieved load-displacement curves successfully fitted the experimental ones.

A number of modifications were introduced in the model to represent and account for inputs that could not be included or to palliate the lack of good data about it, for instance, the expansion to model the effects of the pile installation or the OCR and K_0 values. They turned out to give good results, so, besides confirming some of the conclusions that were seen in the tests or analytical mode, the PLAXIS model could somehow fill one of the gaps existing in the experimental testing: it provided information over the stress state in the soil. Therefore, the soil in the tank can be categorized as overconsolidated, with larger confining horizontal stresses than vertical ones.

As said before, the final global output, the load-displacement curves, may be satisfactory but there were some questions PLAXIS could not answer, it behaves as a black box. A good fit with the experiments was achieved but one has to be realistic and certainly it could not be said that the results of the numerical model could be used as a prediction tool.

11.3   Conclusion

The obtained load-displacement curves fit really well the experimental ones. Besides, they help to corroborate two ideas that had been previously introduced:

- **Drainage**:it is not the case of undrained loading. The soil response is in-between, partially drained.

- **In-situ stresses**:the soil in the tank is overconsolidated.

However, no explicit values of excess pore pressure or effective stresses could be derived, strongly limiting the applicability of the results. The main objective was to gain insight and be able to propose a relationship or predict the response in three points:

- Relationship loading rate-excess pore pressure

- Relationship excess pore pressure-bearing capacity

- Relationship soil strength-excess pore pressure

These three objectives could not be fulfilled.

Therefore it is important to keep in mind that in this particular case at least:

- PLAXIS can be used to analyze or describe the problem up to a certain extent but not as a predictive tool.

Chapter 12

Conclusions and recommendations

The conclusions of each part of the research have been presented already, this chapter wants to provide a global summarizing overview of the results, applications and consequences of the thesis. Also, it is interesting to look back into the definition of the problem and objectives in order to evaluate the satisfaction of those or the existing limitations.

12.1 Conclusions

12.1.1 Global research conclusions

The general aim of the thesis was to extensively investigate quantitatively and qualitatively the generation of excess pore pressures in saturated sand when performing under pseudostatic loading and how those affected the pile bearing capacity. Of course, this is more related to the path to follow, the procedure, the final punctual objectives will be evaluated later. Indeed, the path has been followed from experimental, analytical and numerical points of view.

All-together the investigation proved about the *topic* in question that:

1. **Relationship loading rate-excess pore pressures**: Increasing loading rates do generate larger excess pore pressures. For a velocity augment from 1mm/s to 250 mm/s, hence a 250%, the generation of excess pore pressures increased a tenfold.

2. **Relationship excess pore pressure-pile bearing capacity**: Experimentally the large excess pore pressures did not affect the computed pile's bearing capacity, i.e. tip and shaft resistances. The explanation for this was found by means of the analytical and numerical modeling:

   - The pseudostatic loading in saturated sand, due to the combination sand large permeability-extended loading time, does not occur in undrained conditions. It is a case of partial drainage and consolidations plays an important role in the problem.

   An increase on the force on the pile head was measured experimentally but it was attributed to inertia effect [47].

3. **Soil strength effect**: Could not be investigated.

Besides, other conclusions can be derived:

- To account for all the features of the problem in an analytical model is extremely difficult. An attempt to design a first pseudostatic saturated model has been made. A static analytical model, consisting on an elastoplastic truncated cone, was developed based on the Wolf one, thus, implicitly considering some dynamic features. The calculations, tough, were solely static but they proved quite good agreement with the expected results. It agreed with Dijkstra's conclusion that there was no remarkable rate-effect on the pesudostatic tests and therefore they could be correlated with the static results.

- The numerical model indirectly provided information of the in-situ stress state, it showed that the soil in the tank is overconsolidated and the lateral stresses are larger than the vertical ones.

Moreover, it is desired to evaluate the applicability of the pseudostatic testing methodology in saturated sands. Combined with Dijkstra's [5] and Archeewa's [47] thesis it is a quite complete study. The general conclusion:
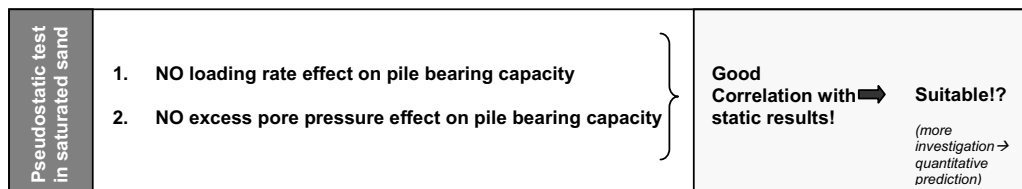

Figure 12.1: General conclusion

However, along the report a series of problems and limitations have been dealt with. Consequently not as much information as desired could be acquainted, mainly, the warning would be:

- Qualitative but not reliably quantitative conclusions⇒The research succeeded in providing some understanding but not enough, especially there is a lack of robust predictive tools⇒The general conclusion cannot be definitive, it is just *the direction results seem to point towards*; more insight is needed.

This will be further developed in the coming subsection.

12.1.2   Evaluation of the fulfillment of the objectives

The *methodology* used can be evaluated by checking the degree of fulfillment of the objectives.

General evaluation

The research took place for almost 9 months, logically the main objective of investigating the topic was fulfilled. It has already been pointed out the weakness of the available tools/results to state quantitative conclusions in a definitive way. The general lines of the loading rate-excess pore pressure-bearing capacity relationship could be defined satisfactorily. Load-settlement curves are available form the experimental and numerical results and they are useful to define the behavior of the soil. The last objective to be met was to consider the suitability of the results to *predict* the response and, if suitable, propose a straightforward way to predict it . This objective could not be met, because:

- From experimental point of view: Extrapolating from the experimental results, taking into account that it is a scaled model, we could roughly try to upscale it and then maybe predict, but the singularity of calibration chamber results can question it. More research is needed, possibly in-situ real scale evaluations.

- From analytical and numerical models: The available/developed methods/models have strong limitations. One of the objectives was to evaluate the suitability of the more 'scientific' state-of-art, this was extensively done and the limitations could successfully be noted. In the end, the available analytical and numerical resources proved good to get some qualitative insight, they could more or less approximately model the experimental test but they could not give enough detail and especially, they can not be used to *predict* the soil response.

Experimental tests

A series of experimental tests have been carried out successfully during 4 months, except for the problems with the preparation system. The research was planified as to take these experimental results as a referent for further investigation and modeling. For this, any results evaluation has always looked back to the experiments for comparison. Experimental results are from far the most satisfactory and reliable, despite the ignorance about the exact soil properties in the tank.

The set-up and designed series satisfactorily represented the different loading-rates for static and pseudostatic load tests, although the shape of the loading pulse for pseudostatic test did differ from the neatly half-harmonic one in theory or numerical models. Dijkstra's device is useful also for saturated sand. It met the main objective, i.e. general quantitative and qualitative investigation. It also resulted in a satisfactory loading rate-excess pore pressure-bearing capacity relationship, and useful load-displacement curves. Looking more into detail in the sub-objectives that had been defined, a good loading rate-excess pore pressure relationship was obtained; also the excess pore pressure-pile bearing capacity relationship was obtained; yet, the third point could not be satisfied, the soil strength effect could not be investigated.

APPLICABILITY OF THE MODEL AND ITS RESULTS: The optimal in-situ testing is expensive and does require much more manpower, for this, scale tests are a very favourable option. The experimental set-up is, considering the current state-of-art of scientific approaches, the most powerful and effective way to obtain directly useful quantitative results. The results were useful to validate and calibrate more 'scientific' models. Upscaling is needed for real in-situ applicability. However, it is difficult for calibration chamber results to be suitable for extrapolation. The results were achieved for a certain type of soil -with a serious lack of data about it-, in a certain type of chamber, with a certain -and unknown-stress state.

Analytical modeling

An analytical model, referred to as *cone model* because it is based in Wolf's theory has been developed to try to represent the soil response that occurs in the tank. None of the available models completely fitted the requirements and cone model was chosen in favor of more widely used cavity expansion; extensive related studies showed that Wolf's theory was precise under dynamic loading. Hence, some implicit dynamic component was considered, though the calculations were static. This 'pseudostatic' model could corroborate the fast plastification that takes place and also the even faster dissipation of excess pore pressures. Therefore, it seems that a satisfactory analytical model for pseudostatic testing could be based in the stress-wave theory but with no need to explicitly perform cumbersome dynamic calculations. It is an interesting first step but its results are not

precise yet, the procedure and developing itself are more interesting in this case than the final results. Besides, no quantitative sub-objectives could be met.

APPLICABILITY OF THE MODEL AND ITS RESULTS: It could explain a bit more the phenomena but not with enough detail. A complete model with plasticity, low frequency dynamic, coupled consolidation and loading, would be useful but very difficult to achieve analytically. Certainly it could not be extrapolated or used for prediction. Not suitable for quantitative analysis.

Numerical modeling

The numerical modeling was done with the finite element program PLAXIS. It is a user-friendly program but behaves as a black-box, just input parameters can be given, no more manipulation that escapes from the 'conventional' design/calculations could be done. This especially affected in two ways:

- Does not account for large deformations: The CPT and installation could not be modeled and its effects should be introduced by other means. It already consists in an approximation then.

- Only 'extreme' cases like drained/undrained or static/dynamic could be implemented, without specifying the loading rate itself and there is no option of partial drainage.

Therefore, it could produce really good load-displacement curves and confirmed the over-consolidation of the soil, but no more detail , for instance distribution of excess pore pressures, was possible. Consequently, as happened with the analytical model, no quantitative sub-objectives could be met. *As Randolph's cite noted in the introduction, also in this thesis the most practical conclusions have to be derived from empirical correlations.*

APPLICABILITY OF THE MODEL AND ITS RESULTS: PLAXIS modeled and corroborated the experimental conclusions in a qualitative way; nevertheless, in this case at least, it can not be used as a predictive tool.

12.2   Recommendations

Once both the satisfactory conclusions and also the limitations of the thesis results are understood, the next step is to define to which extent and how could the limitations be overcome.

Experimental tests

- The soil sample should be improved: New series of tests in a homogeneous sand and with known properties ($E, \phi, c_v, etc.$). Also different densities should be tested to compare effects of the soil strength.

- Piezometers could be installed into the soil at different depth to better explain the generation of excess proe pressures. It would allow to distinguish between shear and compressional generated pore pressures.

- Static loading system should be modified to apply a constant velocity to the pile and not an operator-controlled one.

- The stresses in the soil are unknown and also the residual stresses left behind by the pile installation. The topic itself is already complicated and also the effect of these stresses in the pseudostatic results should be investigated. Also those defined by the calibration chamber. A standard type calibration chamber with known boundary conditions is preferred.

- The prototype should be properly upscaled if the results of the model are to be used for other investigation.

Analytical modeling

- A proper analytical model should be developed, taking into account much more factors. This part needs much more investigation, from extending soil dynamics to plasticity to suitable 3D partial consolidation modeling. It is important to know when the consolidation does start exactly, so, how partially drained is the case. For excess pore pressure prediction considering only the zone below the pile tip can be accepted. But, for the pile bearing capacity this simplification would neglect any shaft resistance component; it should not be used for resistance then, unless the skin friction is introduced by other means in the calculation. Numerical methods will be needed to solve the complexity of the calculations.

Numerical modeling

- If numerical models are to be used for prediction, partial drainage should be included in the calculation. Besides, any calculation for it to be reliable to use in practice should be based in a good knowledge on the input soil parameters. The next step for investigation of the problem with PLAXIS would be to define a user's own soil model based on analytical results and theories. So, is the analytical study would go on, it would be interesting to implement its results in a numerical code in the future.

Bibliography

[1] M.F.Randolph. Science and empiricism in pile foundation design. *Geotechnique*, 53:847–875, 2003.

[2] B.Menzies C.W.W.Ng, N.Simons. *Soil-structure engineering of deep foundations, excavations and tunnels*. Thomas Telford Publishing, London, 2004.

[3] B.Menzies N.Simons. *Foundation Engineering*. Thomas Telford Publishing, London, 2000.

[4] B.Kuiper P.Middendorp, P.Bermingham. Statnamic load testing of foundation piles. *Application of stress-wave theory to piles, F.B.J.Barends (ed.), Balkema, Rotterdam*, pages 581–588, 1992.

[5] J.Dijkstra. Influence of loading rate on pile capacity in unsaturated sand. Master's thesis, Faculty of Civil Engineering and Geosciences, TU Delft, November 2004.

[6] A.I.Al-Mhaidib. Bearing capacity of a model pile in sand under different loading rates. *Proceedings of the 9th international offshore and polar engineering conference, Brest, France*, pages 724–730, 1999.

[7] G.Nasr J-L.Briaud, M.Ballouz. Static capacity prediction by dynamic methods for three bored piles. *Journal of Geotechnical and Geoenviromental Engineering*, 126:640–649, 2000.

[8] M.Novak M.H.El Naggar. Analytical model for an innovative pile test. *Canadian Geotechnical Journal*, 29:569–579, 1992.

[9] W.G.B. Te Kamp. The influence of th rate of penetration on the cone resistance $'q_c'$ in sand. *Proceedings of the Second European Symposium on Penetration Testing, Amsterdam*, pages 627–633, 1982.

[10] E.Rust G.A.Jones. Piezometer penetration testing, cupt. *Proceedings of the Second European Symposium on Penetration Testing, Amsterdam*, pages 607–613, 1982.

[11] J.H.Allen U.Dayal. The effect of penetration rate on the strength of remolded clay and sand samples. *Canadian Geotechnical Journal*, 12:336–348, 1975.

[12] S.Nordal G.Eiksund. Dynamic model pile testing with pore pressure measurements. *Proceedings of the 5th International Conference on Applied Stress-Wave Theory to Piles, Orlando, Florida*, pages 1–11, 1996.

[13] A.Hyde M.Brown, W.Anderson. Statnamic testing of model piles in clay calibration chamber. *IJPMG-International Journal of Physical Modelling in Geotechnics*, 1:11–24, 2004.

[14] E.Garland J-L.Briaud. Loading rate method for pile response in clay. *Journal of Geotechnical Engineering*, 111:319–336, 1985.

[15] T.Issigonis K.D.Eigenbrod. Pore-water pressures in soft to firm clay during driving of piles into underlying dense sand. *Canadian Geotechnical Journal*, 33:209–218, 1996.

[16] W.Broere. *Tunnel face stability and new CPT applications.* PhD thesis, Faculty of Civil Engineering and Geosciences, TU Delft, 2001.

[17] T.Lunne A.K.Parkin. Boudary effects in the laboratory calibration chamber of a cone penetrometer in sand. *Proceedings of the Second European Symposium on Penetration Testing, Amsterdam*, pages 761–768, 1982.

[18] L.D.Wesley. Interpretation of calibration chamber tests involving cone penetrometers in sands. *Geotechnique*, 52:289–293, 2002.

[19] R.Hitchman G.T.Houlsby. Calibration chamber tests of a cone penetrometer in sand. *Geotechnique*, 38:39–44, 1988.

[20] P.Hölscher. *Dynamic response of saturated and dry soils.* PhD thesis, Faculty of Civil Engineering and Geosciences, TU Delft, 1995.

[21] P.Hölscher. Numerical simulation of a fluid-saturated soil under a dynamically loaded pile. *Transport in Porous Media*, 9:73–84, 1992.

[22] F.B.J.Barends P.Hölscher. The relation between soil-parameters and one-dimensional toe-model.

[23] F.B.J.Barends P.Hölscher. In-situ measurement of soil-motion near the toe of a dynamically loaded pile.

[24] H.Modaressi D.Aubry. Dynamic analysis of saturated non-linear media. *Numerical Methods and Consitutive Modelling in Geomechanics; Desai,CS, Gioda, G (ed.), Springer, Wien*, 1990.

[25] M.F.Randolph D.Bruno. Dynamic and static load testing of model piles driven into dense sand. *Journal of Geotechnical and Geoenviromental Engineering*, 125:988–998, 1999.

[26] A.J.Deeks M.F.Randolph. Keynote lecture:dynamic and static soil models for axial pile response. *Application of Stress-Wave Theory to Piles, F.B.J.Barends (ed.), Balkema, Rotterdam*, pages 3–15, 1992.

[27] M.D.Justasson C.D.Ealy. Statnamic and static load testing of a model pile group in sand. *STATNAMIC Loading Test'98, Kusakabe, Kuwabara, Matsumoto (eds.), Balkema, Rotterdam*, pages 169–177, 2000.

[28] J.DiMaggio W.Teferra G.Likins, F.Rausche. A solution for high damping constants in sands. *Application of Stress-Wave Theory to Piles, F.B.J.Barends (ed.), Balkema, Rotterdam*, pages 117–120, 1992.

[29] H.S. Yu I.F.Collins. Undrained cavity expansion in critical state soils. *International Journal for Numerical and Analytical Methods in Geomechanics*, 20:489–516, 1996.

[30] A.F.L.Hyde N.Yasufuku. Pile end-bearing capacity in crushable sands. *Geotechnique*, 45:663–676, 1995.

[31] J.P.Wolf. Spring-dashpot-mass models for foundation vibrations. *Earthquake Engineering and Structural Dynamics*, 26:931–949, 1997.

[32] C.Song J.P.Wolf, J.W.Meek. Cone models for a pile foundation. *Piles Under Dynamic Loads, Geotechnical Special Publication, 34*, pages 94–113, 1992.

[33] J.P.Wolf. *Foundation vibration analysis using simple physical models.* Prentice Hall, Englewood Cliffs, New Jersey, 1994.

[34] J.P.Wolf. *Soil-structure interaction analysis in time-domain.* Prentice Hall, Englewood Cliffs, New Jersey, 1988.

[35] J.P.Wolf J.T.Meek. Material damping for lumped-parameter models of foundation. *Earthquake Engineering and Structural Design*, 23:349–362, 1994.

[36] J.P.Wolf J.T.Meek. Why cone models can represent the elastic half-space. *Earthquake Engineering and Structural Design*, 22:759–771, 1993.

[37] J.P.Wolf J.T.Meek. Material damping for lumped-parameter models of foundation. *Journal of Geotechnical Engineering*, 118:667–685, 1992.

[38] J.P.Wolf J.T.Meek. Cone models for embedded foundation. *Journal of Geotechnical Engineering*, 120:60–80, 1994.

[39] P.W.Mayne S.E.Burns. Monotonic and dilatory pore-pressure decay during piezocone tests in clay. *Canadian Geotechnical Journal*, 35:1063–1073, 1998.

[40] B-A.Torstensson. Het waterspannings-sondeerapparaat. *pt-b*, 33:631–637, 1994.

[41] C.P.Wroth M.F.Randolph. An analytical solution for the consolidation around a driven pile. *International Journal for Numerical and Analytical Methods in Geomechanics*, 3:217–229, 1979.

[42] P.Rocha Filho. Influence of excess pore pressures on cone measurements. *Proceedings of the Second European Symposium on Penetration Testing, Amsterdam*, pages 805–811, 1982.

[43] J.D.McKinley. Coupled consolidation of a solid, infinite cylinder using a terzaghi formulation. *Computers and Geotechnics*, 23:193–204, 1998.

[44] Rosza Imre. Modelling of consolidation around the pile tip. *9th International Conference on Piling and Deep Foundations, Nice, Presses de l'Ecole Nationale de Ponts et Chausees*, pages 513–518, 2002.

[45] A.Verruijt. *Soil dynamics.* TU Delft, Delft, The Netherlands, 2003.

[46] F.P.Smits. Penetration pore pressure measured with piezometer cones. *Proceedings of the Second European Symposium on Penetration Testing, Amsterdam*, pages 871–876, 1982.

[47] E.Archeewa. The effect of loading rate on bearing capacity of saturated sand. Master's thesis, Unesco-IHE, Institute for water education, March 2005.

[48] R.V.Whitman T.W.Lambe. *Mecanica de suelos.* Limusa Noriega, Mexico, 2001.

[49] A.Verruijt. *Grondmechanica.* Delft University Press, Delft, The Netherlands, 1999.

[50] B.M.Das. *Advanced soil dynamics.* Taylor and Francis, Washington, 1997.

[51] J.Atkinson. *The mechanics of soils and foundations.* McGraw-Hill, Maidenhead(UK), 1993.

[52] N.Soliman-Saad A.D.Hanna. Effect of compaction duration on the induced stress levels in a laboratory prepared sand bed. *Geotechnical Testing Journal*, 24:430–438, 2001.